CONTENTS

Page intentionally left blank

1 Introduction

Analytical chemistry has always been a very powerful and essential tool for many branches of natural sciences. Oceanography does not make an exception; this field has been capturing more and more interest in the last decades. It does not have a long history, in fact the HMS Challenger expedition[1], 1872, can be considered as the birth of this research field. The cruise lasted four years, the crew covered almost seventy thousand marine miles during 1606 days (706 offshore). That expedition laid the foundations of modern oceanography, monitoring the water temperature and making several discoveries regarding the marine environment.

Today oceanography is a huge research field, inasmuch it goes through chemical, physical, geological and biological processes. In order to analyze every phenomenon and understand processes in the marine hydrosphere, several major factors should be considered: the ocean circulation [1], the biological and global nutrients cycles [2] and the climate change impact [3-5]. All of these aspects are interconnected and, in turn, depending on numerous variables. Obviously, it is very hard to have a clear overview in this so intricate situation, given the high number of factors and the immense study area. The easiest way to improve the knowledge was to study in independent way the most important topics and, eventually, try to understand their mutual relationships.

The attention of the scientific community was drawn to several issues during time. Many papers have been devoted to ocean acidification and its relation to increasing CO_2 concentration in the atmosphere [6-8], together with the plankton production and the nutrients cycles have been deeply investigated [9-13].

Iron plays a vital role in regulating primary productivity[14]: low iron concentrations consistently found in HNLC areas led to the formulation of the "iron hypothesis", the possibility that iron is the limiting agent for primary productivity in vast areas of the oceans[15]. This limitation has important consequences on the regulation of the global climate via a reduction of the ability of the oceanic phytoplankton to sink atmospheric CO_2 and export a part of it to the deep ocean in a process referred to as the biological pump [16].

[1] Wyville Thomson, C and Murray, J. 1885. The Voyage of H.M.S. Challenger 1873-1876. Narrative Vol. I. First Part. Chapter I.

Iron detection in seawater at the trace level was accordingly encouraged by fundamental research in oceanography based on the oligo-nutrient role of iron [17, 18] and is one of the issues at the forefront of elemental analytical chemistry. Due to the low solubility of Fe(III), the common redox form at the pH and ionic strength of seawater, iron solubility in organic-free seawater is in the narrow range 10-100 pM [19] with natural concentrations increased by organic complexation to the 0.1-10 nM range [20]. Dissolved iron analysis challenges the analytical chemist to reach extreme detection capabilities, prevent the high risk of sample contamination and tackle the issue of a high salinity matrix. .

1.1 Analysis of Iron by CSV-DHN: Analytical Background

The determination of dissolved iron in seawater is a fundamental step concerning the deep understanding of all the mechanisms about primary production. Currently, iron concentrations in the open ocean are mainly measured by chemiluminescence [71, 72], spectrophotometry [73] and ICP-MS [74, 75] after pre-concentration by co-precipitation with $Mg(OH)_2$, liquid/liquid extraction or strong acid elution following pre-concentration in columns packed with different resins. Mass spectrometric methods require sample pre-concentration and matrix modification whereas chemiluminescent and spectrophotometric methods require of sample pre-concentration and modification/homogenization of the redox state of iron (see [76] for methods based on pre-concentration and mass spectrometry detection and [77] for chemiluminescence and spectrophotometric methods: reviews on iron determination in seawater in [78, 79]).

Up to now, only cathodic stripping voltammetry (CSV) is able to detect natural concentrations of iron in seawater at the ultra-trace level without requiring a pretreatment step. Accordingly, several methods have been developed based on CSV, with [80, 81] and without [82, 83] catalytic enhancement of the signal. Despite the great advantage of being easily adaptable to onboard operation in oceanographic cruises (an anti-vibration support only is required), these methods did not find extensive application and their use seems to be abandoned in favor of pre-concentration procedures coupled to spectrophotometric, chemiluninescent (both easily adaptable to onboard operation) or mass spectrometry detection.

As an example, the two extensive inter-calibration exercises concerning iron determination in oceanic waters featured a limited number of methods based on cathodic stripping: one out of 24 for the IRONAGES exercise[84] and four out of 21 for the SAFe inter-calibration [85] (regarding the latter, the updated version of the reference value features only one method based on CSV out of 29, see http://es.ucsc.edu/~kbruland/GeotracesSaFe/kwbGeotracesSaFe.html). Further evidence comes from a recent (2012) survey including >13000 dissolved iron data [86]: 62 % were obtained by chemiluminescence, 20% by spectrophotometry, 8% by ICPMS, 6.5% by GFAAS and 3.5% by CSV (if papers instead of number of measurements are used for the calculation, the data change to 54%, 12%, 11%, 12%, 11%, respectively). Several difficulties are associated with CSV detection: the use of mercury

as electrode material which is a regulated substance, the stability of the Hanging Mercury Drop Electrode (HMDE) itself on a moving lab surface, the need for a pretreatment to get rid of organic species (UV digestion), the challenging cleaning of reagents needed to reach a blank at the pM level, and the inconvenience of spiking reagents to an open cell [87].

Previous efforts to determine iron concentration via CSV have made use of the following commercial ligands: dihydroxynaphthalene (DHN) [80], salicylaldoxime (SA) [88], 1-nitroso-2-naphthol (NN) [89] and 2-(2-thiazolylazo)-p-cresol (TAC) [90] with limits of detection close or below the lowest iron concentrations reported for open ocean waters. Nevertheless, improvements in the performance and reliability of analytical methods are actively sought [84, 91]. The voltammetric procedures for the determination of iron in seawater are reported in the Table 1.1.

Table 1.1 – Pool of analytical procedures for the determination of iron in seawater.

Analytical method	Sensitivity-CSV ($nA\ nM^{-1}\ min^{-1}$)	LOD	Ref
Pre-concentration free methods (CSV)			
CSV-TAC	17	100 pM	[90]
CSV-SA*	16	10 pM	[88]
CSV-DHN/BrO_3^- (pH=8)	8	13 pM	[80]
CSV-NN	3	90 pM	[92]
Methods requiring a pre-concentration step			
ICPMS $Mg(OH)_2$ co-precipitation		2 pM	[75]
GFAAS after APDC/DDDC solvent extraction		30 pM	[93]
ICPMS Pre-concentration on NTA		6-28 pM	[94]
Chemiluminiscence luminol/H_2O_2 Pre-concentration in oxine		50 pM	[71]
Catalytic spectrophotometry Pre-concentration in oxine		25 pM	[95]

*only for speciation analysis, the reported LOD is an estimation with 10 min of deposition time.

The DHN/BrO_3^- provide the better performance in terms of LOD and sensitivity. Furthermore the DHN/BrO_3^- is a catalytic method, this being a very important feature

enabling extensive optimization. In Table 1.1 non-voltammetric methods for analysis of iron in seawater are also reported and they all require intensive pretreatment steps.

1.2 Iron in Seawater[2]

Despite being one of the most abundant elements in the Earth crust (5%), iron concentrations in seawater are particularly low (nano-molar to pico-molar range) due to a combination of minute solubility [19], effective removal caused by biological uptake [21, 22] and particle scavenging [23]. Moreover, co-precipitation with flocculating organic matter at low salinities in estuarine water [24] drastically reduces potential inputs from rivers and run-off waters [25].

Iron is present in seawater in multiple forms, particulate and dissolved, organic and inorganic and all these species can occur in different physical size classes. The fraction removed by filtration through 0.2 or 0.4 μm pore size filters, is commonly definite as particulate Fe. Particles of alumino-silicate clays, the intact cells of marine microorganisms and a variety of biogenic detritus are the sources of particulate iron [26]. Dissolved Fe consists in the fraction not removed by filtration, it is mainly complexed with organic molecules, containing numerous classes of organic chelators, humic compounds and cell lysis products [27]. A small part of dissolved iron is formed by inorganic iron hydroxides, while free iron (Fe^{3+}, Fe^{2+}) is practically absent. Dissolved iron is actually formed by small colloidal particles (0.02 –0.45 μm), the percentage of this species depends from the water sample origin and can reach very high value, even 90 % of total iron for coastal waters [28, 29]. Dissolved iron has traditionally been supposed to be bioavailable mainly thanks to the colloidal fraction but part of the dissolved iron is not bioavailable due to ligand binding [29].

Iron in seawater is also present in two different oxidation states: Fe(III) and Fe(II). Fe (III) is predominant in oxic environments and it characterized by a high reactivity, thermodynamic stability and a very low solubility as free ion. Despite the tiny concentration of free ion there are a multitude of Fe(III) hydrolysis products Fe(III)' [30]. The precipitation of the iron hydrolysis species starts at concentrations of 0.7 nM [31]; but their solubility strongly decreases with time [19, 32]. Fe(III) reduction leads to species of the more soluble and kinetically labile Fe(II). Fe(III) reduction occur via absorption of low UV light or high frequency radiation in the visible region (photo-reduction) in the surface ocean [33], and via biologically-mediated reactions at cell

[2] Metal Ions in Biological Systems, Volume 43, edited by A. Sigel, H. Sigel and R. K. O. Sigel, CRC Press 2005

surfaces [34]. Inorganic Fe(II) species Fe(II)' are very soluble, despite the Fe(III) homologous, and Fe(II)–organic complexes are not strongly bound. For these reasons, reduction processes can cause a sporadic increase in the availability of dissolved and labile Fe species. Dissolved Fe(II)' species are rapidly re-oxidized by H_2O_2 [35] or dissolved oxygen if in contact with oxic waters. The re-oxidized species may follow two different routes: re-precipitate as Fe(III) hydroxides or be reincorporated into complexes with organic ligands. These sequence of reactions generate a redox cycle, the final result is a rise of the concentrations of the Fe(II) and Fe(III) hydrolysis products in seawater. Moreover, these species are the main source of iron for phytoplankton blooms.

The concentration of dissolved iron in ocean is obviously not homogenous; there are several factors involved that need to be considered in order to understand the iron distribution. External inputs, chemical processes, physical processes and the vertical and lateral distributions are the principal source of variations concerning dissolved iron.

The dissolved iron concentrations vary in a very wide range: the high nutrients low chlorophyll regions (HNLC) and the deep water are characterized by a low concentration of iron, it is usual to measure concentrations below 1 nM, instead in areas close to hydrothermal vent fluids can reach concentrations around 3 nM.

Atmospheric dust deposition, river input, hydrothermal vents, and release from marine sediments are all external sources of iron, their contribute are widely inhomogeneous in time and space for several reasons including chemical and physical processes. The most important external input in the marine environment is the atmospheric deposition of the continental dust. The deposition can be dry or wet, in both cases the amount of iron that becomes actually bioavailable is minimal because the particles and the colloidal Fe(III) solubility is very low. On the other hand, it is clear that aerosol has a role on the chlorophyll and biomass production. Bottle incubation tests highlighted an increase in phytoplankton production when iron particles are added to the cultures [36].

As mentioned before currents and other mixing processes have a very important role in the oceans and they also impact atmospheric particles when they get into the water. The consequence of the transport from a source area to another area due to a gradient in iron concentration is the equatorial Pacific region close to the Galapagos Islands. In this area the dissolved iron concentration change from 0.05 to 3

nM depending on the measure being performed up-current (higher concentrations) or down-current (lower concentrations) [37]. The vertical transport of iron acquire more relevance in remote zone of the open ocean when the external dust input is almost irrelevant [38]. In fact in the Southern Ocean, one of the known HNLC areas, the iron input is guarantee by the winter mixing, enhanced by the summer upwelling of circumpolar deep water at the polar front of the Antarctic current [39].

The sum of all the mixing processes in the oceans usually gives as a result a similar dissolved iron vertical distribution. The vertical concentration profile of iron is comparable to other biological nutrients like nitrate and phosphate: (a) depletion at the surface, determined by biological uptake; (b) a mid-depth maximum, linked to the rate of export production from the photic zone and the result of microbial regeneration of exported material; (c) reasonably stable concentrations at depth (Figure 1.1) [40].

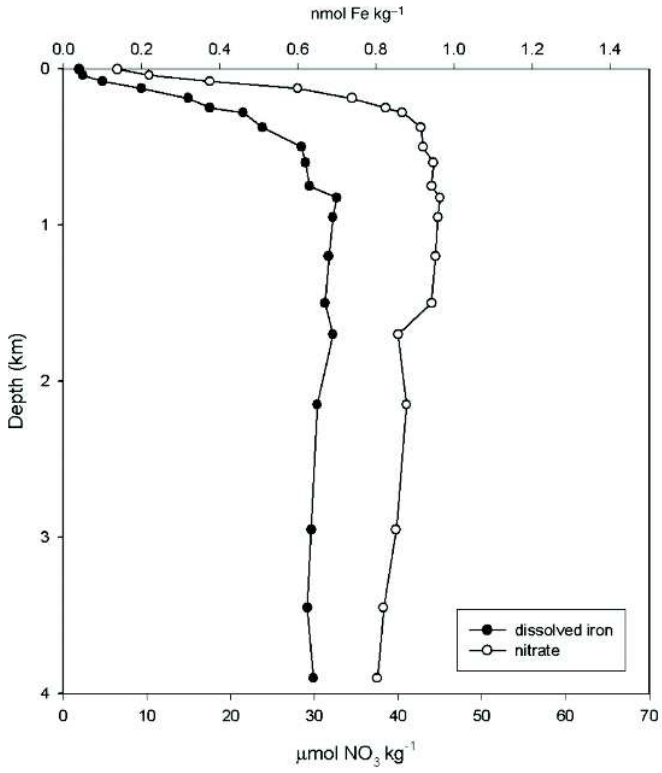

Figure 1.1 - Vertical distribution of dissolved Fe and nitrate in the central Subarctic Pacific at Ocean Station Papa, 508N, 1458W. Adapted from Ref. [41].

Very low concentration of nitrate and phosphate have been detected during the subtropical gyres of all the principal oceans during the summer suggesting the N limitation of new production. Instead the North Atlantic , the Arabian Sea and various coastal upwelling regions showed high nutrient concentrations (*i.e.* nitrate above 2 µM) keeping the high chlorophyll concentration (> 0.5 mg m^{-3}). On the other hand,

other oceans region have a similar nutrients concentration on the surface but a lower chlorophyll presence (<0.5 μg L^{-1}). These areas, called HNLC, comprehend the eastern equatorial Pacific, subarctic Pacific, and the Southern Ocean. All of these regions, even if located in very different part of the globe, show a good provision of nutrients able to guarantee a better primary production compared to the existent one [42-44].

It was hypothesized that the motivation of this incongruence is the role of iron in the primary production in the HNLC areas [45, 46]. Before the 1980s the absence of adequate trace metal clean sampling techniques made hard the investigation of this hypothesis. The HNLC regions gave very low values of iron concentrations when accurate measurements were possible, particularly in the Southern Ocean and the equatorial Pacific [37, 42, 43, 47]. On support of this thesis initial bottle incubation experiments showed an increasing of chlorophyll a and nutrients depletion after iron enrichment in the nano-molar scale. [17, 41, 48, 49]. Following study completed the first outcomes [36, 50-53], recording quick physiological responses by phytoplankton (increased ^{15}N uptake, nitrate reductase expression) to Fe addition [51]. Other studies demonstrated that even pico-molar additions of Fe could produce assessable consequences [54]. The effect of iron on the primary production has been demonstrated for different kind of phytoplankton communities. Incubation studies, from nano and pico-sized phytoplankton to diatoms, showed the reduction of nutrients and an increasing of phytoplankton flora.

Clearly the incubation conditions are different than the ocean ones and many restrictions limit the applicability of these data. For instance the fixed light insensitivity during the experiments and the presence of containers walls themselves are a strong limitation to recreate the marine environment. For all these reason incubation experiment are not the best way to describe this phenomena as it actually happen in nature [43]. In situ Fe enrichment mesoscale experiment were performed by researchers trying to bypass the limitations reported before. Large areas of the ocean were seeded with iron and sequentially the response of the system, in terms of phytoplankton bloom, was monitored for several days.

To date, thirteen *in situ* mesoscale iron enrichment experiments have been performed in the HNLC regions, everyone with its own acronym: IRONEX I [43] and II [47] in the equatorial Pacific south of the Galapagos Islands; FeeP [55] in the North Atlantic Ocean, SOIREE [42], EisenEx [56], EIFEX [57, 58], SAGE [59] and SOFeX in various sectors of the Southern Ocean south of the Polar Front; SEEDS I [54], SEEDS II

[60] and SERIES [61] in western and eastern gyres of the subarctic Pacific, respectively. The SOFeX experiment consisted of two distinct enrichments, one (SOFeX S) in the high silica waters south of the Polar Front [62, 63], the other (SOFeX N) in low silica waters to the north [62]. The last iron enrichment experiment is the LOHAFEX [64, 65], which was carried out in the South Atlantic Ocean. The LOHAFEX expedition parted after two weeks of suspension due to an environmental group's protest against the experiment. As a result of this protest the iron enrichment was limited to a smaller scale and only for coastal water[64].

The procedure for the iron enrichment experiment is similar for all the expeditions performed: an HNLC surface water area (50–225 km^2) was seeded with ferrous sulfate to increase the ambient iron concentration, simultaneously sulfur hexaflouride(SF_6) was added as inert tracer. After the iron enrichment the concentration of dissolved iron was several times bigger (even around 4 nM) compared to the pre-experiment condition. The chemical, biological, and physical variations in the experiment area were monitored for many days after the seeding, the longest mesoscale iron enrichment experiment (SOFeX S) lasted 28 days. Figure 1.2 indicates the location (blue stars) of the in situ mesoscale iron enrichment experiments.

Figure 1.2 - Location of in situ mesoscale iron enrichment experiments (stars).

As reported before, *in situ* mesoscale iron enrichment experiments have used a mutual framework that allows comparison between their chemical, physical and biological results. Other outcomes were noted during the enrichment experiments beside the iron essential role. For example it was discovered that warmer waters

permit a faster phytoplankton growth [66] (this was already predicted by algal physiological relationships [67]). Moreover, all the observed blooms highlighted an inverse relationship between mixed-layer depth and chlorophyll concentration [68, 69]. Aside from the reported results, all thirteen mesoscale enrichment iron experiments brought detailed extra observations covering the entire experimentations time scale. It is possible to find further information, and the experimental data of all the mesoscale enrichment experiments, except LOHAFEX, in the work performed by Boyd et. al. [66].

Up to now, it is not clear how natural or anthropogenic variability in Fe supply affects ocean biogeochemistry and global climate [70]. The duration of the enrichment experiments is another significant issue; in fact they had a relatively short-term duration, specifically designed to test whether Fe supply limits primary production in HNLC waters. All the considerations made before are based on a temporally and spatially scale up of the findings from the enrichment experiments. Four issues are essential to testing the validity of such extrapolation: macronutrient uptake, bloom time scale, modes of iron supply and iron-carbon biogeochemistry [66].

1.3 Thesis Outline

Aim of this thesis was to create a new CSV method suitable for the determination directly on board of iron in seawater during scientific cruises. The adsorptive cathodic stripping voltammetry was chosen as analytical technique because it offers the possibility to reach this goal without pre-concentration step. Obviously the new CSV method should have better performance in comparison with the pre-existent ones and, if possible, further advantages like the reduction/simplification of used chemicals and an overall simplified procedure.

The first step was the choice of the artificial ligand. After a long and accurate evaluation of the existing voltammetric methods (reported in Table 1.1), 2,3-dihydroxynaphthalene (DHN) was chosen as the artificial ligand for the development of the new CSV method.

After the ligand choice, a new CSV method for the analysis of iron was optimized (Chapter 2). It was based on a previous work on the determination of iron using DHN as a ligand in the presence of potassium bromate as a catalytic agent [80]. The achieved procedure improved significantly the performance of the prior one but it still uses $KBrO_3$ as the oxidant.

In the meanwhile, the optimization of a new voltammetric cell was started with the purpose to reduce the sample size required for each analysis (Chapter 3). The development of this new hardware went across the realization of several prototypes and ended with a new voltammetric cell enabling the use of 500 µL sample aliquots. This new cell was also a key point during the optimization of another voltammetric method (Chapter 4) related to iron determination. The latter led to a strong reduction in sample volume, amount of reagents and a significant increase in sensitivity.

More than one procedure for the analysis of iron in seawater was created during this work. Any of these were fundamental to achieve the final result: Chapter 5 presents the comparisons between the developed CSV methods, existing ones and analytical procedures based on other detection schemes including future implementations and foreseen trends.

2 Analysis of Iron by CSV-DHN with Potassium Bromate

This chapter reports on the foremost optimization introduced for the challenging analysis of total dissolved iron at the low picomolar level in oceanic waters suitable for onboard analysis. As mentioned in the Introduction, the method is based on the adsorptive properties of the iron-2,3-dihydroxynaphthalene (DHN) complexes on the hanging mercury drop electrode (HMDE) with catalytic enhancement by bromate ions. Although based on a previously proposed reagent combination, the optimized method shows that the addition of an acidification/alkalinization step is essential in order to cancel any organic complexation and it allows avoidance of the UV oxidation stage before the voltammetric analysis. Moreover, an increment of the pH to 8.7 leads to the definition of a pre-concentration-free procedure with the lowest detection limit described up to now, which was equaled by the method described in Chapter 4. The new method was validated onboard via the analysis of reference material and via inter-calibration against FIA-chemiluminescence on North Atlantic Ocean samples.

2.1 Method Optimization

In the following sections, the steps leading to the definition of the improved procedure are described, starting from the evaluation of the effect of pH on sensitivity and acidification on iron recovery, following with the validation of the procedure, ending with a tentative elucidation of the mechanism responsible for the sensitivity increase.

2.1.1 pH dependence experiments

Early experiments led to the discovery that pH was the most important parameter controlling the detection capability of the voltammetric analysis of iron in the presence of DHN and bromate.

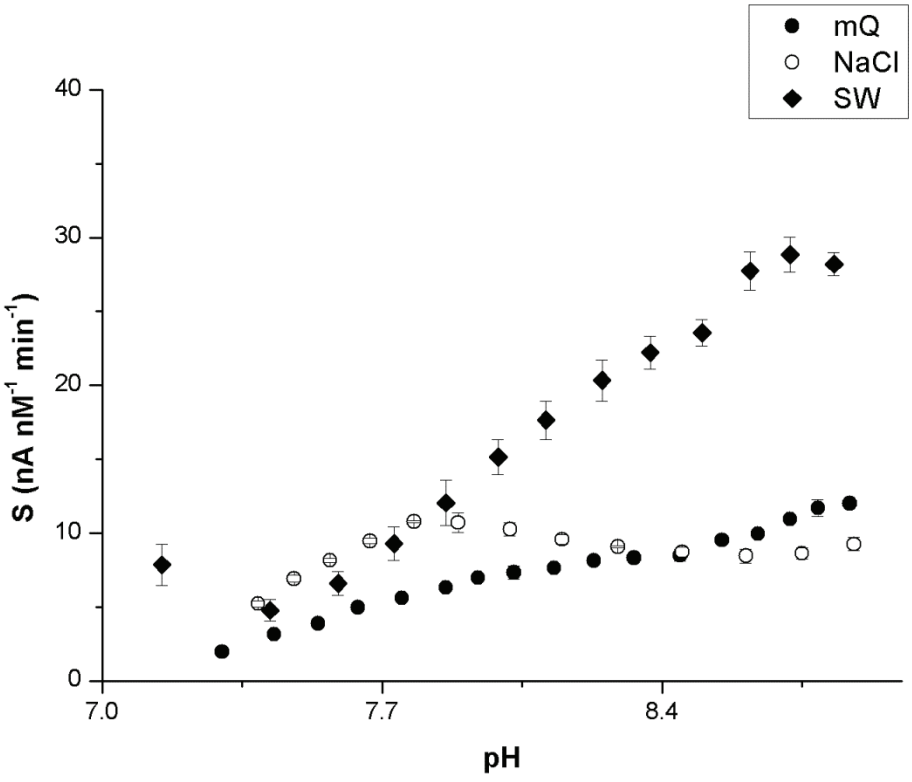

Figure 2.1 – pH dependence experiments. All solutions: 20 mM bromate, 5 mM POPSO buffer and 30 µM DHN.

Figure 2.1 shows the effect of pH on the sensitivity of Fe-DHN complex in the presence of BrO_3^- in three different solutions: ultrapure water, NaCl (0.72 M) and Southern Ocean UV digested seawater. Iron concentrations were established before the

beginning of the experiments by two standard additions, thus allowing the calculation of the sensitivities (S reported as nA nM^{-1} min^{-1}). The pH was initially moved to 7.2-7.4 by an HCl addition to explore the pH range from circumneutral to alkaline and subsequently increased by successive NH_4OH additions (the acidic range was not investigated as it showed low sensitivities and/or strong interferences).

The Fe-DHN signal increased steadily as a function of the pH in the whole range of study with the exception of the response in 0.72 M NaCl (Figure 2.1). This followed the behavior of seawater up to a maximum at pH 7.8 with a nearly constant value at higher pH, similar to the ones found for ultrapure water at pH > 8.4. The sensitivity increased by a factor of 2 in NaCl, 5 in seawater and 12 in ultrapure water. This effect was completely different to that observed in the Obata and van den Berg paper [80], where a maximum response was found at pH=8.0 (~8 nA nM^{-1} min^{-1}) as they only checked the effect of pH in the absence of bromate. For seawater, the sensitivity grew up to 30 nA nM^{-1} min^{-1} whereas for ultrapure and 0.7 M NaCl the maximum was around 10 nA nM^{-1} min^{-1}. Because the addition of the HCl/NH_4OH pair improved substantially the sensitivity and further NH_4OH additions increased additionally the sensitivity, the first hypothesis was that NH_4OH had a direct role in the signal enhancement. Nevertheless, when the experiment was repeated with ultrapure water and seawater after an acidification/alkalinization cycle by consecutive additions of HCl and NH_4OH prior to the analysis (~ 3x the original NH_4OH concentration provided by the POPSO/BrO_3^-/NH_4OH reagent) the relation sensitivity vs pH did not change substantially, reaching for seawater again a maximum of ~ 30 nA nM^{-1} min^{-1} at pH 8.9 (data not shown). This ruled out any significant effect caused by ammonia. The sensitivity achieved was an improvement by a factor of four with respect to the Obata and van den Berg settings at the same bromate and DHN concentrations.

The features and reproducibility of the signal in the pH range 8-9 was also investigated. Figure 2.2 shows the scans obtained from the analysis with standard addition calibration of the same ocean water at two different pH. There is an obvious increase of the sensitivity and a moderate broadening of the Fe-DHN peak. In order to discard a negative effect of pH, Figure 2.3 shows 3 raw scans from the analysis of the same sample analyzed at pH = 8.1, 8.4 and 8.7 (Fe-DHN peak magnified in insert plot).

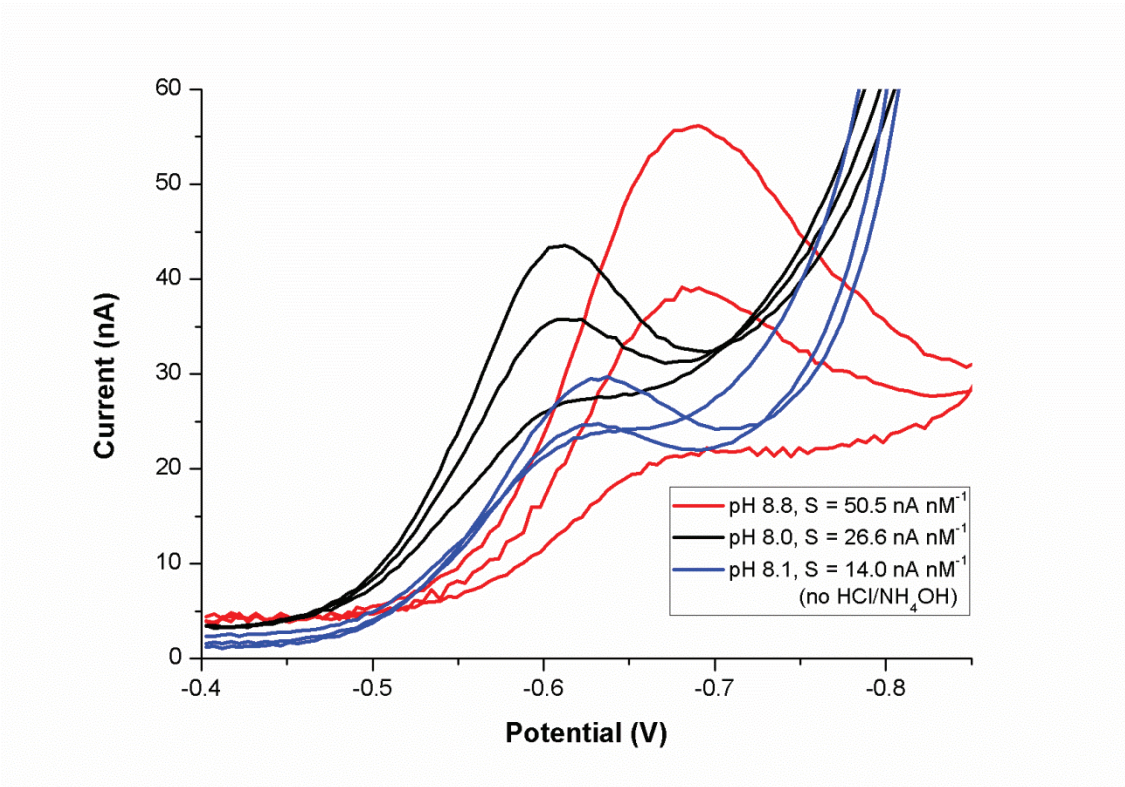

Figure 2.2 – Raw voltammetric scans obtained in different seawater samples under the following conditions: all samples 30 µM DHN, 20 mM BrO_3^-, 90 seconds deposition at 0V. In all cases calibration by two additions of 0.3 nM Fe. Blue line: equilibrated and analyzed at pH=8.1 (0.26 nM Fe); black line: equilibrated pH=2.0 and analyzed at pH=8.0 (0.19 nM Fe); red line: equilibrated for 24 hours at pH=2.0 and analyzed at pH=8.8 (0.16 nM Fe). Blue scans were brought down 15 nA for the sake of clarity.

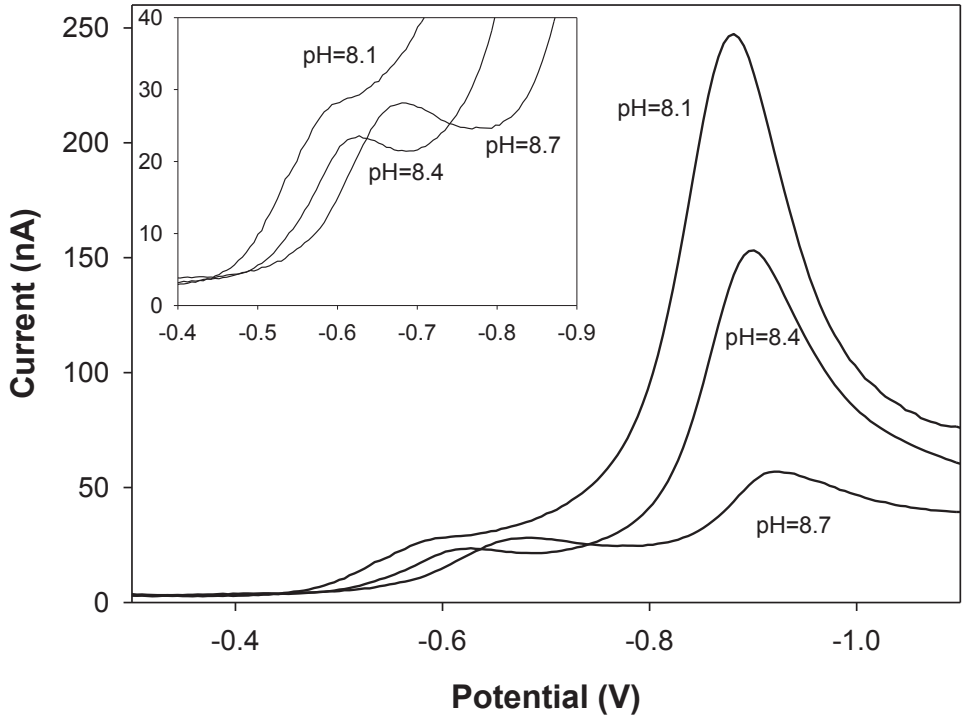

Figure 2.3 – Effect of the pH on the catalytic AdCSV determination of iron in the same Southern Ocean sample. All in the presence of 30 µM DHN, 20 mM BrO_3^- and 5 mM POPSO buffer. Insert: magnification of the Fe-DHN peak.

The pH shift moved the Fe-DHN peak towards more negative potentials and substantially reduced the vanadium peak: as a consequence, the peak changed from a poorly resolved shoulder to a well-defined peak. The magnitude of the peak increased from 11.8 nA (pH=8.1) to 17.4 nA (pH=8.7) but the sensitivity (determined after two 0.3 nM additions) increased accordingly from 20.3 to 36.5 nA nM^{-1} min^{-1}. Iron concentrations determined in 5 different aliquots were: 0.39 ± 0.02 (pH = 8.1), 0.36 ± 0.01 and 0.31 ± 0.01 (pH = 8.4), 0.35 ± 0.01 (pH = 8.5), and 0.32 ± 0.02 (pH = 8.7). Therefore, the performance and accuracy of the method were not a function of the pH in the range 8-8.8. At pH ≥ 9 we found in some samples serious difficulties in defining the end of the Fe-DHN peak in its intersection with the residual V-DHN signal and advise against its use for analysis (Figure 2.4).

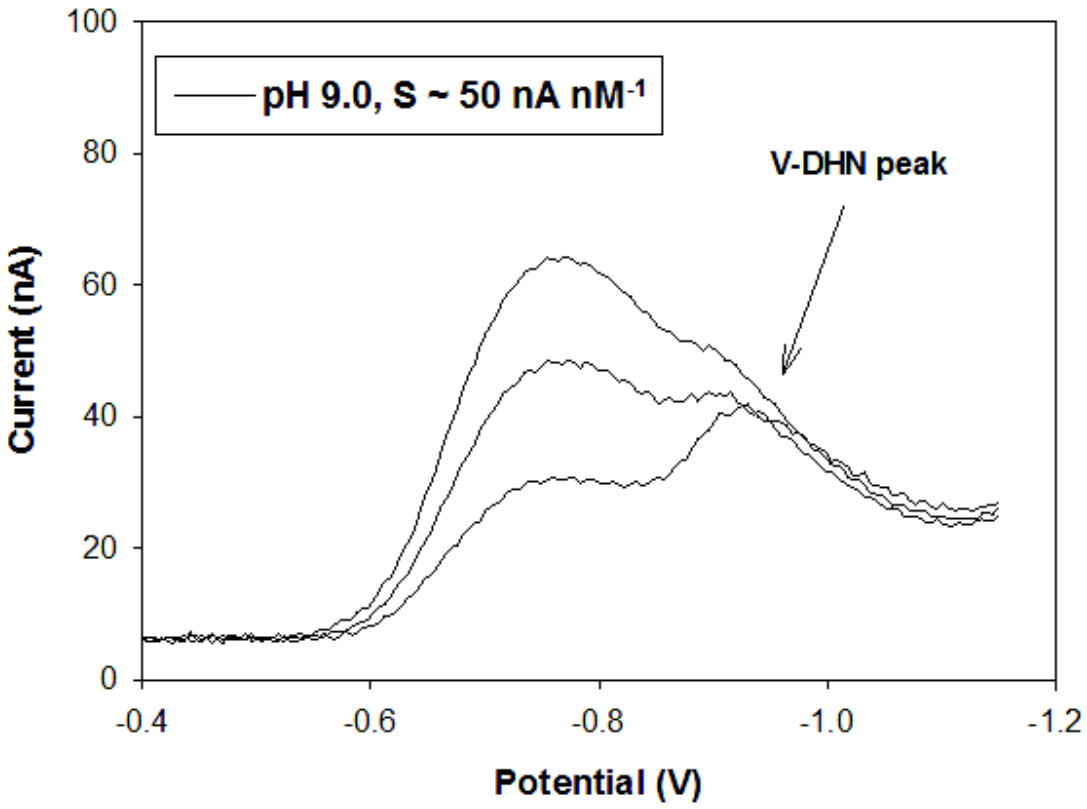

Figure 2.4 – Determination of the iron concentration in a Souther Ocean surface sample by AdCSV in the presence of 30 µM DHN, 20 mM BrO_3^- and 5 mM POPSO buffer at pH=9.0. The plot presents potential scans for the sample and two 0.3 nM internal additions for calibration

Buffering capacity in the analytical range All the experiments presented in this work were carried out in the presence of the buffer POPSO (piperazine-N,N′-bis(2-hydroxypropanesulfonic acid). The pH range where we found optimum analytical conditions (8.5-8.8) was at the edge or beyond the buffering interval of POPSO (7.2-8.5; pK_a = 7.80, information provided by the manufacturer). Instability of pH in the bulk of the solution or in the limit layer of the electrode could cause analytical problems. The easiest solution would be to use a buffer with a pK_a close to 8.7. The obvious candidate, frequently used in CSV, would be borate buffer. However, UV digested borate additions suppressed the Fe-DHN peak in the presence of BrO_3^-. Figure 2.5 shows the buffering capacity (here defined as µL of 0.9 M NH_4OH per pH increment) as a function of pH for ultrapure water and UV digested seawater after alkalinization by ammonia additions in the presence of 5 mM POPSO buffer (initial NH_4OH concentration ~ 6 mM from the BrO_3^-/POPSO solution). The buffer capacities did not decrease until pH around 8.5, but there was a steep increase up to the end of the pH range tested (7.2-9).

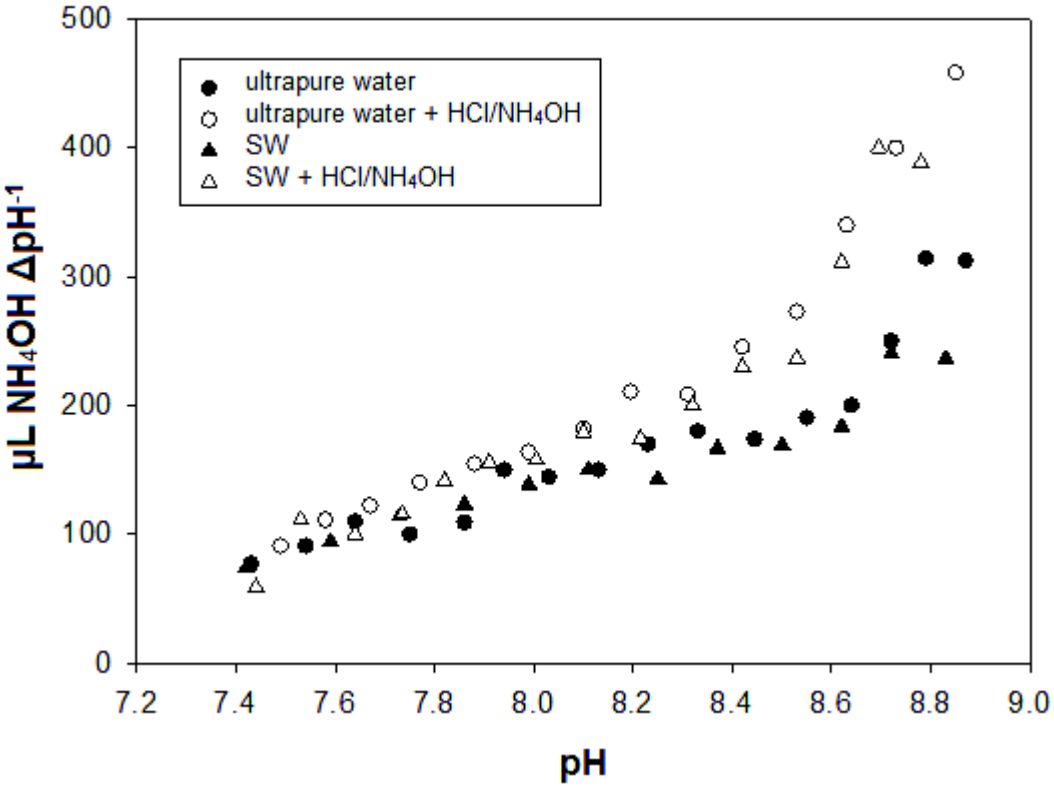

Figure 2.5 – Effect of successive ammonia additions in the relationship in between the pH and the buffering capacity (here defined as µL NH_4OH per pH increment) of ultrapure water and UV digested seawater in the presence of 30 µM DHN, 20 mM BrO_3^- and 5 mM POPSO buffer. The experiment was repeated after acidification to pH=2 and neutralization which approximately tripled the concentration of ammonia in the samples (open symbols).

When the experiment was repeated after acidification/neutralization (increasing the initial concentration of NH_4OH by a factor of 3), the buffering capacity increased further to pH > 8.4, ultrapure water and seawater responded identically. The deviation from the behavior expected for POPSO, and the extra increment caused by an increment of the ammonia concentration indicated the formation of an ammonia/ammonium chloride buffer (pK_a (NH_4OH/NH_4Cl) = 9.25, the effective pH range for this buffer is 8.8-9.9).

The experiment was repeated by HCl additions after an initial NH_4OH addition to study the effect of pH at a constant NH_4OH concentration. The HCl addition brought the pH close to 9 (Figure 2.6), the buffering capacity decreased in the range 8.6-9 and then it remained constant down to pH 7.2. The pH was varied by adding either small volumes of 20-fold diluted acid (HCl) or base (NH_4OH) solutions kept airtight in between experiments.

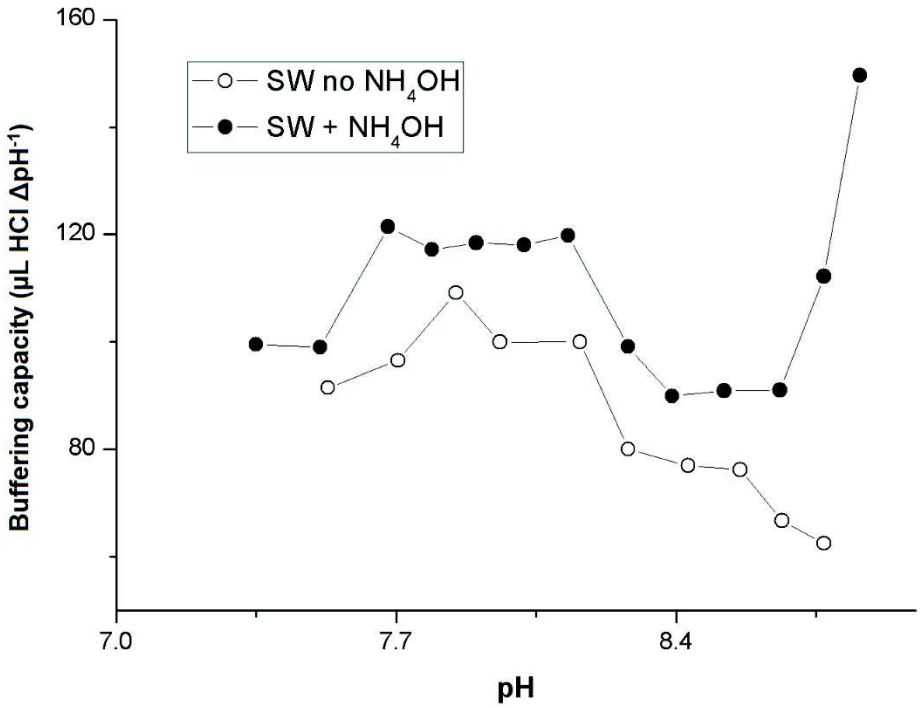

Figure 2.6 – Effect of successive HCl additions in the relationship in between the pH and the buffering capacity (here defined as µL NH_4OH per pH increment) of UV digested seawater in the presence of 30 µM DHN, 20 mM BrO_3^- and 5 mM POPSO buffer. The experiment was repeated using an ammonia free BrO_3^-/POPSO solution.

2.1.2 Acidification neutralization and its effects

The determination of total metal concentration by CSV at circumneutral pH is strongly affected by the non-lability of the fraction that outcompeted the artificial ligand (AL) added to the sample. This problem cannot be circumvented increasing several orders of magnitude the AL concentration because, at some point, AL excess forces a substantial decrease of the sensitivity by saturation of the HMDE surface. Moreover, the slow dissociation kinetics of natural complexes could hinder the ligand exchange reaction leading to unreliable results. The removal of organic complexation prior to analysis is usually achieved by a period of strong acidification, digestion by UV irradiation or both. This is also the case for the determination of many other trace metals [96, 97]. The use of DHN presents a clear advantage with respect to the rest of the voltammetric methods based on other AL (NN, TAC and SA): the possibility of increasing the DHN concentration about 30 times (from 1 μM to 30 μM) with respect to the concentration used for speciation studies [80, 98] which is not the case for the rest of the AL that operate for complexation studies at the upper limit of the AL concentration linear range. This DHN concentration (30 μM) is the equivalent to a log $\alpha_{Fe'\text{-}DHN}$ of 4.6 ($\log K'_{Fe\text{-}DHN}$= 9.1) [99], a side coefficient 1 to 2 orders of magnitude higher than those reported for the other AL. Possibly, that strong Fe-DHN complexation was behind the reason to keep untested the recovery achieved in the absence of sample acidification in previous uses of the DHN/BrO_3^- pair [80].

Iron recovery in open ocean seawater after 24 hours equilibrium with 30 μM DHN at pH 8.0, without further treatment, was measured as a percentage with respect to the iron recovered if the sample was acidified for the same period at pH 2.0. Figure 2.7 shows that in those experimental conditions only 42 ± 7 % of the total dissolved iron was labile indicating the requirement for an acidification prior to analysis.

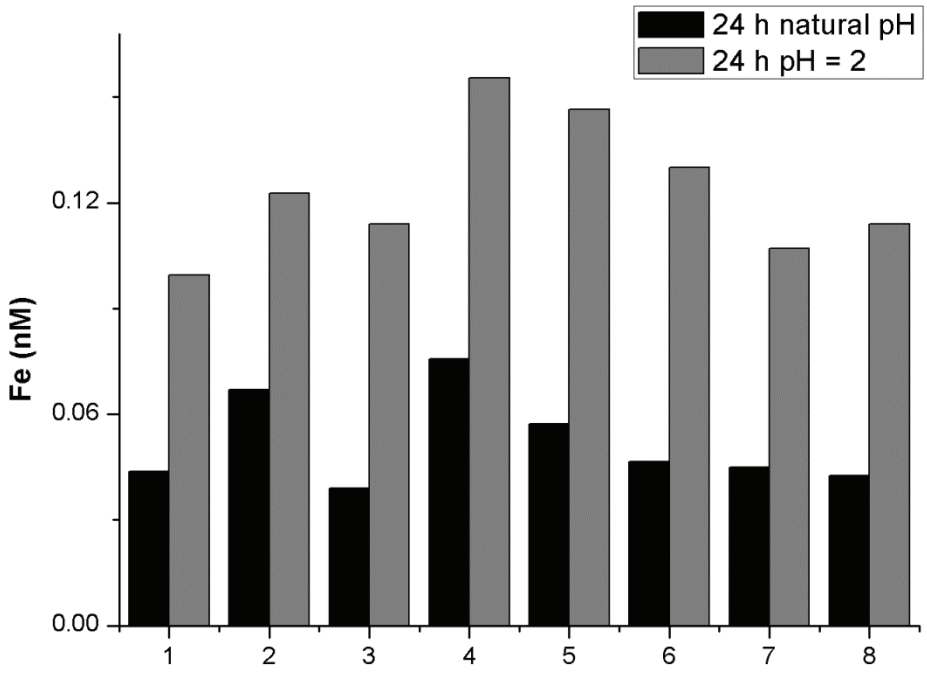

Figure 2.7 – Effect of 24 hours equilibrium with 30 µM DHN at natural pH and at pH=2.0 on the recovery of total dissolved iron in different Southern Ocean surface seawater samples.

This process is in agreement with the reported presence of strong binding ligands in all open ocean waters [87]. This test is not definitive in order to validate the method as the pH could not be acidic enough to break all natural complexes or the pH neutralization could lead to the formation of not only Fe-DHN complexes but also Fe-natural ligands complexes that would outcompete DHN leading to underestimations of the iron concentration. For that purpose, the same sample was measured after UV digestion to cancel any organic complexation. Figure 2.8 shows the iron recovery caused by the acidification to pH 2.0 as a function of the acidification time prior to the analysis at pH 8. The result was a full recovery after 2.5 hours that was unaffected for 24 hours. We decided to keep an acidification period of at least overnight in order to follow recommendations presented in other publications.

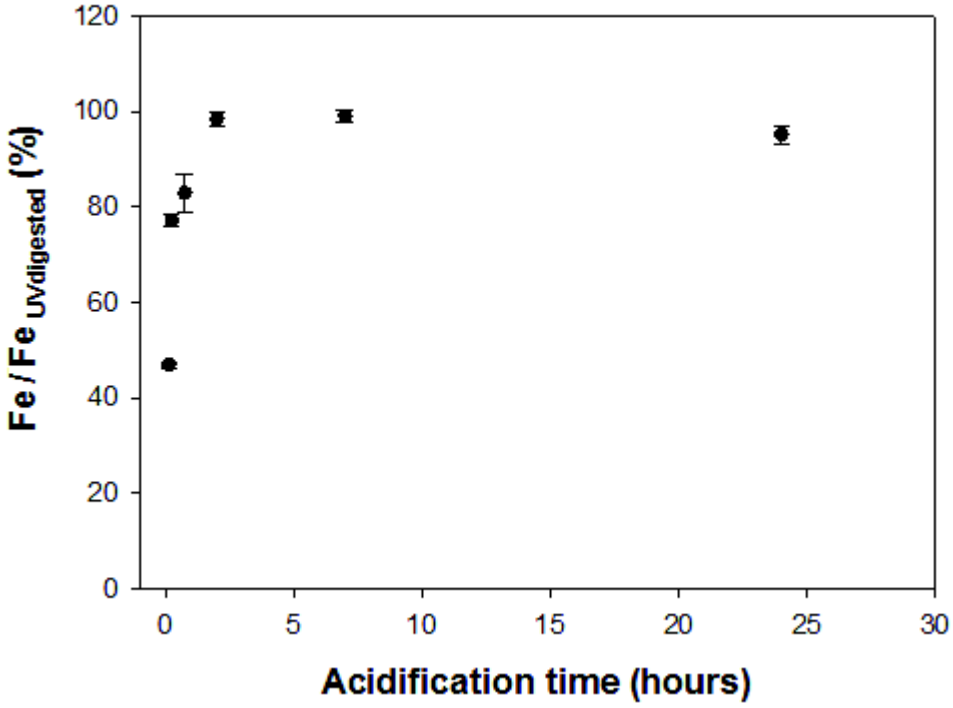

Figure 2.8 – Effect of the acidification time (pH 2.0) on the percentage or iron recovered with respect to acidification plus UV digestion. Sample: Southern Ocean surface seawater.

2.1.3 Vanadium interference

During the analysis of a sample with consensus values or reference materials, a persistent trend was observed obtaining slightly higher concentrations than the given ones. Careful inspection of the scans obtained from iron standard additions showed that as the iron peak grows and broadens, its increasing overlapping with the V-DHN peak lifted the right end of the Fe peak and introduced a bias in the calculation of its height (detailed in Figure 2.4), leading to an underestimation of the sensitivity. At pH > 8.6 and despite its declining, the V-DHN signal still constitutes a serious interference.

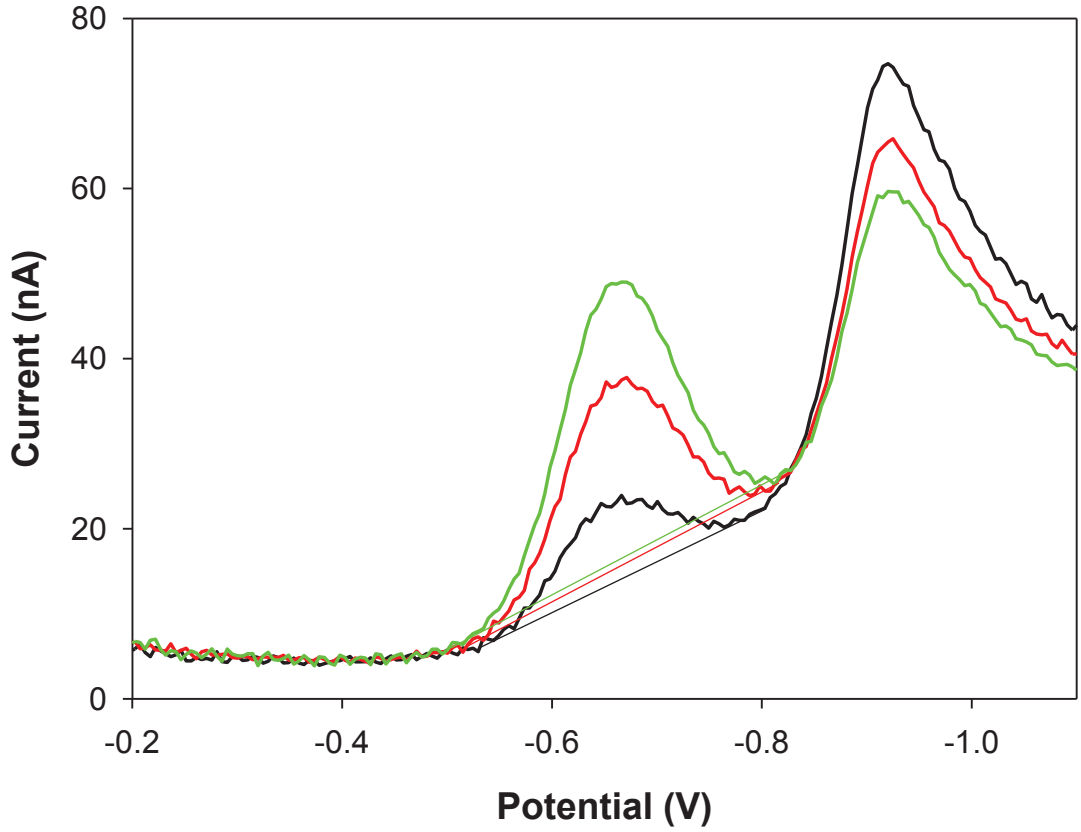

Figure 2.9 – CSV determination of the iron concentration in a SAFe deep seawater reference material at pH 8.7. Black scan: sample, red scan: sample +1 nM Fe, green scan: sample +2 nM Fe. Straight lines: tangents that delimit the edges of the peak according to the color code to demonstrate the effect of vanadium in the estimation of the peak properties.

This effect could be minimized by the use of the peak area. Table 2.1 gives examples of the extent of the enhancement of the accuracy obtained for the analysis of different samples and reference materials. The use of peak area consistently lead to lower estimations for all CRMs which are closer to the certified value. The peak area use is possible even if it does not have a clear physical meaning as in the non-catalytic analysis.

In order to prove that the effect was caused by the V-DHN peak we studied the recovery via analysis of fortified ocean and ultrapure (V free) waters (Table 2.1). Fe concentrations before fortification were determined as 0.12 ± 0.01 (ultrapure water) and 0.23 ± 0.02 (ocean sample) respectively. The error comes from the average of the results obtained from the use of peak height and peak area. Both samples were fortified to 2.12 and 4.23 nM respectively. After a new internal calibration, the iron recovery in ultrapure water was very close to 100% independently of the use of peak height or

area. For seawater, again the peak area gave a lower and significantly better estimate of the Fe concentration. (Table 2.1).

Table 2.1 – Recovery comparison using the peak height and the peak area. All the concentrations in nM.

	Consensus concentration	Peak height (% recovery)	Peak area (% recovery)
CASS-5 (diluted 1:5)	25.8 ± 2.0	28.6 ± 0.2 (111 %)	27.2 ± 0.8 (105 %)
SAFe-S	0.097 ± 0.043	0.123 ± 0.009 (127 %)	0.094 ± 0.010 (96.9 %)
SAFe-D2	0.91 ± 0.17	1.00 ± 0.01 (110 %)	0.86 ± 0.03 (94.8 %)
Milli-Q + 2 nM Fe	2.12 ± 0.02	2.10 ± 0.05 (99.1 %)	2.08 ± 0.07 (98.1 %)
St 146 + 4 nM	4.23 ± 0.02	4.47 ± 0.04 (105 %)	4.32 ± 0.04 (102 %)

2.2 Figure of Merit & Validation

2.2.1 Limit of detection, limit of quantification and precision

The limit of detection (as 3 times the standard deviation of repeated scans divided by the sensitivity) for the determination of iron in seawater using DHN/BrO_3^- at pH=8.0 without previous acidification/neutralization has been determined at 13 pM elsewhere [80]. This limit of detection, considering the reported sensitivity of 7.9 nA nM^{-1} min^{-1} results in a lowest detectable signal of 0.1 nA peak. Despite being determined by established methods, this limit is clearly unrealistic. A 0.1 nA peak approximately equals the common level of noise in an unsmoothed scan working in optimum conditions and it is much lower than the common baseline of 2-4 nA. Visual inspection of plot 6 in [80] clearly shows that a 0.1 nA peak would be hard to resolve. In our case, after acidification and alkalinization to a pH in the range 8.5-8.7, sensitivities were in the range 25-35 nA nM^{-1} min^{-1} which is a major improvement (~ 4 fold) at no cost of baseline or noise enhancement. Repeated analysis of the same sample gave a LOD in seawater of 0.005 nM Fe (n = 5; iron concentration 0.098 nM; pH = 8.8, 90 s deposition time). For instance, the limit of quantification of 0.018 nM (10x standard deviation, 90 s deposition time), would translate in a peak of 0.45 nA height or 0.073 nW area. Moreover, the limit of detection (LOD) and the limit of quantification (LOQ) could be improved increasing the bromate concentration although at the cost of increasing the blank level.

The precision of the method, calculated from the average of the relative percentage standard deviations of duplicate samples (filtered and unfiltered) analyzed during a Southern Ocean cruise across the concentration range 0.06 - 2.45 nM Fe (n=148) was 13%.

2.2.2 Analysis of samples with consensus values

The performance of the analytical method was assessed by analysis of Nearshore seawater Reference Material for trace metals (CASS-5, National Research Council, Canada) and of three of the seawater samples with consensus value produced in the framework of the SAFe (Sampling and Analysis of Fe) program [91] and

GEOTRACES programs (updated consensus values in: http://es.ucsc.edu/~kbruland/GeotracesSaFe/kwbGeotracesSaFe.html).

For convenience, the nearshore seawater was diluted 5 times with ultrapure water previously acidified to pH 2.0. Reference values and the result of our analyses with DHN/BrO_3^- at pH 8.7 are shown in Table 2.2. In all cases, the values obtained were in excellent agreement with the target concentrations.

Table 2.2 – Results of the cathodic stripping voltammetry (CSV) analysis with DHN/BrO_3^- at pH=8.7 of Reference Material (RM).

RM	Fe declared (nM)	$Fe_{CSV\text{-}DHN}$ (nM)	n
SAFe-S	0.097 ± 0.043	0.12 ± 0.04	5
SAFe-D2	0.91 ± 0.17	1.00 ± 0.02	3
GEOTRACES-S	0.52 ± 0.07	0.47 ± 0.07	2
CASS-5*	25.8 ± 2.0	27.2 ± 0.8	3

*after 5 fold dilution in acidified ultrapure water

2.2.3 Comparison of the CSV-DHN method with FIA-CL analysis

In order to further validate the method, an inter-calibration against the most used method for onboard analysis, chemiluminescence after FIA, was also carried out. During a Southern Ocean cruise, seawater was sampled in the water column down to 300 m at the same location in the time span of three weeks. The oceanographic, meteorological and biological conditions in that spot remained stable and big changes in total dissolved iron were not expected. Dissolved iron profiles obtained by both methods are shown in Figure 2.10.

Despite a few minor discrepancies, there is a good agreement between methods. All common features could be observed in both sets of results: nearly constant concentrations in the mixing layer (range 0.07-0.15 nM, down to 100-120 m) with slightly lower values in the range 60-100 m and a significant constant increase with depth at depths >100m.

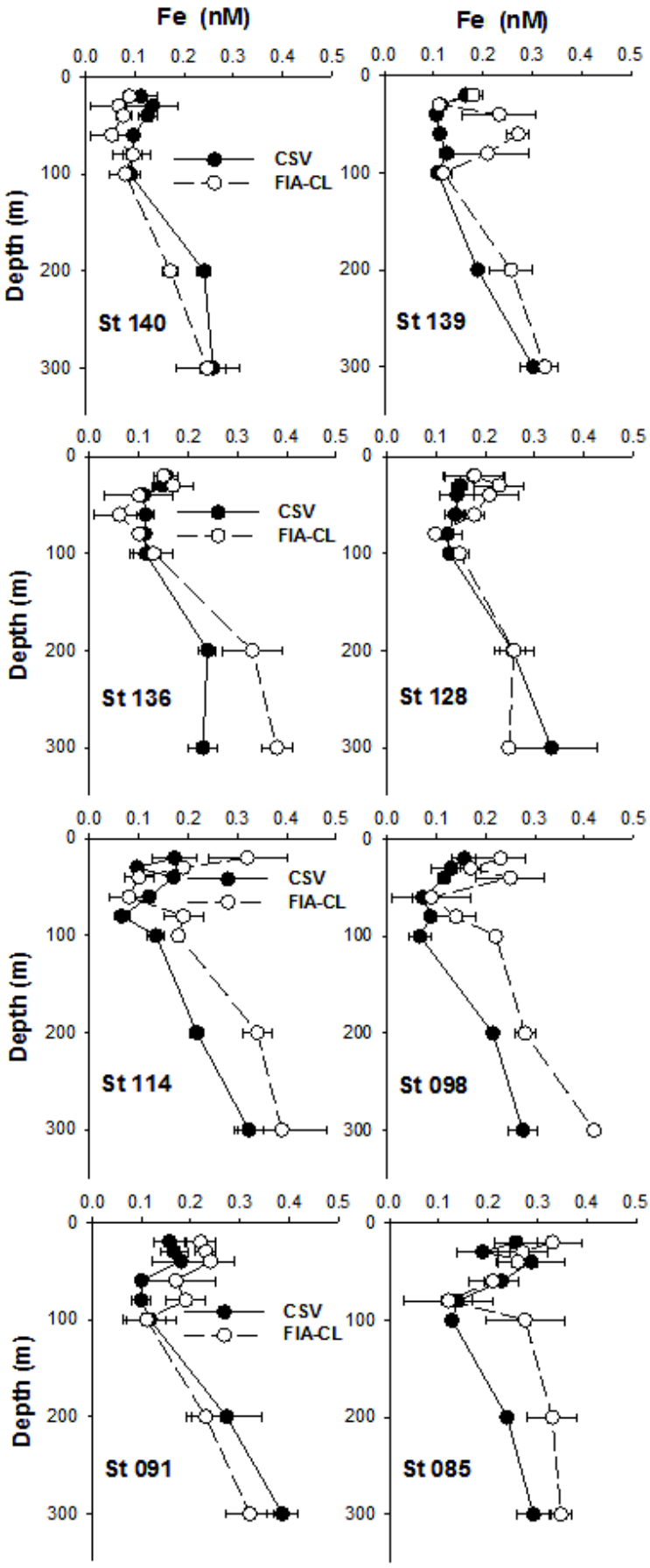

Figure 2.10 – Determination of the concentration of Fe-DHN by CSV and FIA-CL in filtered seawater samples collected during the EDDY PUMP cruise in waters of the Southern Ocean.

2.3 Mechanism Elucidation

The great increase in method performances as a function of pH noted during the optimization process led to additional experiments aimed at a better understanding of the reaction mechanism during the voltammetric scans. The hypothesized mechanism is reported in Figure 2.11.

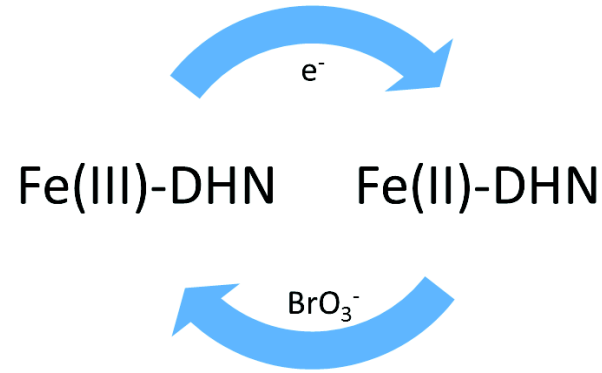

Figure 2.11 – General mechanism of the catalytic process. The complex Fe(III)-DHN is reduced at the electrode surface by electron transfer in the first step. The formed Fe(II) complex is back oxidized by the dissolved potassium bromate.

Several tests were performed trying to understand the effect of each experimental parameter. The almost direct proportionality between sensitivity and pH was tested reversing the experiment, i.e. by acidifying samples brought to alkaline pH (see also Figure 2.1 for the alkalinization experiment) . The experiment was repeated for ultrapure water and seawater plus POPSO buffer, but initially brought the pH close to 9 followed by acidification via HCl additions. The sensitivities obtained (Figure 2.12) followed a completely different pattern from the one reported in Figure 2.1.

For seawater, the sensitivity increased slightly from 25 to again 30 nA nM^{-1} min^{-1} at pH 8.4 remaining constant down to pH 7.7 where it started to grow exponentially. However, at pH < 7.8 the V-DHN peak is so massive that the Fe-DHN peak becomes a poorly defined shoulder of no analytical value. For ultrapure water, the sensitivity plot took a domed shape with a maximum value of ~ 10 nA nM^{-1} min^{-1} in the pH range 7.7-8.4. In this case, two final NH_4OH additions showed that now the system became reversible to pH changes and at pH 8.0 and 8.4 the sensitivity came back to that obtained during the acidification (see arrows in Figure 2.12). It is plausible, analyzing the Figure 2.1, that a non-reversible transformation of the DHN/BrO_3^- system takes place at high pH in a time scale of minutes. To study the specific effect of NH_4OH we

repeated the experiment in seawater replacing it with NaOH in all solutions. Figure 2.12 shows that in the pH range of analytical interest (8.4- 9.0) the absence of NH_4OH did not lead to any significant difference. However, the exponential rise of sensitivity found at pH < 8.0 seemed to be related to the presence of NH_4OH in solution.

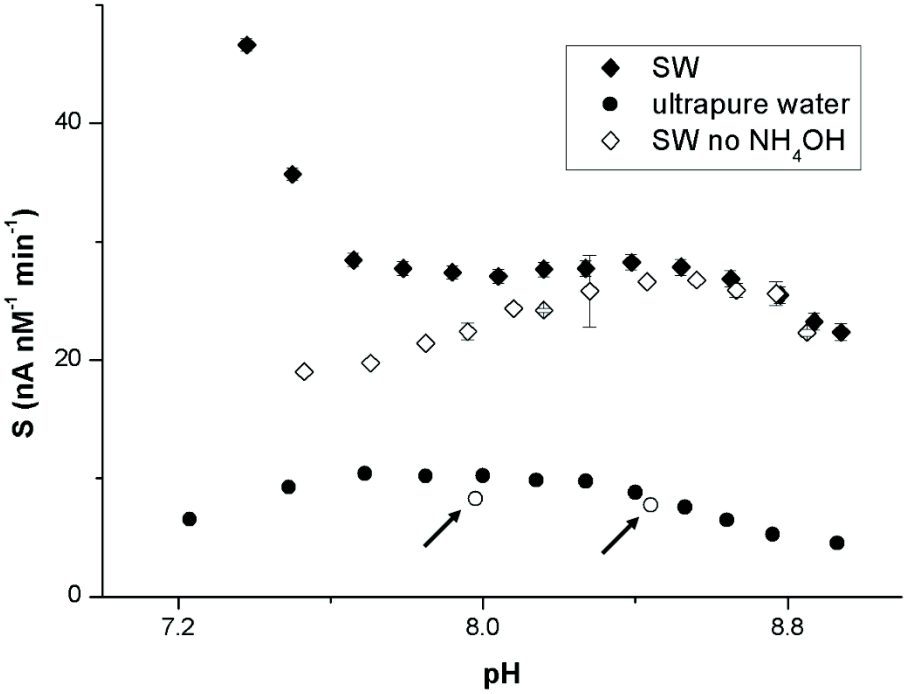

Figure 2.12 – Sensitivity dependence experiments. All solutions: 20 mM bromate, 5 mM POPSO and 30 µM DHN

Several possible mechanisms leading to an irreversible transformation of the involved chemical species were investigated. Ammonia could be oxidized to hydroxylamine and/or brominated amines (NH_2Br and $NHBr_2$) by the action of bromate ions which are strong oxidizing (E^0 = + 1.5 V) and possible brominating agents. Hydroxylamine was recently shown to be a good catalytic reagent to enhance sensitivity during the CSV cobalt determination [100]. However, the formation of these oxidation products can be discarded as none of them could be detected in UV digested seawater by UV-vis spectrophotometry at pH 8 and 9 (see [101] for the UV-vis spectra of these species).

Dihydroxynaphthalene is also known to be prone to oxidation in alkaline solutions [102]. This mechanism is known for a similar system, the vanadium/catechol/BrO_3^- CSV method [103], where an irreversible oxidation

involving the binding ligand prior to its use for catalytic CSV has been described. However, in that case, catechol was mixed with BrO_3^- and heated prior to the analysis to force its oxidation to 1,2-benzoquinone. One may speculate that this oxidation takes place at different rates depending on the solution pH, thus accounting for the different sensitivity via a change in the ligand structure.UV-Vis experiments were carried out to understand if the pH has a role in this process and, accordingly, the sensitivity changes were related to the oxidation of the ligand.

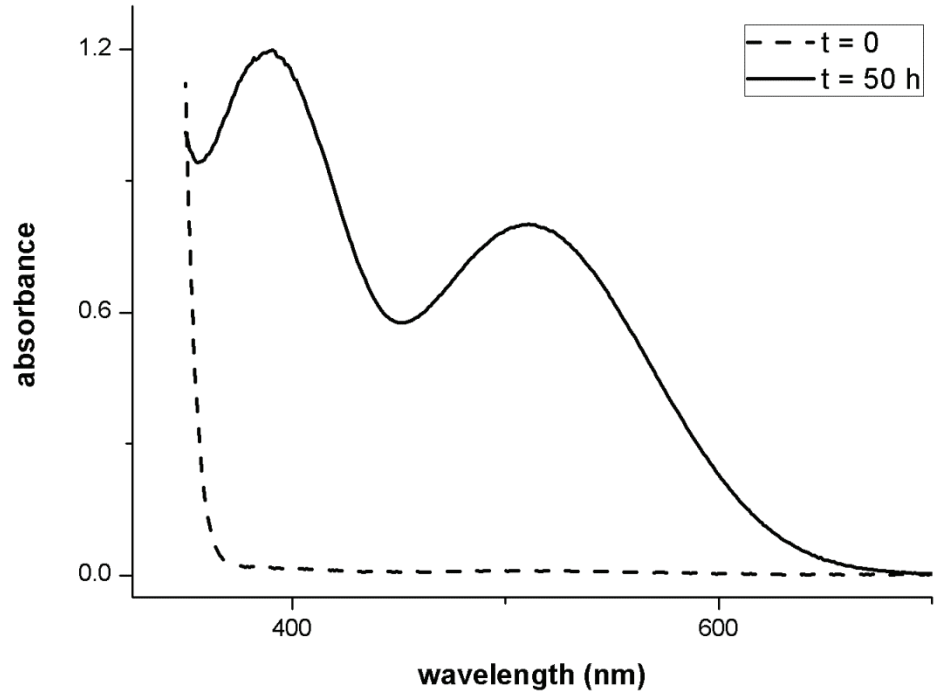

Figure 2.13 – UV-Vis spectrophotometry of ultrapure water in the presence of DHN (50 µM) and HEPPS buffer (10 mM) after different equilibrium periods at room temperatures

Figure 2.13 show the visible portion of the UV-Vis spectra of a 1 mM solution of DHN at pH 9 at time zero and 50 hours, clearly showing that dihydroxynaphthalene undergoes oxidation in the presence of oxygen at alkaline pH [102]. Nevertheless, setting the pH to 8 was also able to induce its oxidation: a different reaction rate, i.e. a faster oxidation at higher pH values, could explain the different behavior at the two pH values. Kinetic measurements of DHN oxidation showed that the reaction rate is similar for the two pH values, as showed in Figure 2.14. The kinetics is first order (or pseudo first order as the role of oxygen was not investigated) and the two kinetic constants are

$1.15 \cdot 10^{-5} \pm 2.1 \cdot 10^{-7}$ and $1.04 \cdot 10^{-5} \pm 2.6 \cdot 10^{-7}$ sec^{-1} for pH 8 and pH 9 respectively, evidencing no significant difference.

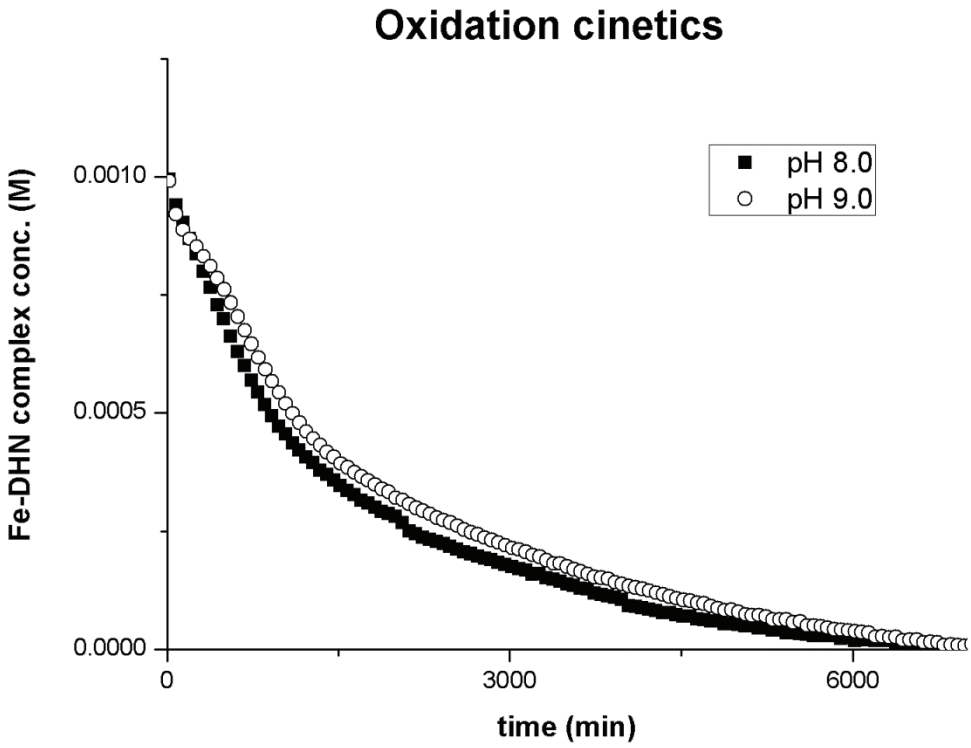

Figure 2.14 – UV-Vis kinetic measurements of ultrapure water in the presence of DHN (1 mM) and HEPPS buffer (10 mM) at two different pH.

In conclusion, DHN oxidation does not appear as a significant explanation for the difference in sensitivity found in the previous experiments.

The complex stoichiometry at this point could be another aspect worthy of attention: the formation of complexes with different stoichiometry at different pH (reasonably, with ratio 2:1 or 3:1 between DHN and iron) could again explain the difference in sensitivity. The Job's method, also known as continuous variations method, was applied to get this information [104]: solutions containing different ratios of iron and DHN (between 0.1 and 4, depending on the pH) were prepared keeping the sum of metal and ligand concentrations constant and their UV-vis spectra registered. The absorbance values reported were taken in correspondence of the maximum and the results are reported below in Figure 2.15.

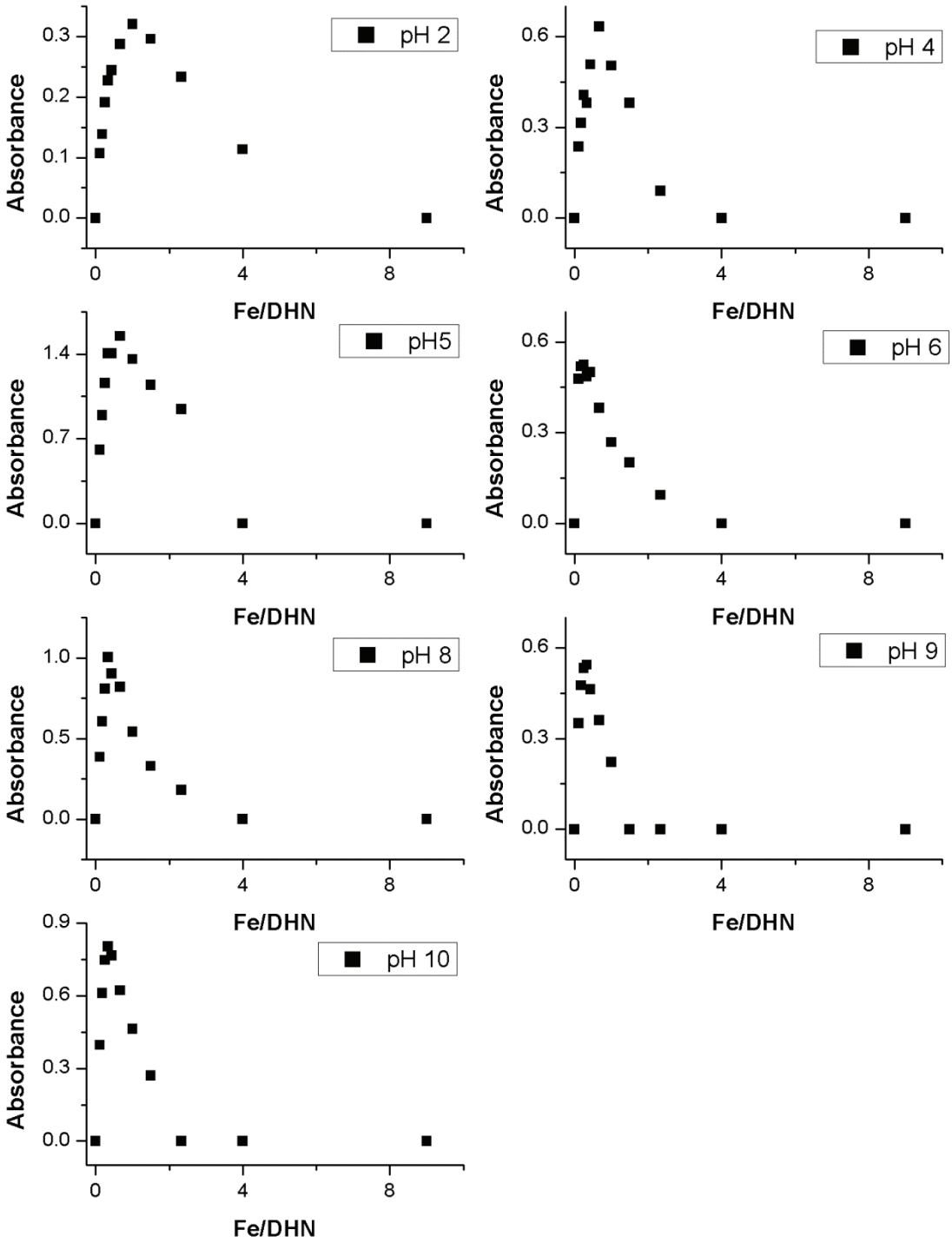

Figure 2.15 – Job's method graphs at different pH. The iron and DHN concentrations sum is constant and it is equal to 1 mM. λ_{max} changes as a function of pH, they are respectively 595, 554, 530, 523. 509, 460, and 453 nm from pH 2 to pH 10.

The stoichiometry ratio of the complex responsible for the UV-Vis absorption corresponds to the intersection of the two straight lines formed by the A vs ratio data (or, in a simplified procedure, to the point of maximum absorbance). As it is showed in the graphs above the stoichiometry ratio is constant in the pH range 8-10 and it is equal to 1:3 (Fe-DHN). The stoichiometry at pH 6 is complicated by the difficulty in

determining the absorbance at low Fe/DHN ratios, whereas the ratio moves to 1:2 Fe:DHN at pH 4 and 5. Finally, at pH 2 an equimolar, 1:1, iron DHN complex is formed.. These data clearly show that changing the pH from 8 to 9 does not lead to the formation of complexes with different Fe/DHN ratio. The acidification/alkalinization process could be responsible for changes in the prevailing species, given the observed difference in stoichiometry between alkaline and acidic pH values. The concentration ratios between iron and DHN are much lower in the Job method with respect to the ones used during real analyses, being the Fe/DHN ratio at least 1:1000 during the latter. On the other hand it is not possible to carry out these experiments with the real Fe-DHN ratio because of the limited solubility of DHN and the sensitivity of the UV-Vis measurements. Nevertheless, the high excess of DHN is expected to cause the formation of the $Fe(DHN)_3$ complex, as higher stoichiometries may be difficultly possible. Accordingly, the great DHN excess would trigger the formation of the 1:3 complex at lower pH, not undermining the conclusion that iron and dihydroxynaphthalene form a 1:3 complex in the pH range 8-9.

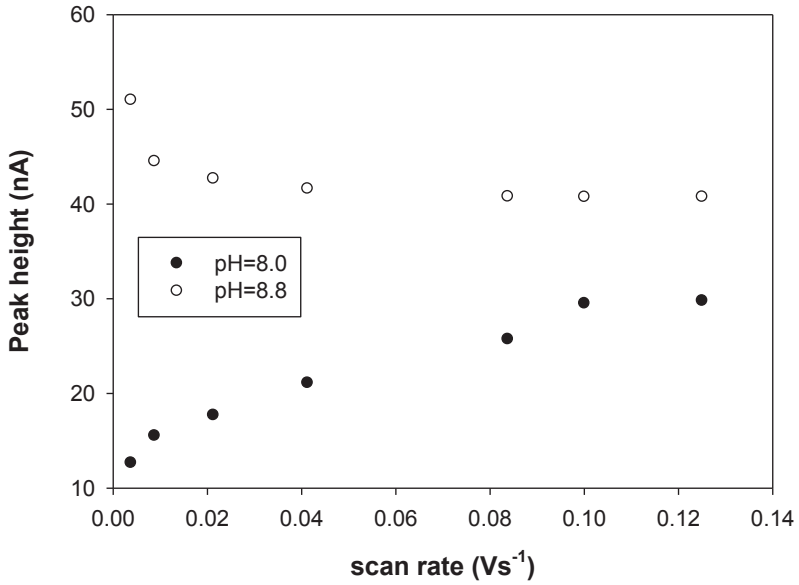

Figure 2.16 – Effect of the scan rate on the peak height of Fe-DHN complexes in seawater (30 µM DHN, 20 mM BrO_3^- and 5 mM POPSO buffer) at pH=8.0 (full circles) and at pH=8.8 (open circles).

Understanding the intimate chemical mechanism involved revealed itself as a difficult task, we could not find the species involved that would explain the irreversible behavior with respect to pH changes and the differences found in between ultrapure water and seawater that cannot be ascribed to the presence of NaCl (Figure 2.1). Changes in the nature of the reaction with pH could also be inferred from the

dependence of the Fe-DHN peak height on scan rate. For that purpose, the effect of the scan rate in UV digested seawater in the presence of DHN and BrO_3^- was studied before and after shifting its pH from 8.0 to 8.8. Figure 2.16 shows that at pH 8.0 the sensitivity followed the expected increase in a less than linear fashion with respect to the scan rate observed before by Obata and van den Berg. This is caused by the limited diffusion of the catalytic reagent on the time scale of the stripping when the scan rate increases [105].

However, at pH 8.8 the trend is opposite with a decrease up to a rate of 40 mV s^{-1} where the Fe-DHN signal reaches a plateau. This is characteristic of surface catalytic systems where the relative weight of the catalytic reaction is strongly accentuated with respect to the kinetics of the redox reaction [106]. Incidentally, Figure 2.16 shows that slower scan rates could slightly improve the sensitivity, but would increase the stripping period to the order of minutes. This would damage the reproducibility during onboard analysis beside increasing excessively the analysis time: a scan rate of 50 mV s^{-1} was selected.

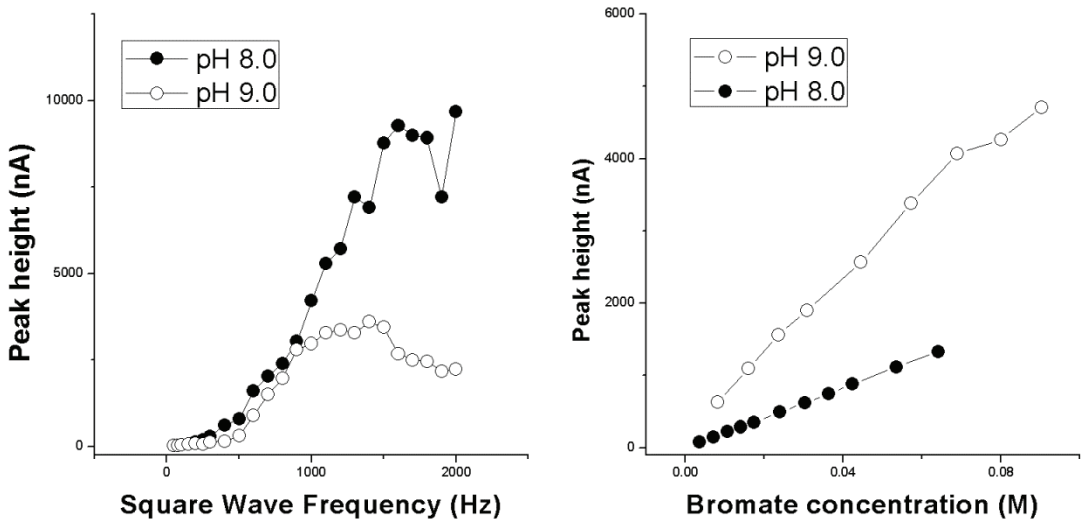

Figure 2.17 – A: Effect of the square wave frequency on the peak height of UV digested seawater sample in the presence of 30 µM DHN in the absence of bromate at pH 8 and 9. B: Effect of increasing bromate concentrations on the analytical signal of UV digested seawater sample in the presence of 30 µM DHN. Square wave frequency: 100 Hz.

In order to give a more accurate picture of the process involved, we started by investigating the kinetics of the redox surface reaction and of the catalytic reaction using square wave voltammetry [106, 107]. The current signals in the absence of bromate at different square wave frequencies (see Figure 2.17 A) clearly showed that

the kinetics of the redox surface reaction were slower at pH 9 than pH 8 in agreement with [80], where a decrease in sensitivity at pH >8 was observed in the absence of bromate. This is against the important increase of sensitivity observed at higher pH. Nevertheless, investigating the kinetics of the catalytic mechanism increasing bromate concentration at constant square wave frequency showed that the slope of the signal vs. BrO_3^- concentration is higher at pH 9 (Figure 2.17 B), ratio between slopes around 3). This is a clear indication that the catalytic mechanism is much more efficient at higher pH.

Summarizing it is clear that an increasing of the operational pH lead to an improvement of the performance mainly due to a higher sensitivity. Regarding the mechanism responsible for such increased performance, no changes in the ligand due to oxidation and of the Fe-DHN complex stoichiometry were evident when changing the pH from 8 to 9. On the other hand, the catalytic mechanism, i.e. the electron transfer from the iron complex to bromate, became much more efficient at higher pH, thus explaining the raise in sensitivity. The description of the mechanism responsible for the sensitivity raise was achieved, although a deeper explanation for such behavior is still missing.

3 Miniaturization of the Voltammetric Cell

Standard procedures in ultra-trace analysis make use of 10 mL aliquots for quantification, whereas the CLE – CSV speciation protocol requires no less than 120 mL, strongly limiting the application of these procedures. Actually, at least 12 sample aliquots with increasing metal additions have to be analyzed for the CLE–CSV procedure. Accordingly, reducing sample size would assure the extension to limitedly available specimens, concurrently reducing reagent consumption and possibly analysis time, as is usually true for other analytical methods (e.g. micro and nano HPLC [108]). Sample size reduction in voltammetry has mostly been achieved by miniaturization and the development of dedicated electrodes (see [109] for a review of pre-1997 papers). Microfluidic devices featuring solid state microelectrodes have been developed in the last two decades, with dramatic reduction in sample requirements [110-112]. However, application at the trace and ultra-trace level in environmental samples is presently limited to 10, rarely 5, milliliter samples.

The aim of this project was to introduce a simple sample holder enabling the reliable determination of total concentration and speciation of metals at the ultra-trace level in a small sample volume. A new procedure operating with small volume sample could include many advantages beside the sample volume requirements. Two definitive advantages are the decreasing waste generation and increasing sample throughput by reducing the purge time. Each of these points are listed in the twelve principles of the Green Analytical Chemistry (GAC) [113]. Naturally, it was necessary to achieve these results with a minimum replacement of commercial hardware in order to adapt the new system to the existing instrumentation.

The new cell was applied to both freshwater and seawater environments to determine total concentrations and to perform speciation analysis of trace elements: comparison with reference materials or standard procedures, led to a successful validation of the proposed apparatus.

3.1 New Cell Development

The initial aim of this project was to develop a new instrumental hardware able to work with a 1 mL sample size. This conspicuous reduction of the volume needed for each analysis could generate various advantages in the prospective of the green analytical chemistry (GAC), as discussed in Conclusion section (Chapter 6).

Figure 3.1 depicts the standard configuration of the voltammetric system where a 10 mL sample was transferred into the standard glass cell. The system, also using the standard cell, looks crowded (Figure 3.1). In fact, five different probes need to fit in a very small space, three of which are electrodes: working electrode, reference electrode and counter electrode. An additional two pieces are also included: the stirrer and the degassing tube. Clearly, it is understandable that fitting all of these probes in a ten time smaller volume was a big challenge.

Figure 3.1 – Photo of standard configuration of the voltammetric system (Metrohm 757 VA)

Moreover, it was decided to apply as few changes as possible to the standard three electrodes configuration in order to achieve a versatile hardware capable of on-site operation and still compatible with standard instrumentation. Several prototypes were realized before the final, optimal configuration was achieved. The step-by-step development of the new cell is reported in the next paragraph (3.1.1).

3.1.1 Cell prototypes timeline

The initial idea was to build a completely new cell system. In collaboration with the University workshop, it was decided to use plastic material on the way to simplify and speed up the manufacturing of the prototypes besides ensuring minimum contamination. The first attempt involved the lathing of two different pieces: a black support (made in Delrin, see Figure 3.6) and a bottom part, the actual sample cell made in polystyrene (Figure 3.2), able to slide in the black support and be positioned at the desired height. A T-shaped hole was realized in the polystyrene piece (Figure 3.2) in order to limit the required sample volume while accommodating the three electrodes, the stirrer and the purge tubing (see also Figure 3.1).

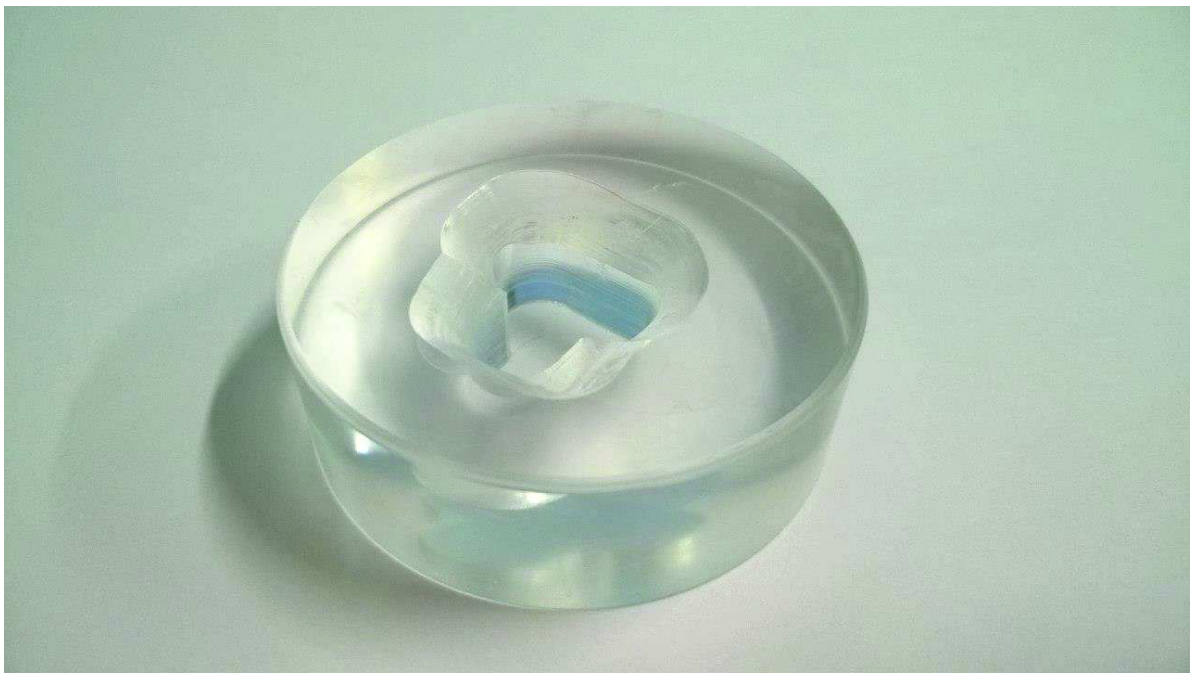

Figure 3.2 – Bottom part of the first prototype photo. This portion was realized in polystyrene.

The idea, in fact, was to fit the three system electrodes in the upper part of the T-shape and the stirrer in the bottom and narrower part. The technical drawing with the quotes is reported in Figure 3.3.

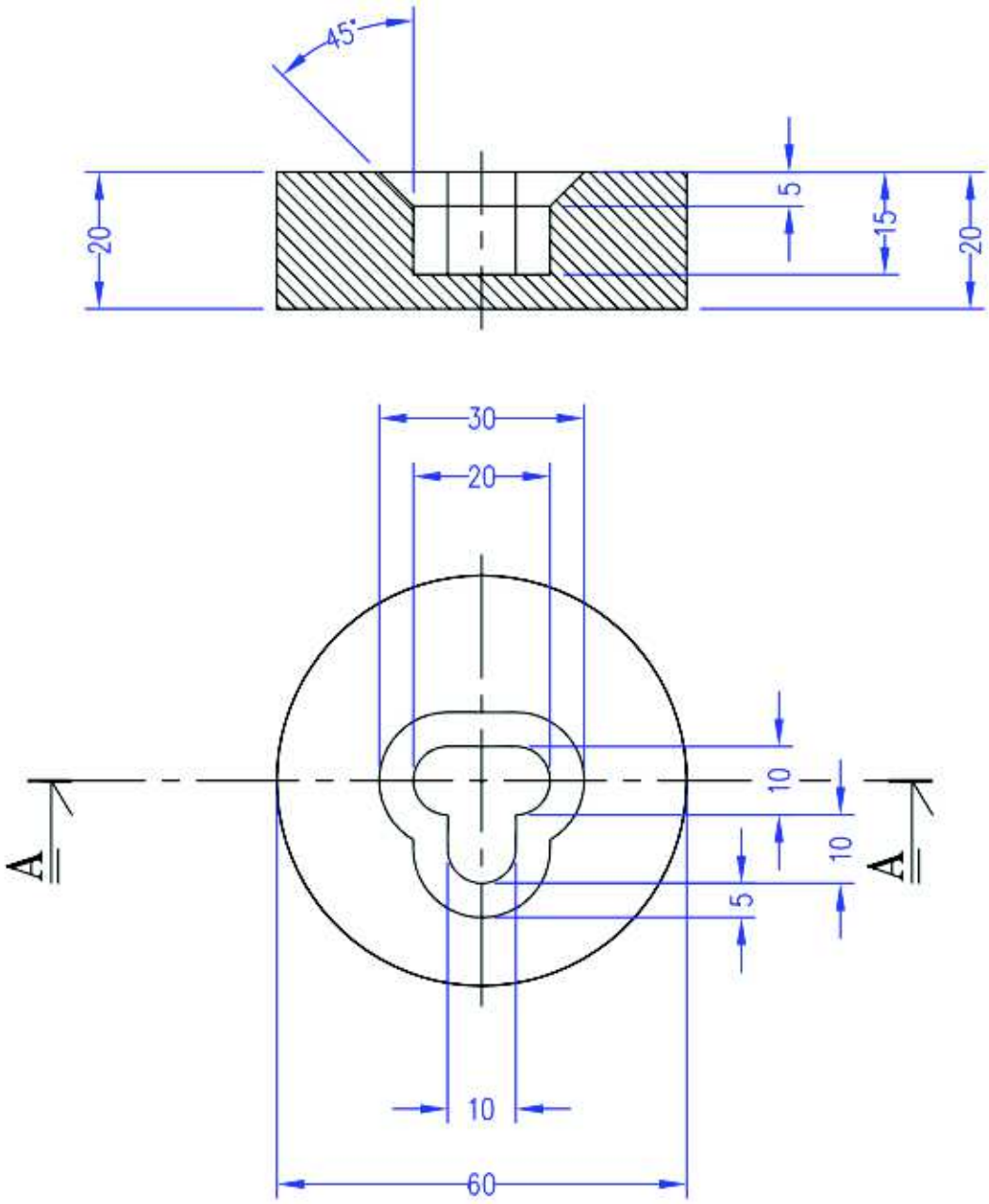

Figure 3.3 – Technical drawing of the bottom part made in polystyrene with quotes.

Unfortunately, the tests did not lead to good results. The two-piece system proved to be consistent concerning height regulations, but was completely unreliable during the sample preparation and the sample change steps. In addition, the T-shaped hole guaranteed the use of a small volume but the precise housing of the three

electrode and especially the stirrer revealed a major issue, with the latter occasionally hitting the cell walls.

The standard stirrer with its diameter of about 7 mm was a big obstruction in such a small environment. The solution of this problem was to build a new stirrer (Figure 3.4), with a small final diameter, able to fit in the new cell and assure adequate stirring to the system.

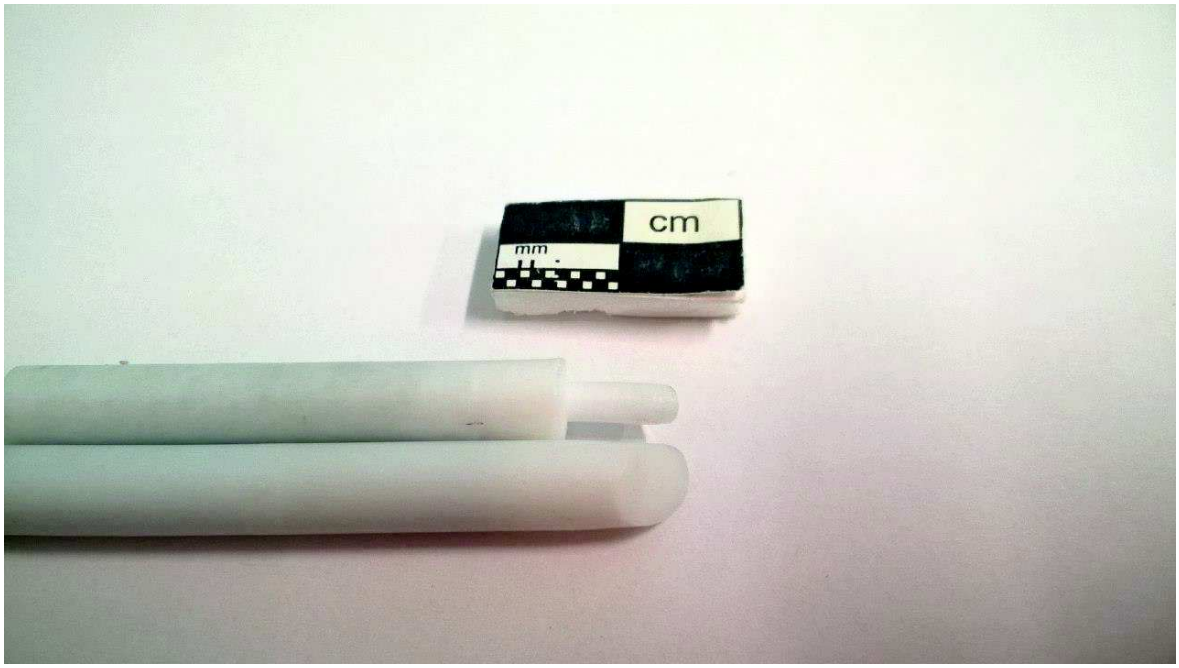

Figure 3.4 – Comparison between the standard stirrer and the modified one. The final part of the modified stirrer was reduced in diameter to fit better in the new smaller system.

This part of the project was without a doubt one of the most difficult during the workshop realization. It is possible to have an idea of the complexity around this small piece by reviewing the technical drawing (Figure 3.5). The modified stirrer is shown in two separate sections. The internal part, in Derlin, guarantees the connection with the instrumentation through a screw. The external part, made in PTFE, acts like the real stirrer, it ends with a very small diameter in order to take as little space as possible in the new cell.

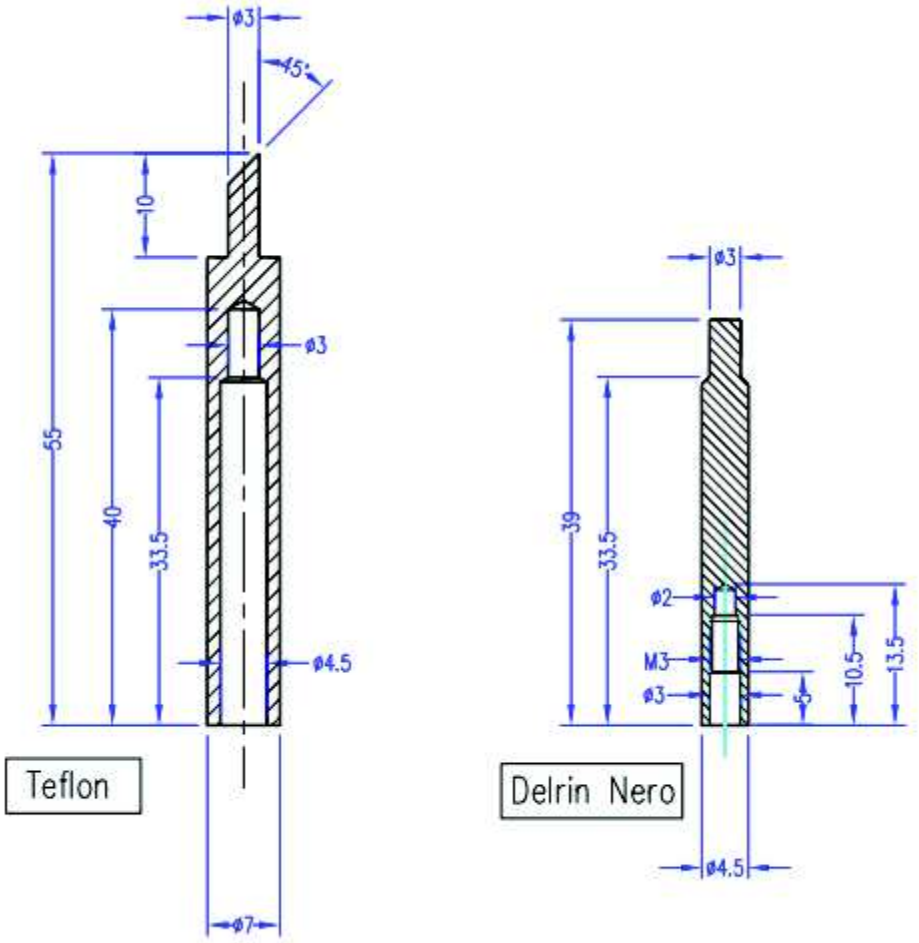

Figure 3.5 – Technical drawing of the new stirrer. It is formed by two different parts: the external made in PTFE and the internal made in Derlin (connection with the head instrumentation).

The new stirrer with a 3 mm diameter was able to fit in the polystyrene cell but because of the cell shape it was not able to give a consistent and homogeneous agitation. After this evidence, it was clear that the round shape was the only one suitable for the new cell.

All the information gained with the first prototype was valuable during the design of the new model. The new hardware was formed by three different pieces (Figure 3.6): the same black support (made in Derlin), a bottom part (made in polystyrene) and lastly the round cell (made in polytetrafluoroethylene). In this prototypal version, an O-ring was placed around the bottom part for two reasons: guarantee the air tight seal of the system and facilitate the movements.

Figure 3.6 – Photo of the second prototype. The black support was unchanged, the bottom part is formed by two pieces now: a support in polystyrene and the actual cell in PTFE.

The idea behind the development of a cylindrical cell was to decrease the depth of the cell itself, which in turn required additional adjustments regarding the electrodes. In fact, in the normal, 10 mL sample configuration, every electrode is set at a different height, which is not an issue due to the large sample volume employed. The three electrodes were accordingly set at the same height by placing PTFE tape around the upper part of the electrodes where they enter the head of the voltammetric stand. The performances of this new system improved drastically over the previous ones and therefore additional tests were performed to validate whether or not the prototype could be a viable candidate to work as a small volume cell.

The Cd and Pb ASV analysis was used as a benchmark of the performance. The first tests with this new cell were not encouraging. The signals were not stable and showed a decreasing trend with time. The PTFE could be the possible cause of this trend and also of the instability of the signals. This material shows chemical inertness, but it also includes negative characteristics such as porosity and apolarity. The apolarity of the PTFE permits adhesions phenomena (adsorption) on the cell walls, which can cause signal instability, especially for real samples. Alongside, the porosity could be the reason for the decreasing trend; metal ions can penetrate in the bulk of the cell because of the gradient concentration. PTFE cells are currently used for voltammetry analysis but they require an equilibration period prior the use, and that treatment is needed every time the analyte changes.

All these reasons supported the decision to change the cell material, even if it was not the only problem noticed during the tests with this first prototype. Additionally, the black support does not allow visibility inside of the cell during analysis. Often, lack of visibility is a problem as all of the electrodes need to be dipped into solution and the operator should be given the choice to visually check in case of trouble.

Actually, the second prototype was, without a doubt, a starting point in order to perform analysis with 1 mL of sample size. It is also true that many problems needed to be fixed, the most important of which are schematized in Figure 3.7.

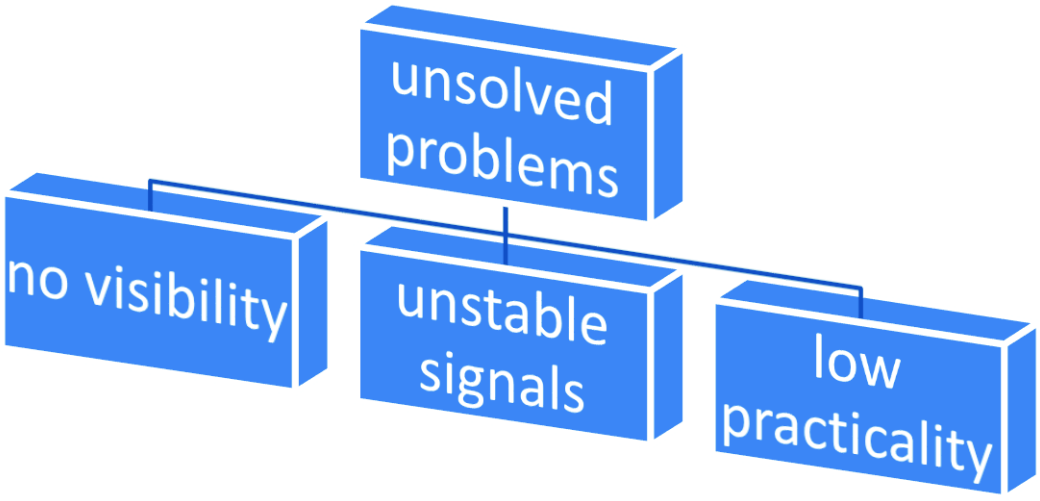

Figure 3.7 – Scheme of unsolved problem related to the second prototype.

The criticisms of the second attempt are summarized in the above scheme: the ideas and solutions that lead to devising a new cell solving these issues are presented in the following sections.

As aforementioned, the cause of the instability of the signal was the cell material (PTFE). Few materials are available when considering voltammetric cells and they are typically produced with plastic material (PTFE, LDPE, HDPE, etc.), glass or quartz. The plastic materials were discarded after the attempt with PTFE, and the choice was limited to glass and quartz. Both materials have a common problem, being much more

difficult to be shaped than polymeric materials. Quartz was chosen to ensure minimum memory effects and contamination: a cell with 20 mm of internal diameter; 6 mm height and 2 mm of wall thickness was blown and subsequently lathed starting from a 20 mm internal diameter quartz tube. The cell dimensions were set after a careful measurement of the three electrodes system and subsequently blown and lathed by a master glassmaker. The quartz cell id depicted in Figure 3.8 together with the first prototype in PTFE for comparison. The quartz cell presents a small handle in order to make the system more user-friendly.

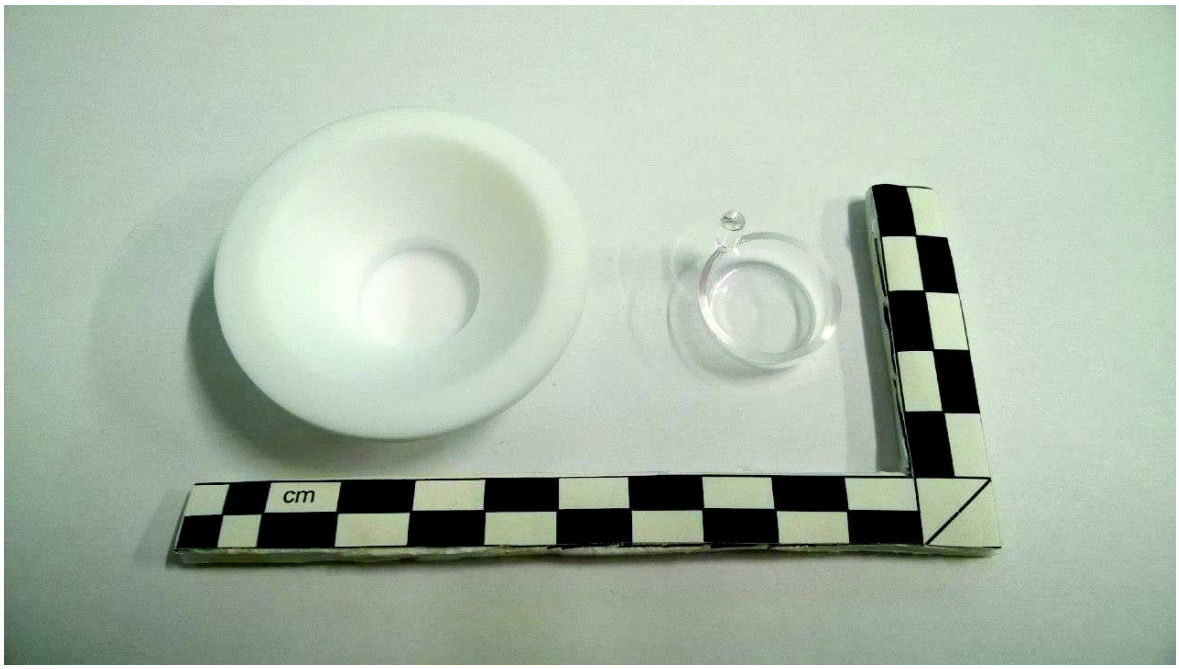

Figure 3.8 – Comparison between the cell made in PTFE and the new cell made in quarts.

Once the cell material issue was resolved, the focus turned to the absence of visibility. The most logical decision was to adopt a standard glass cell as a support. The use of the standard cell gives an airtight system and simplifies the accessibility of the new hardware. Obviously using the glass cell is not enough, the new quartz cell needs a lodging to be placed. This stand must guarantee stability and the right position.

An internal stand was projected with the help of the University workshop. This new piece, in Figure 3.9, was conceived to be placed in the bottom of the glass cell keeping the quartz cell at the correct height to warrant the dipping of the electrodes. This piece was lathed from PTFE in agreement with the workshop technician (Mr. Sergio Grigioni) being an easy to work with material.

Figure 3.9 – Photo of a PTFE cell stand and quarts cell. The stand was necessary in order to use the standard glass cell available from Metrohm.

The photo of the new prototype as described above (Figure 3.10), shows that the visibility is optimal and comparable with the classic cell that acts like the support. The PTFE stand fits perfectly in the bottom of the glass cell and gives stability to the quartz cell and practicality to the entire system.

Figure 3.10 – Aspect of the new cell system using the new PTFE stand and the quarts cell.

This configuration lead to solve the criticisms that affected the first prototype (see Figure 3.7). The new prototype is easy to use and surprisingly it is able to work with a 500 µL sample, half of the set goal (1 mL). Cadmium and lead analysis by ASV

were used as benchmark to test this cell too. Figure 3.11 shows an example of the scans obtained under typical conditions employed in ASV (differential pulse conditions: pH 2, purging time 150 sec, dep. time 60 sec, dep pot. – 1.15 V, scan range from –0.15 to 0.05 V, pulse amplitude 50 mV, pulse time 0.04 sec, voltage step 6 mV, voltage step time 0.15 sec). Signals are stable and not affected by noise and replicated analyses are consistent. Taking into consideration the above, it was possible to deem this last prototype as a real and functioning voltammetric cell.

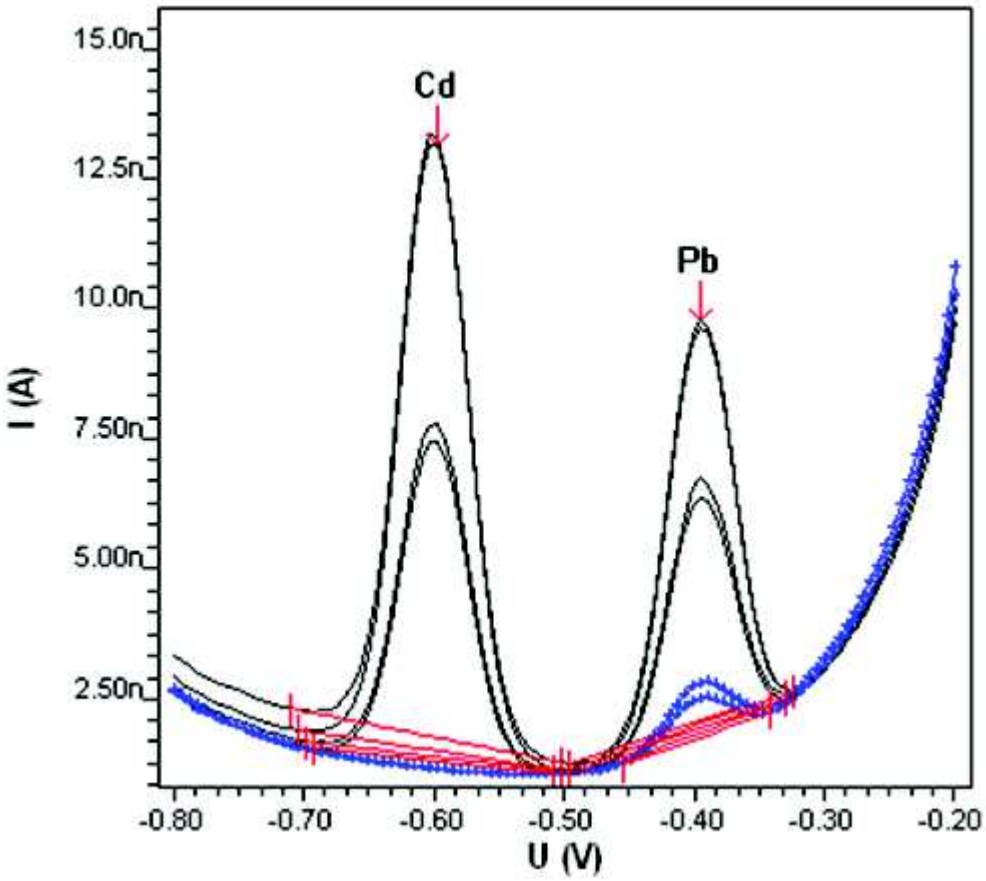

Figure 3.11 – Voltammetric scans for the determination of Cd and Pb using the new hardware configuration.

Figure 3.12 reports what the entire system looks like during the performance of a real analysis. Working electrode, reference electrode, counter electrode and modified stirrer all fit in a very small area with only 500 µL of sample volume. This tiny volume is translated into a low height of the liquid (around 2 mm) inside the cell, resulting in an elevated surface/volume ratio. This profitable ratio will be valuable during the parameter optimization, especially for the purge time, and most significantly during the optimization of the new method for the voltammetric determination of iron in the presence of atmospheric oxygen (Chapter 4).

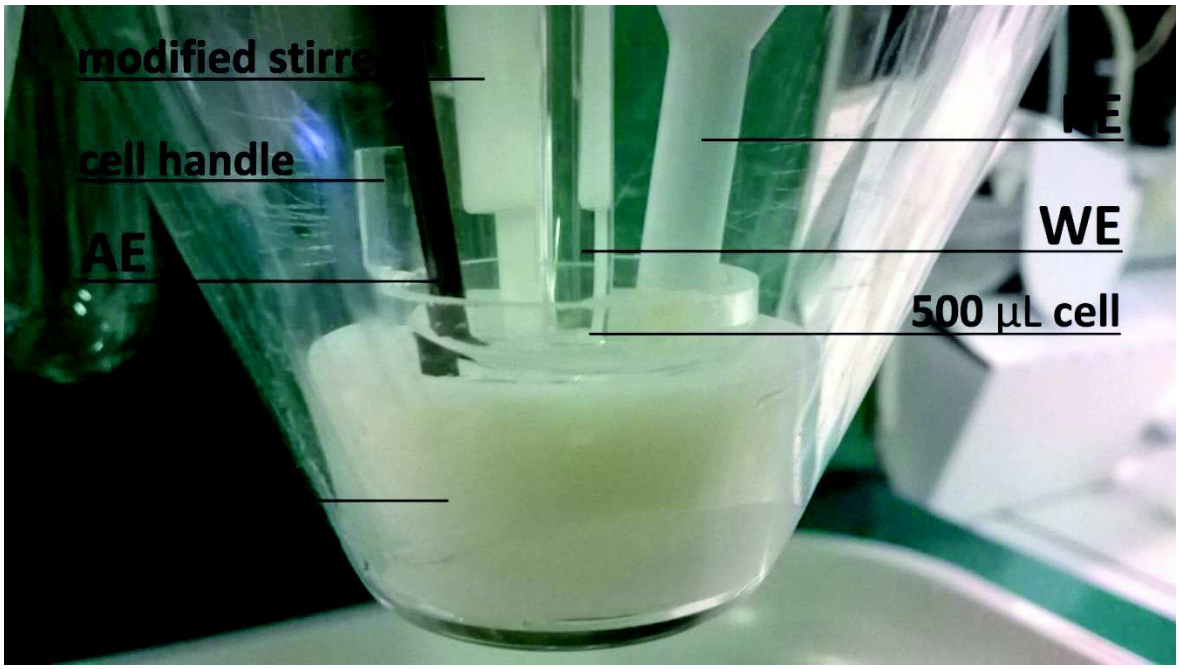

Figure 3.12 – Picture of the new hardware: the 500 µL cell, the modified stirrer and the polytetrafluoroethylene stand placed in the standard glass cell. Abbreviations: RE, reference electrode; WE, working electrode; AE, auxiliary electrode.

3.1.2 Procedure optimization

Once a consistent hardware configuration was achieved and promising results obtained, it was necessary to define a standard procedure for voltammetric analysis as the different sample size implies some changes in the operations. As a first point, the small volume hindered the usual degassing procedure, *i.e.* blowing nitrogen directly into the solution from a small diameter tubing. In fact when nitrogen was blown into the cell, splashing caused part of the sample to be ejected from the cell due to the gas pressure and the very small volume. For that reason the purging procedure was extremely simplified and nitrogen was introduced into the cell headspace. The possibility to purge the headspace only is due to the high aspect ratio of the sample volume, being the sample height and diameter 1.6 mm and 20 mm, respectively. This feature ensures a fast diffusion of the gases to and from the sample volume: actually, early experiments in which the purge time was systematically changed demonstrated that 150 seconds are enough to achieve a satisfactory baseline with negligible changes observed for longer purge time. A two-fold reduction in the purge time was accordingly achieved with respect to the normal 300 seconds required by the 10 mL sample. For copper determinations, an even lower 120 s purge time could be used: a slightly higher

baseline was registered although it did not interfered with the determinations. The reduction in purge time was an unexpected outcome of the sample volume reduction.

Another practical aspect that required a revision is the handling of the samples. Removing the sample from the small cell by pouring demonstrated an uneasy and unreliable procedure. Filling and removal of the sample were performed by a 100-1000 µL micropipette, ensuring a faster and more reliable procedure. Higher, random blanks were conversely obtained when the sample was poured out of the cell as usually done: actually, incomplete sample removal and/or contact of the specimen with the rims of the cell could lead to contamination.

3.2 Real Samples Analysis

3.2.1 Cu speciation in seawater

The apparatus was initially validated for the determination of total copper concentration by CSV using 25 µM of SA (see section 5.3.2 for experimental details) in a low level inter-laboratory standard (SAFe D1 [91]). Three batches of the SAFe D1 standard were analyzed for copper: 2.5 ± 0.73 (n=9), 2.6±0.49 (n=7) and 2.0±0.15 (n=3) nmol/kg were determined in 500 µL aliquots (mean ± standard deviation), with no significant difference from the consensus value of 2.27±0.11 nmol/kg. Detection capabilities were also similar to the ones found in previous papers for 10 mL samples: a limit of detection of 0.13 nM was determined for copper (deposition time 60 s) against a 0.1 nM reported in the paper presenting the salicylaldoxime method [114] (note that the latter refers to seawater, whereas the one determined here to ultrapure water).

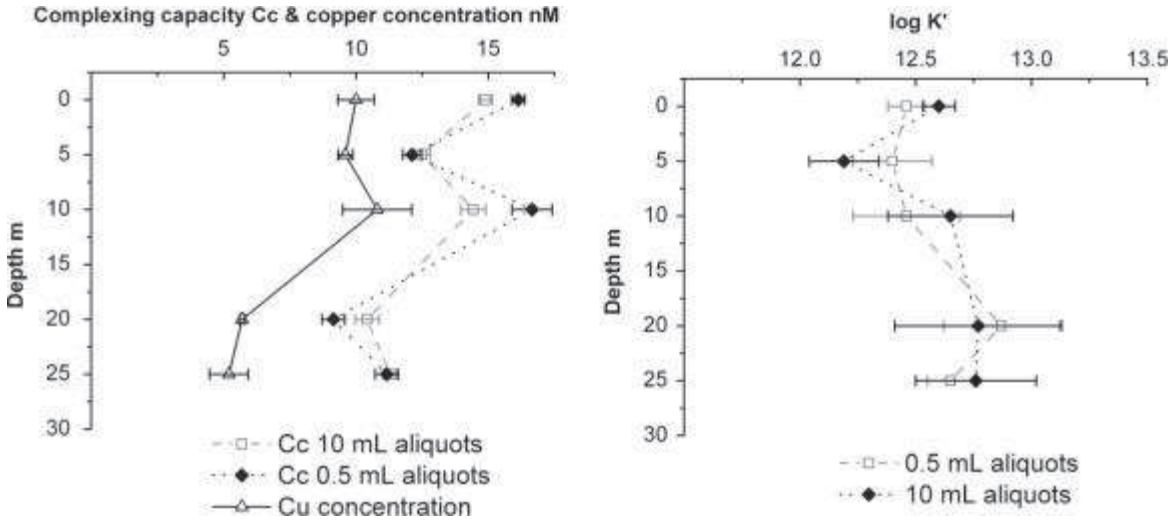

Figure 3.13 – Speciation analysis results: comparison between the proposed new method (0.5 mL aliquots) and the standard procedure (10 mL aliquots). Total copper concentration in the water column is also reported.

Speciation analysis was validated by comparison with the standard procedure involving 10 mL aliquots using seawater samples from a surface-bottom vertical profile at the deepest point of Mahon bay (Minorca, Balearic Islands, Spain). Results are reported in Figure 3.13 (see also Figure 3.14). Both ligand concentrations and conditional stability constants K' did not show statistically significant differences if the random errors associated to the procedure are taken into account [115] (see also

Figure 3.14). Relative percentage standard deviations on real samples are around 10% for ligand concentrations and 50% for conditional stability constants (approx ± 0.2 on the log unit scale), making the differences observed here easily accounted for by the uncertainty associated to the result, with the possible exception of the ligand concentration for the 20 m depth sample. Nevertheless, the latter showed the lowest concentration among the samples and literature data show that at low ligand concentration, less than 10 nM, a constant standard deviation around 0.8 nM must be expected [115]: it would be difficult to consider the difference observed in the data as significant. Neither was a significant difference evident in the precision of the results (compare error bars in Figure 3.13).

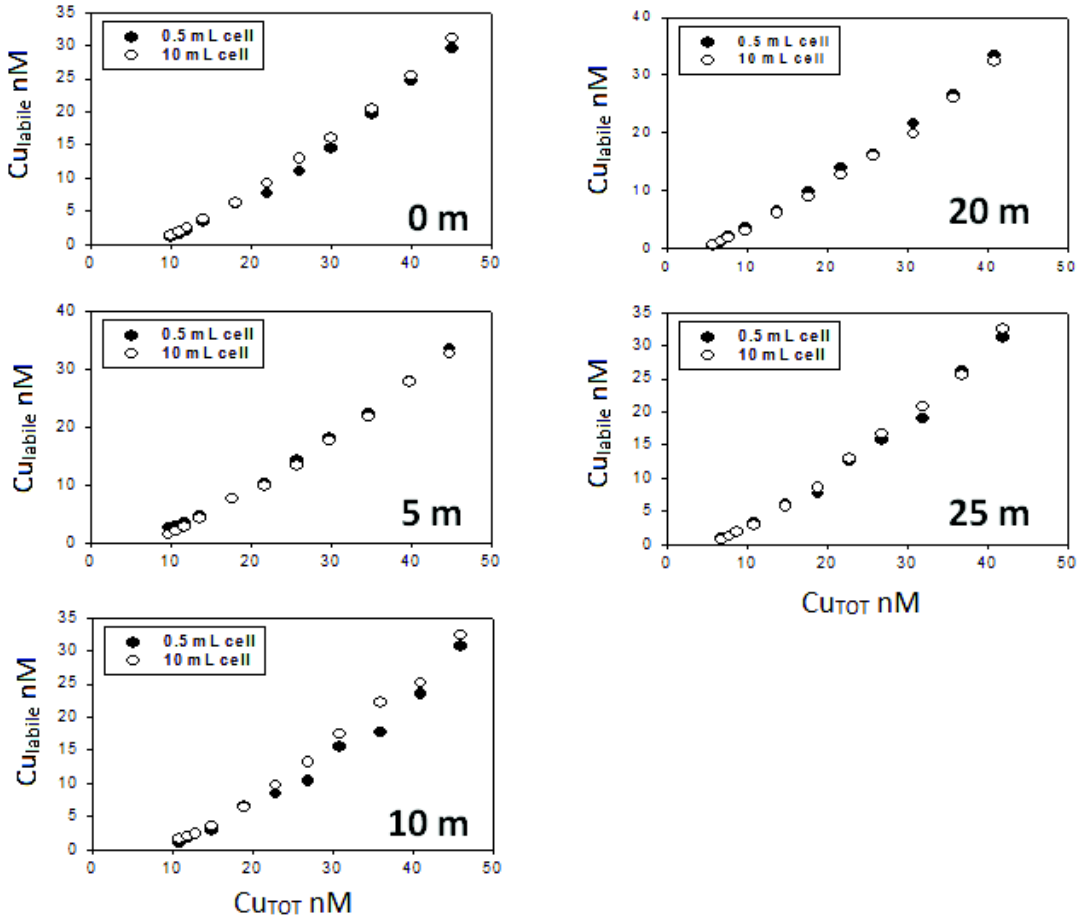

Figure 3.14 – Labile copper vs total copper for the tirtration of the five sample using 0.5 mL and 10 mL aliquots.

3.2.2 Rain samples total concentrations

The validation of the small cell for freshwater was performed on rainwater samples collected in Como, Italy: methods based on both anodic (Cd, Pb and Cu) and adsorptive (Ni and Co) stripping voltammetry were tested. Detection capabilities as measured by limits of detection (LODs) were determined and compared to figures obtained by some of us in a recent paper with a similar apparatus and a standard 10 mL cell (a VA stand 663 in this circumstance vs. a 757 Computrace voltammeter in the previous work [116], both from Metrohm). As a result, no significant difference may be observed (Table 3.1): accordingly, detection capabilities were not deteriorated by the reduction in sample volume (see also the previous section for seawater conditions and copper analysis).

Table 3.1 – Comparison between LODs determined in the present work and literature data. Note the different deposition times.

	Dep. Time (s)	Limit of Detection (nM)				
		Cd	Pb	Cu	Ni	Co
500 µL (this thesis)	60	0.27	0.17	1.0	0.14	0.20
10 mL (literature [116])	90	0.16	0.10	1.7	0.46	0.15

Table 3.2 reports the trace element concentrations determined in the five rainwater samples: reference values obtained by ICP–MS are reported for comparison purposes. Standard deviations for voltammetric measurements are referred to triplicate independent measurements of sample aliquots, whereas uncertainty in ICP-MS data refers to triplicate readings of the same sample (i.e. it is an estimate of the short term repeatability).

No statistically significant difference was evidenced for all of the sample and analytes but in four cases (two tailed t test, p=0.05). This consistency between the data obtained with the two different techniques is shown also in Figure 3.15 for concentrations below 30 nM. Only four values failed the two tailed test: nevertheless, three of them showed differences below 25%, whereas the difference in nickel concentration in sample 5 was highly significant and possibly due to the contamination of the aliquot used for CSV.

Table 3.2 – Result of the analysis of the five rainwater samples by stripping voltammetry (ASV and CSV) and Inductively Coupled Plasma-Mass Spectroscopy (ICP-MS). Data are reported as mean ± one standard deviation in nM.

Sample #	Cd		Pb		Cu	
	ASV	ICP-MS	ASV	ICP-MS	ASV	ICP-MS
1	<LOD	0.267±0.027	1.9±0.77	1.52±0.010	59±1.0	56.6±0.91
2	<LOD	0.151±0.009	1.2±0.25	1.40±0.077	27.8±0.88	27±1.6
3	<LOD	0.116±0.018	1.4±0.23	1.11±0.010	15 ±1.3	14.8±0.20
4	<LOD	0.116±0.027	0.97±0.07*	1.16±0.005	21.2±0.72	21.4±0.11
5	<LOD	0.107±0.036	1.30±0.06	1.30±0.014	21±1.2*	18.4±0.19

	Ni		Co	
	CSV	ICP-MS	CSV	ICP-MS
1	123±15	103±15	0.61±0.14	0.47±0.034
2	22±1	20.4±0.19	0.46±0.10	0.59±0.051
3	8.7±0.89*	7.0±0.10	<LOD	0.14±0.017
4	24±2.2	23.3±0.17	<LOD	0.19±0.017
5	13.0±0.61*	6.46±0.068	<LOD	0.10±0.017

* Values with statistically significant differences from ICP–MS data (two tailed t test, p=0.05).

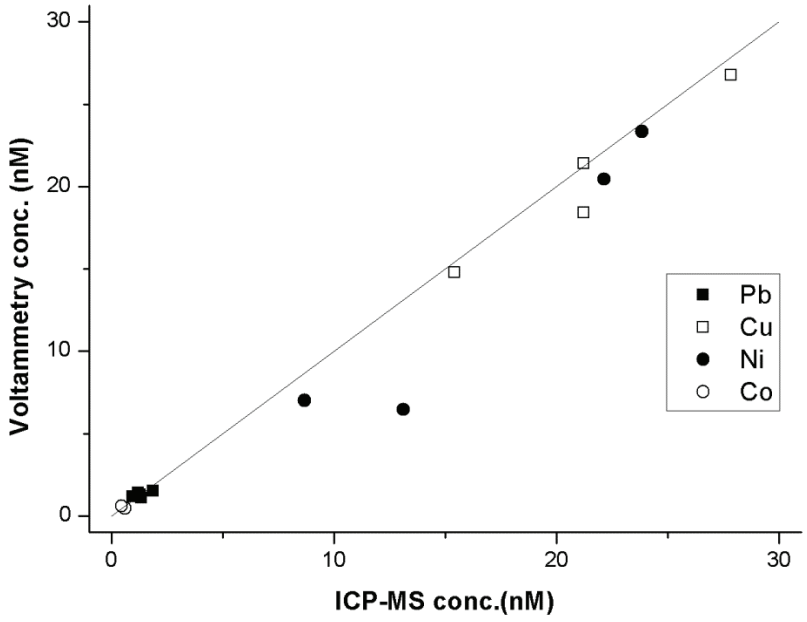

Figure 3.15 – Comparison between the values obtain with voltammetric technique and ICP-MS. The straight line x = y was drawn to facilitate interpretation of the graph.

4 Analysis of Iron by CSV-DHN with Atmospheric Oxygen

After the optimization of the bromate method, the next challenge was to develop a completely new procedure for the analysis of iron in seawater more performing than previous approaches. Major improvements would include sample size and analysis time reduction, limited number and amount of reagents and reduced toxicity of the employed chemicals while keeping the detection capabilities described in Chapter 1. The goal of the new procedure would be to employ the small volume cell described in Chapter 3 and, at the same time, reducing the employed reagents (see also section 6.2 for recent evolutions in this direction). As a matter of fact, the employment of potassium bromate is a weak point of the method described in Chapter 2. Potassium bromate, which is classified as a carcinogenic chemical, poses significant consequences, the most relevant of which are the high cost of waste treatment and possible effects on the operator's health. Cost and safety are crucial in an analytic laboratory, specifically if the laboratory is located on a research vessel. In this singular environment, it is very important to protect the researcher from exposure to contamination and toxic chemicals. While the boat is offshore or moored in remote areas, the toxic waste will need to be stored on the same vessel with no means of treatment. On the other hand, the proper disposal of carcinogenic chemical wastes has greater costs when compared with standard wastes.

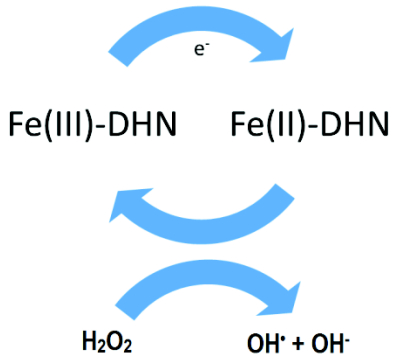

Figure 4.1 – Simplified mechanism of Fenton reaction.

At this point of the project, for the aforementioned reasons, the objective was to create a new carcinogenic-free method. This goal, combined with the employment of the small cell described before (Chapter 3), lead to an impressive improvement for the voltammetric determination of the iron on board.

This chapter describes the steps taken to define the final methodology: initially, the catalytic enhancer bromate was changed with tank oxygen in a standard voltammetric cell (10 mL), hydrogen peroxide was then used and, finally, atmospheric oxygen in combination with the small sample cell. The idea is to enhance the sensitivity by a Fenton like reaction [117] as reported in Figure 4.1.

4.1 Tank Oxygen

The first evidence of a catalytic effect of oxygen on the reduction of the Fe-DHN complex was observed when the sample was not purged with nitrogen in the absence of bromate. As a result, a CSV wave was present and repetitions showed a decreasing signal due to the presence of an additional nitrogen input in the cell headspace that slowly removes oxygen from the sample (this is a typical unavoidable feature of the Metrohm voltammetric stands).

After this observation, the initial thought was to exchange the potassium bromate with tank oxygen. Finding an alternative to bromate is a requirement to keep the higher sensitivity of catalytic methods

In order to use the tank oxygen as an oxidant in the voltammetric procedure, it was necessary to build a system capable of mixing oxygen and nitrogen from two different tanks before the inlet into the voltammetric cell. This apparatus warrants the possibility to change the percentage of oxygen blown into the cell. Two needle valves, quick-fit fittings, a bubbler to humidify the mixture and various tubing were used to set up the apparatus (Figure 4.2).

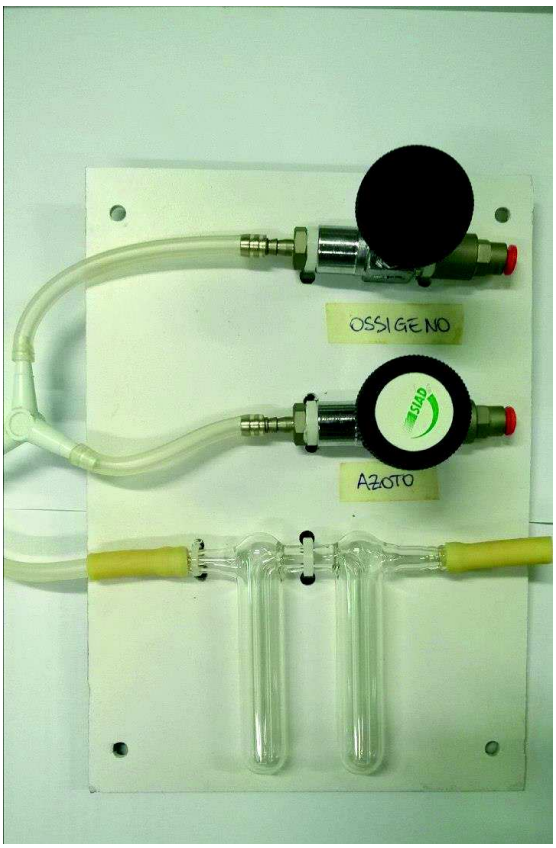

Figure 4.2 – Mixture apparatus composed by two needle valves, fittings and a bubbler.

The oxygen, coming from the tank and mixed with nitrogen gas, was sent directly to the voltammetric cell, as shown in Figure 4.3, using the lined usually employed for purging.

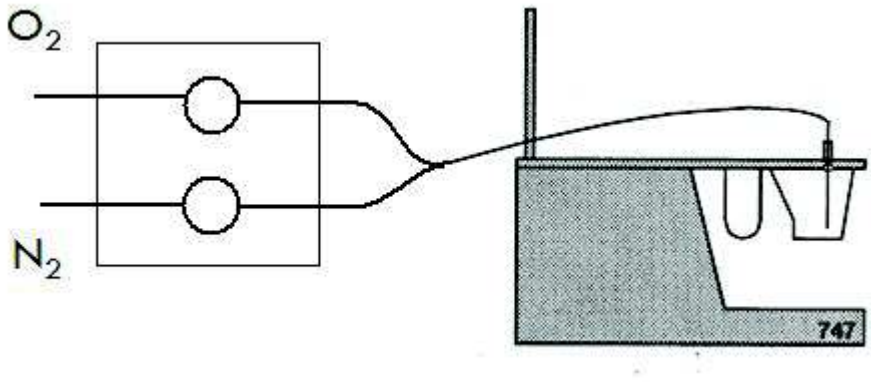

Figure 4.3 – Scheme of the voltammetric system using the mixture apparatus.

Adding oxygen into the voltammetric cell guaranteed the catalytic effect. In fact, it was possible to observe the peak related to the complex Fe-DHN and its height was proportional to the iron concentration in the cell. Figure 4.4 displays scans obtained for the blank analysis with two additions. The blank was around 1 nM, a high value due to the fact that the instrumentation was not located under a laminar hood

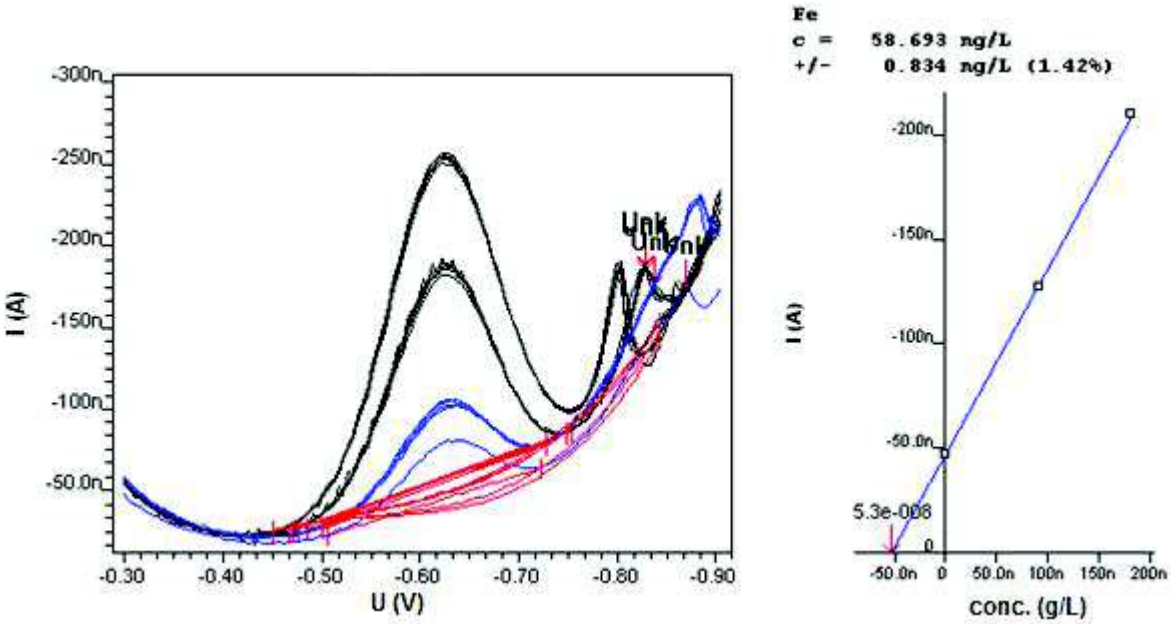

Figure 4.4 – CSV determination of the iron concentration in a blank at pH 8.0. Blue scan: sample, blacks scans: sample + 1.5 and + 3.0 nM Fe. 20 µM DHN, 1 min deposition time and 10 mM HEPPS buffer.

Given these encouraging preliminary results, it was decided to better explore the catalytic effect of oxygen. New experiments were performed using the possibility to change the percentage of oxygen in the gas mixture.

4.1.1 Catalytic effect

The catalytic effect caused by oxygen was demonstrated by blowing mixtures of nitrogen and oxygen at different ratios in the voltammetric cell mentioned in the previous section (see Figure 4.5).

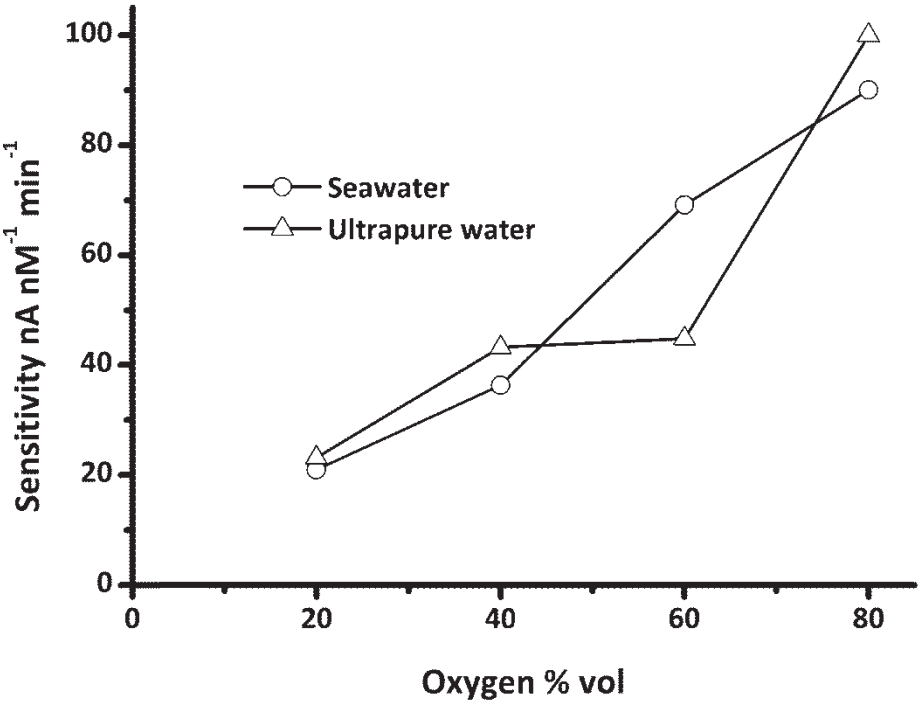

Figure 4.5 – Effect of percentage of oxygen on the voltammetric signal in seawater and ultrapure water. The voltammetric cell contained 10 mL of ultrapure water or seawater, 1 nM of iron, 10 mM of HEPPS buffer and 2 µM of DHN, the scan was preceded by 30 sec of deposition time at - 0.1 V. RSD% of the sensitivities were between 1.5% and 5%.

The experiments were carried out in the presence of simulated seawater (NaCl solution 35 g/L) and ultrapure water. In both cases the sensitivity grows with the increase of oxygen percentage: in simulated seawater the trend is almost perfectly linear with maximum sensitivity of around 90 nA nM^{-1} min^{-1} (RSD% of sensitivity values are below 5%). Using ultrapure water there is still a linear trend, but the experiments at percentages of oxygen equal to 40 and 60% gave very similar results.

Moreover, in ultrapure water the values of RSD% are generally higher and up to around 10% with 80% oxygen and 20% nitrogen.

The almost linear relationship between O_2 volume percentage and sensitivity is a good indication of the catalytic effect of oxygen in this system [81, 118]. Beside the value at 60% oxygen in ultrapure water, which is possibly an outlier, the voltammetric scans were noisy and not suitably stable. The instability is more than likely do to the high concentration of gasses during the analysis. In fact, for the standard voltammetric procedure, the potential scan is preceded by a degassing time. The usual degassing time for ten milliliters of sample is 300 s. The hypothesis was made that taking the oxygen/nitrogen mixture and blowing it directly into the sample for three minutes in addition to the continuous flux of nitrogen from the head space can cause unstable scan and noisy signals.

During these experiments, the limits of detection were calculated for every percentage of oxygen and for the two matrixes. The best result was obtained in simulated seawater at 60% oxygen, with an estimated LOD of 0.23 nM. The high noise during the scans, the non-optimal LOD and the feeble reproducibility of the peaks headed to leave the optimization with this operative system.

These experiments were repeated employing the small cell developed as described in Chapter 3. The oxygen/nitrogen mixture was blown in the headspace in a closed system (Figure 3.12) because of the difficulty in blowing a gas in the limited operating volume of 500 µL only.

The outcomes of these experiments are reported in Figure 4.6. Increasing the percentage of O_2 causes the sensitivity to grow to very high values for both matrices: in 80% of oxygen, the sensitivities are 160 and 90 nA nM^{-1} min^{-1} for ultrapure water and seawater, respectively. The sensitivity was around twice in ultrapure water with respect to seawater (1.9 on average). Increasing oxygen percentage (i.e. the concentration of the catalysts) is the main way to increase sensitivity, this is consistently true for catalytic systems in cathodic stripping voltammetry [118]. It is important to point out that no cost, in terms of blank level, is paid when oxygen partial pressure is raised. As two gas cylinders and a gas flow regulation system would be needed, an increase in the complexity of the apparatus would nevertheless result which may be an issue during field analysis.

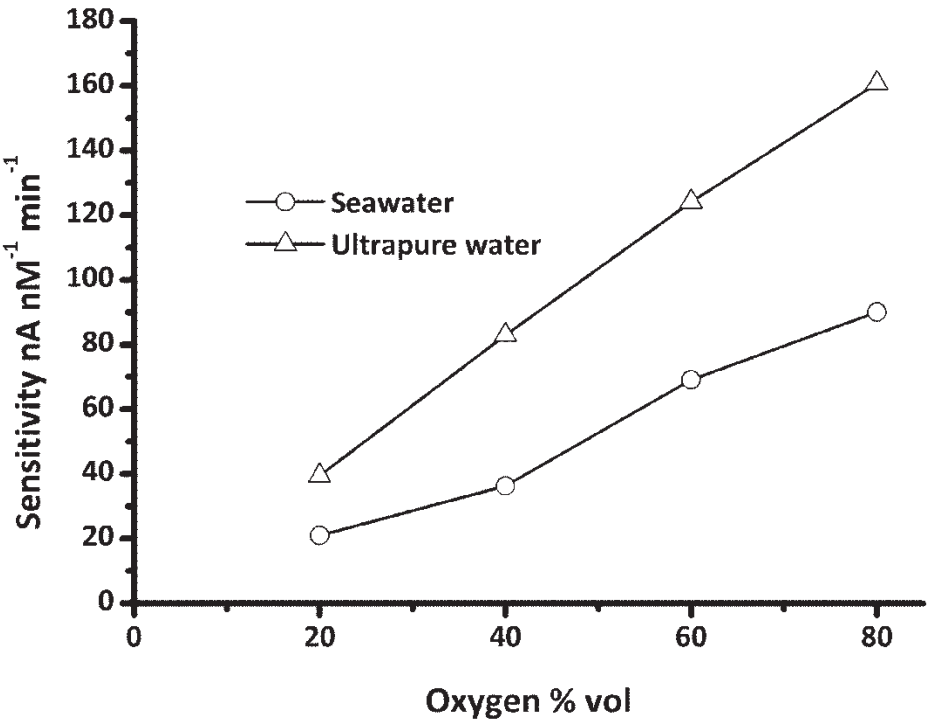

Figure 4.6 – Effect of the percentage of oxygen on the voltammetric signal in seawater and ultrapure water. The voltammetric cell contained 500 µL of ultrapure water or seawater, 1 nM of iron, 10 mM of HEPPS buffer and 2 µM of DHN, the scan was preceded by 30 sec of deposition time at - 0.1 V. RSD% of the sensitivities were between 2.5% and 5%.

4.2 Hydrogen Peroxide

Experimental evidence suggests that hydrogen peroxide generated by oxygen reduction during the deposition time at -0.1V or during the potential scan is responsible for the catalytic effect, as already advised for the analogous method based on salicylaldoxime [81]. As one would expect, while observing the voltammogram of oxygen in an air saturated solution (Figure 4.7) the oxygen in the diffusion layer is reduced into hydrogen peroxide. Finally the hydrogen peroxide, in situ produced, performs as the oxidant in the catalytic mechanism. As a matter of fact, hydrogen peroxide added to the sample was already demonstrated to catalytically enhance the signal in the original study on iron determination in seawater employing DHN [80]. The mechanism behind this catalytic effect deserves a clarification. The Fe-DHN voltammetric peak is at the positive potential end of the peak due to the reduction of H_2O_2 to H_2O, -0.58 V, whereas O_2 reduction to H_2O_2 occurs at much higher potentials. The iron complex acts as a catalyst in this reaction, as it facilitates the electron transfer among the electrode and the H_2O_2 molecule. The latter is not a catalyst as it is the final electron acceptor: the usual representation of the oxidant being the catalyst that reoxidizes the freshly formed reduced species of the electroactive metal complex is not the correct description of the mechanism [118].

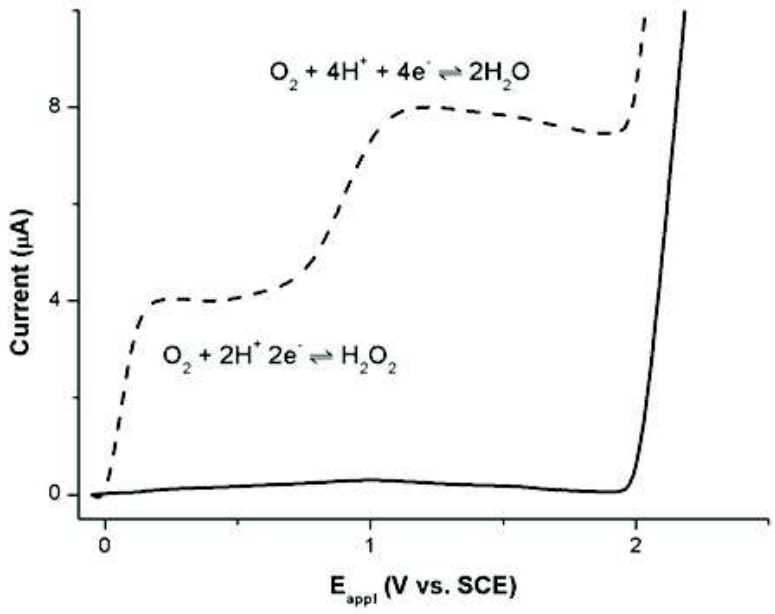

Figure 4.7 – Voltammogram related to the oxygen reduction in a 0.1 M KCl solution saturated with air. The lower scans refers to 0.1 M KCl solution short of oxygen.

4.2.1 Catalytic effect

In order to prove and verify the catalytic behavior of hydrogen peroxide, several tests were performed using both of the configurations available: the new hardware configuration (0.5 mL sample volume) and the standard one (10 mL sample volume). Figure 4.8 reports the results of the scans obtained with different concentration of H_2O_2 and DHN in the standard, 10 mL sample cell. For each hydrogen peroxide concentration, the signal grows linearly with DHN concentration up to 20 µM. After this point, the signal departs from linearity and eventually reaches a plateau value up to very high DHN concentrations (100 µM).

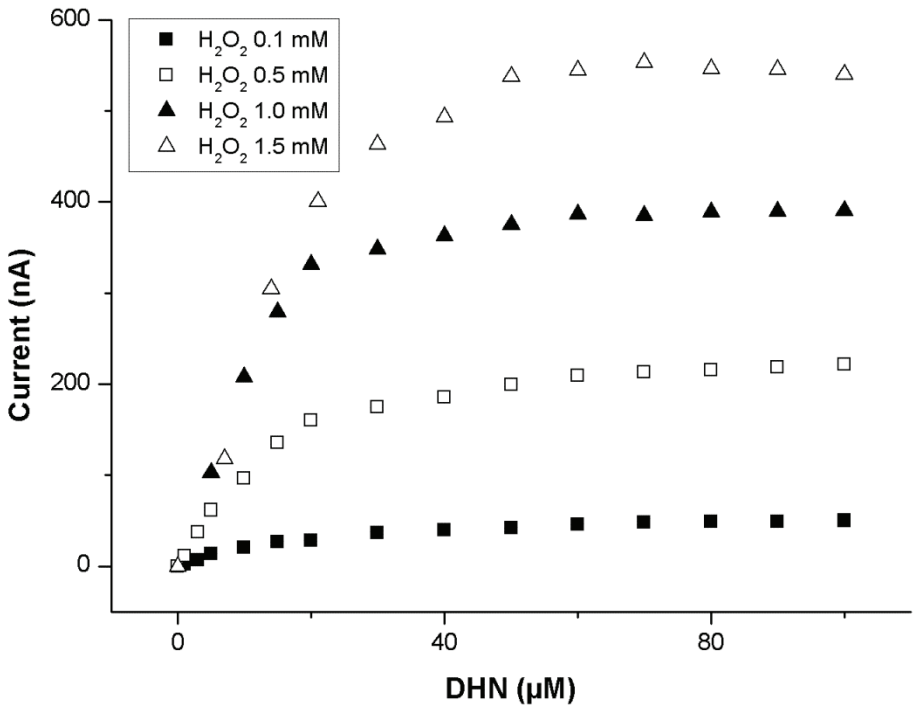

Figure 4.8 – Effect of different concentrations of hydrogen peroxide and DHN on the voltammetric signal in ultrapure water. Conditions: 10 mM POPSO buffer pH 8.0, 300 s purging time and 1 min deposition time.

Additionally, different scan rates were investigated. In this case, no significant differences in sensitivity were observed in the range between 0.005 and 0.15 V s^{-1} (Figure 4.9) and the signal seems to be only dependent on hydrogen peroxide concentration, with the possible exception of the lowest investigate sweep rate. The highest variability was measured at 2 mM peroxide and can be easily attributed to the increase of the baseline and the consequent instability of the signal (Figure 4.10).

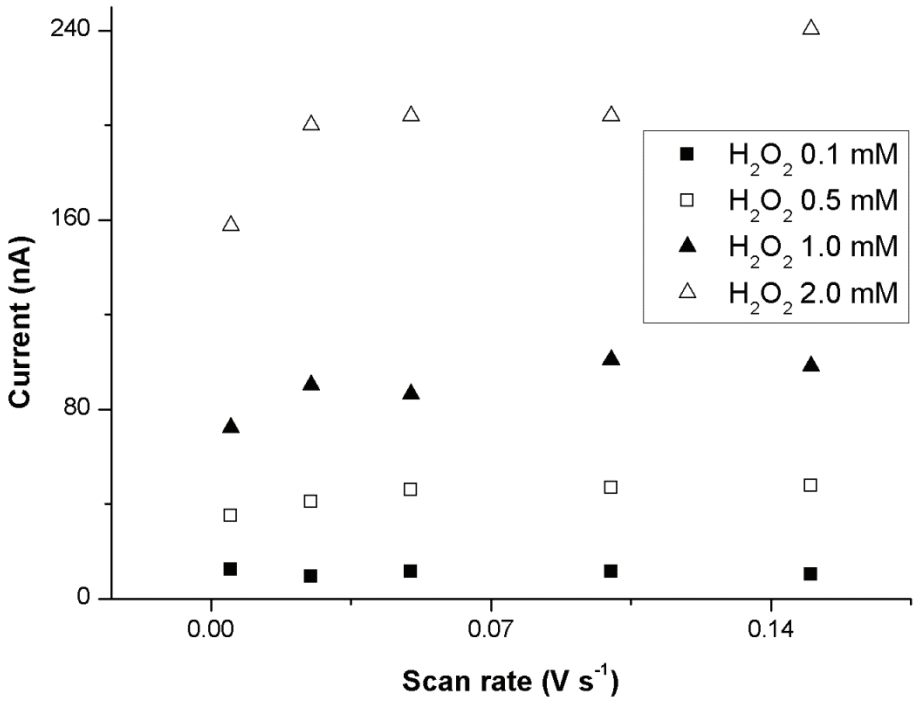

Figure 4.9 – Effect of the concentration of hydrogen peroxide and scan rate on the voltammetric signal in ultrapure water. Same experimental conditions as Figure 4.8.

As is always true for analytical methods, the raise in sensitivity does not effort by itself better detection capabilities, as the signal to noise ratio should be evaluated. An analysis of the four scans in Figure 4.10 shows that with 2 mM of H_2O_2 the sensitivity is higher, but also the baseline grows significantly. At negative potentials, the baseline reaches significantly higher values and the peak loses its symmetry. In addition, the baseline seems to depart from linearity, making its definition more complicated. For each of these reasons, 0.5 mM of hydrogen peroxide was selected as the best compromise between sensitivity, easiness of baseline interpolation and noise reduction. This choice was confirmed by the LODs values obtained during these measurements. The best LOD was found with 0.5 mM of hydrogen peroxide and is equal to 0.03 nM. All the other LODs were higher and the worst performance (LOD 0.50 nM) was registered with H_2O_2 0.1 mM, that circumstance was mainly due to the tiny sensitivity.

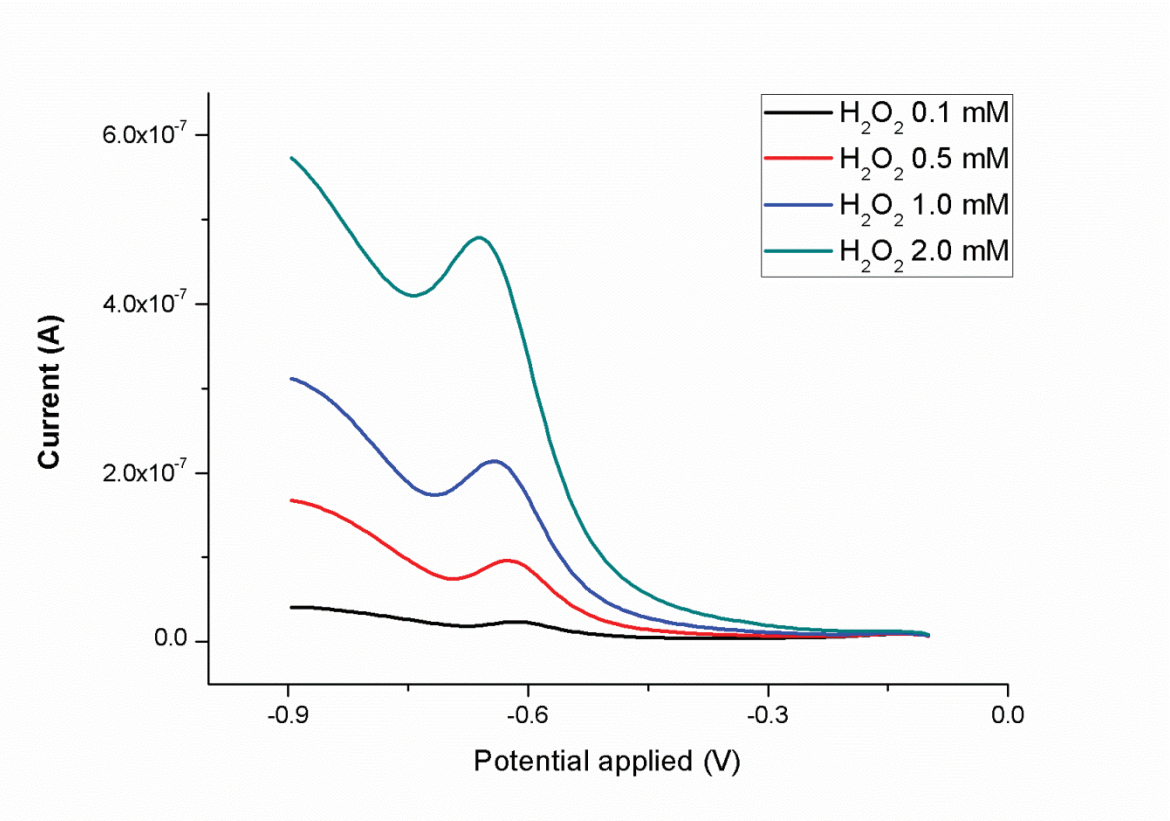

Figure 4.10 –Voltammetric scans varying the hydrogen peroxide concentration in ultrapure water plus 1 nM iron. Same experimental condition as Figure 4.7.

After the tests reported above one additional parameter was checked: the signal stability. The same sample was analyzed every 5 minutes for 3 hours, the results of which are displayed in Figure 4.11. The relative standard deviation of all measurements during three hours was below the 3 %. Considering the fact that the average analysis time is around 10 minutes, this is an optimal result.

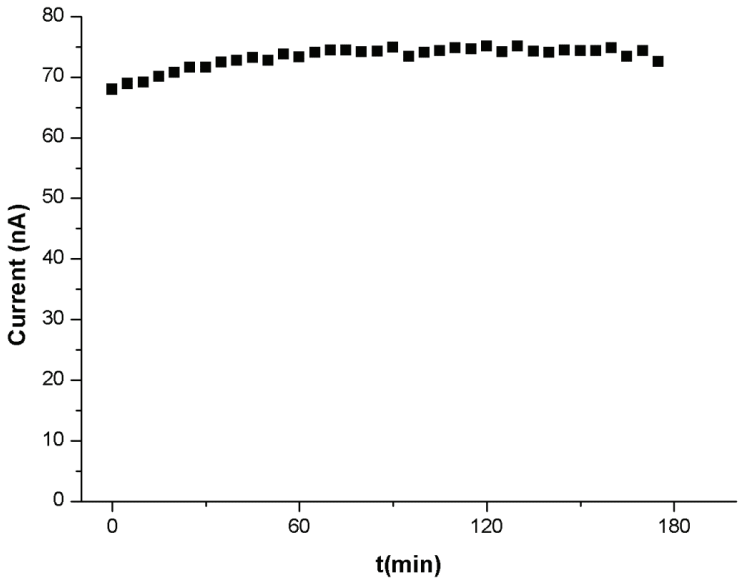

Figure 4.11 – Stability of the measures over three hours, The scans was performed every 5 min in ultrapure water plus 1 nM iron. Same experimental condition as Figure 4.7.

The availability of the new voltammetric cell (Chapter 3) allowed the application of the hydrogen peroxide method to a 500 µl sample. Different concentrations of hydrogen peroxide were tested as before and the LOD was calculated for each of them together with sensitivity (Figure 4.12). Specifically, oxygen linearly increases with hydrogen peroxide concentration in accordance with the results of Obata et al. [80] and the catalytic mechanism.

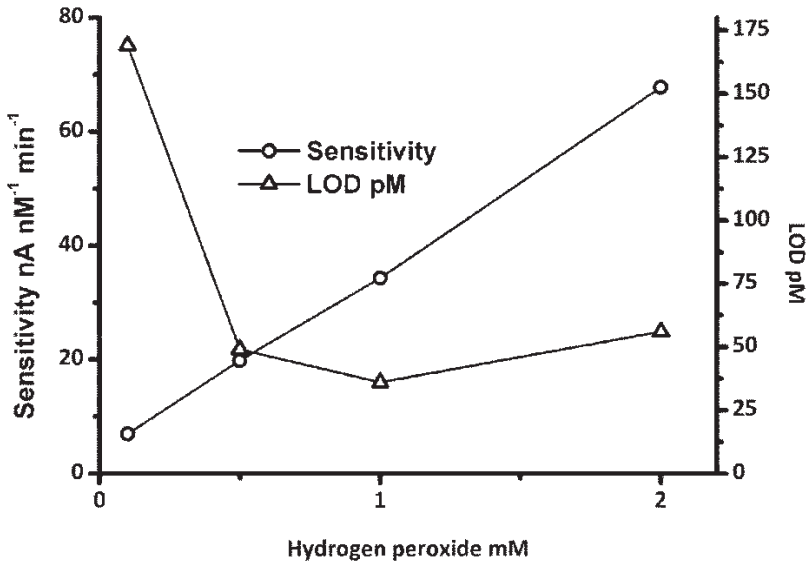

Figure 4.12 – Effect of variation of H2O2 concentration in ultrapure water using the 500 µL cell. Same experimental conditions as Figure 4.8.

Nevertheless, the signal became unstable when the H_2O_2 concentration was increased, leading to a deterioration of the LOD at hydrogen peroxide concentrations higher than 1 mM. The best performances were obtained with a concentration of hydrogen peroxide equal to 1 mM: sensitivity 34 nA nM^{-1} min^{-1} and LOD 36 pM (30 s deposition time).

Besides its possible use for analytical purposes, the enhancement of the analytical signal caused by hydrogen peroxide is a further indication, although indirect, that it is responsible for the catalytic effect in the iron DHN system.

4.3 Atmospheric Oxygen

It was proven that the oxygen has a catalytic behavior, but the adopted system was still complicated and unpractical. The next step was the removal of the gas tanks and the use of atmospheric oxygen as the oxidant. For this reason, another hardware modification was implemented: four large holes were made in the cell support starting from the first prototype (Figure 4.13). These four large holes permit to the air to pass over the small cell. The voltammeter was placed inside a laminar flow hood to prevent the contamination. The elevated volume/surface ratio guaranteed the contact between the atmospheric oxygen and the sample, as described in Chapter 3. Removing the need for gas cylinders makes the method practical and suitable in every contest, also for analysis on board.

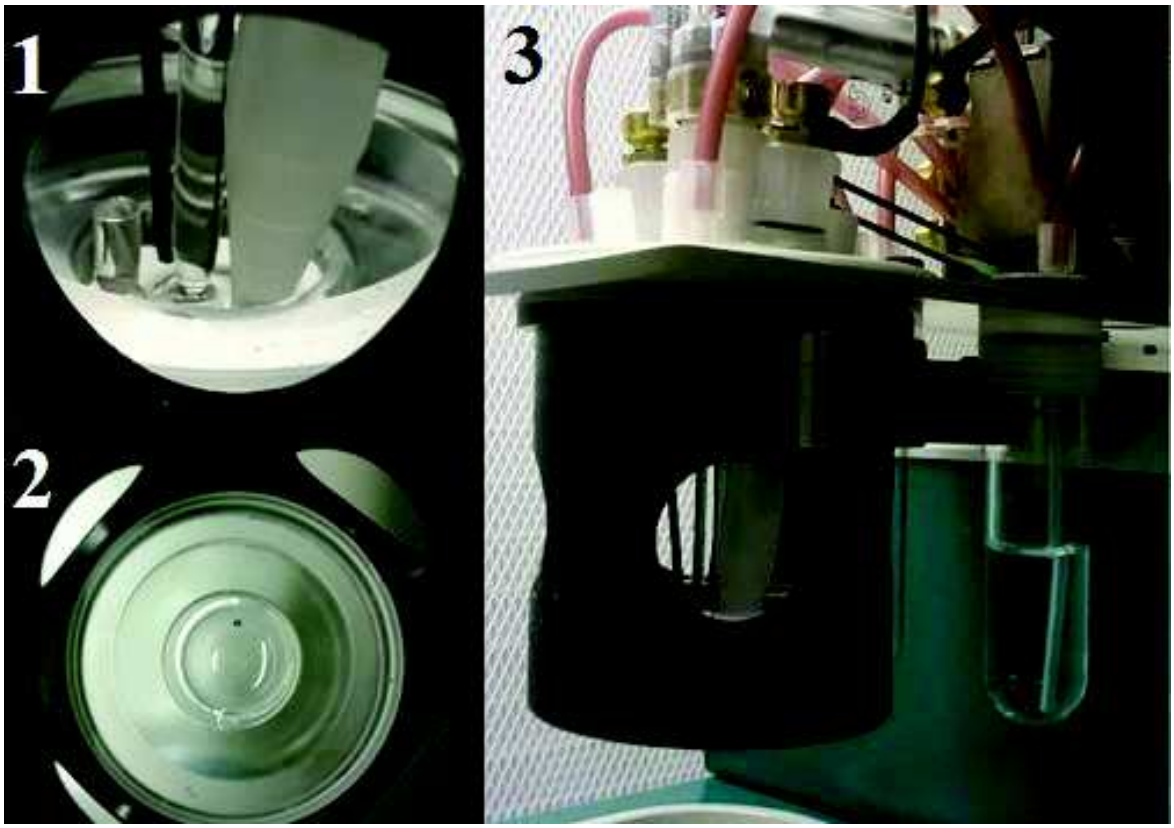

Figure 4.13 – Images of new instrumental cell: 1) view through an hole, the positioning of the three electrodes system is visible; 2) view from above of the new cell inserted in its stand; 3) overview of the whole system.

4.3.1 Method optimization

Purging time Voltammetric determination usually need a purging step prior the potential scans. The purging time aims at removing the dissolved oxygen in the sample, but the oxygen is the catalyst in the new method and so this step is not required. Nevertheless the firsts attempts showed an instability at the beginning of the analysis. The iron peak had an increasing trend for a couple of minutes and then it became stable. The initial hypothesis was that during the first minute of the analysis the equilibrium between the atmospheric oxygen and the dissolved oxygen in the sample was not reached. It was decided to start the acquisition of the scans after 120 sec of waiting time in order to obtain the oxygen equilibrium and get stable and consistent signals. Concluding this methods do not require the purging time but needs a waiting time of 120 sec because of the oxygen use as catalyst.

Scan mode Linear scan, differential pulse (DP) and square wave (SqW) scan modes were investigated: preliminary tests showed a very high baseline using a linear scan, whereas DP and SqW showed a much lower baseline. The best result in terms of signal to noise ratio was obtained with the square wave modulation.

The frequency of the square wave was subsequently optimized in the range between 1 Hz and 500 Hz. The signal increased up to 10 Hz, then it remained constant up to 25 Hz and finally decreased down to be undetectable at the highest investigated frequencies. The range between 5 and 50 Hz was better investigated to assess the best value of this parameter: four different frequencies were chosen (5, 10, 25 and 50 Hz) and the sensitivity and the LOD calculated for each of them (Figure 4.14).

Sensitivity and LOD show the same behavior in seawater (Figure 4.14) and ultrapure water (Figure 4.15). The 10 Hz modulation was the best choice in terms of LOD as it benefits from a high sensitivity and a limited baseline value. Accordingly, all the following analyses were carried out using a square wave sweep with a 10 Hz modulation.

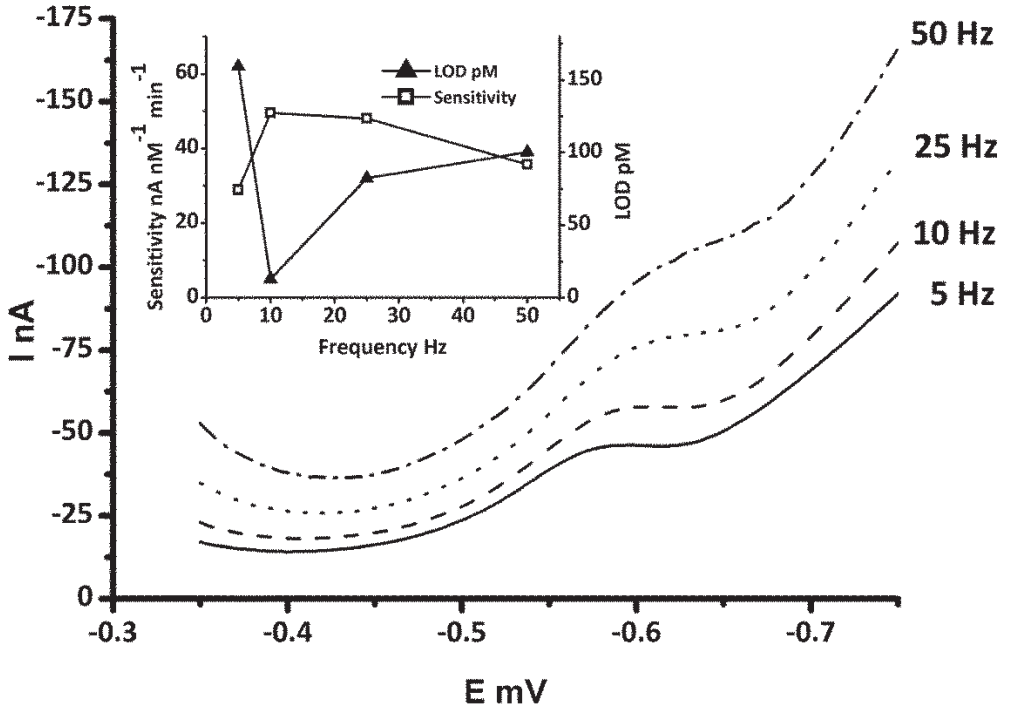

Figure 4.14 – Comparison between different square wave frequencies in seawater. The sensitivity and the value of the LOD were calculated for each frequency (0.5 nM Fe, 10 mM HEPPS, 10 µM DHN).

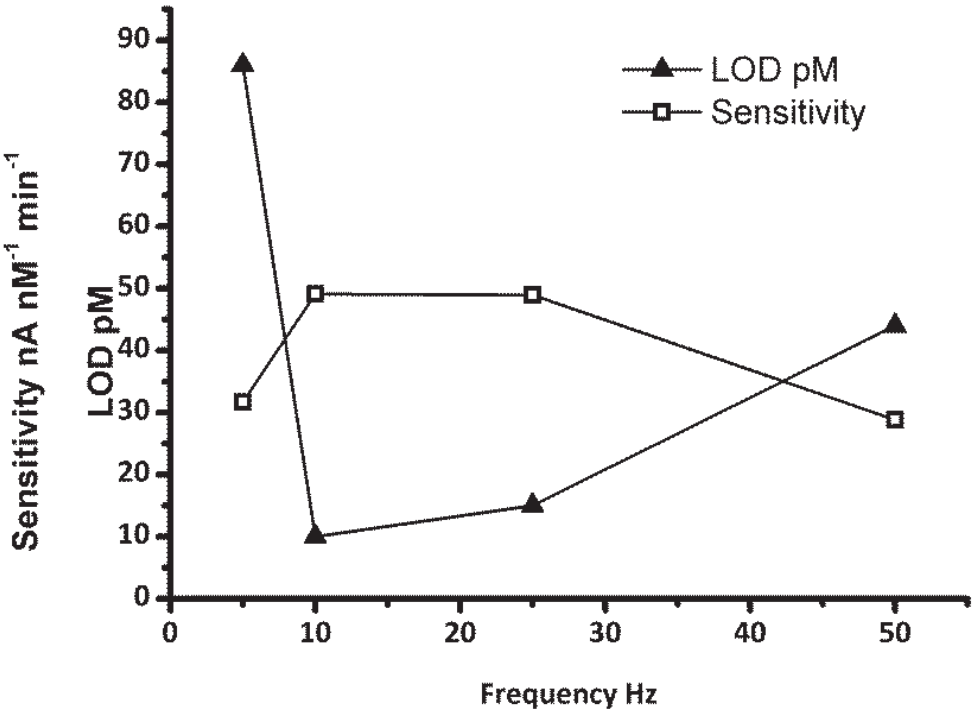

Figure 4.15 – Limit of detection and sensitivity as a function of square wave frequency in ultrapure water.

DHN concentration The concentration of the added ligand is known to exert a great effect on the analytical signal: accordingly, its effect was systematically investigated in both ultrapure water and seawater. Figure 4.16 shows that the sensitivity increased almost linearly with DHN concentration up to 400 μM, decreasing thereafter (note the logarithmic scale for DHN concentration).

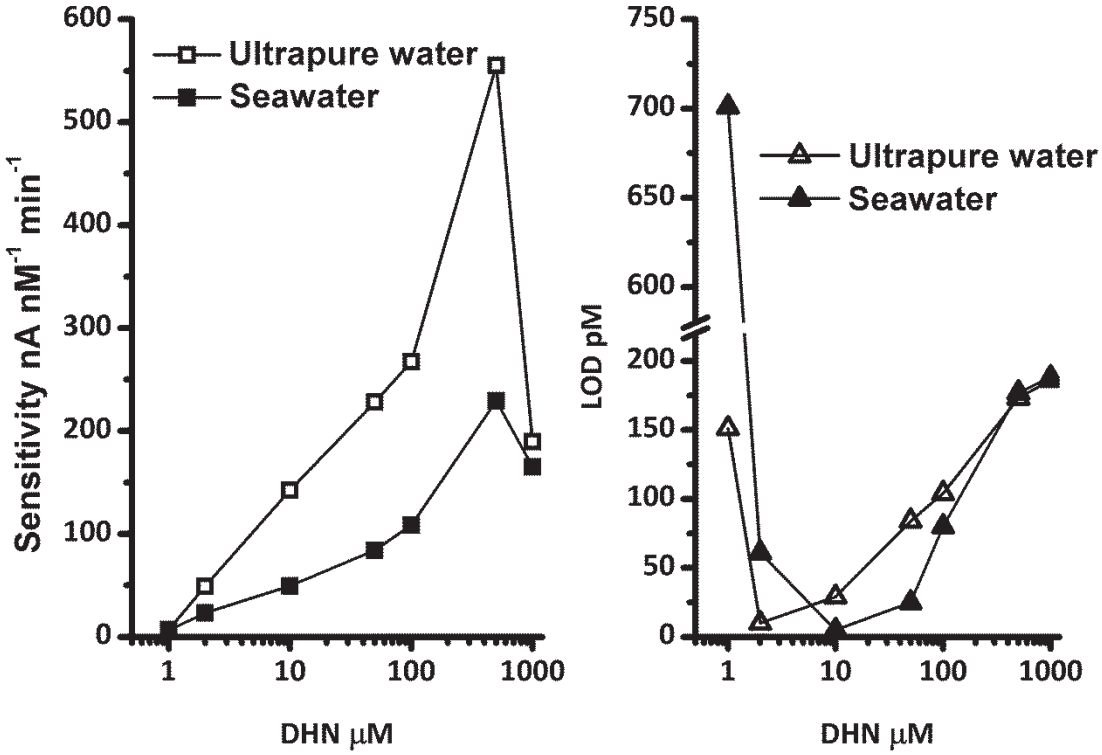

Figure 4.16 – Variation caused by the concentration of DHN in terms of sensitivity and LOD, in ultrapure water and seawater. All the solutions were 10 mM HEPES and 0.5 nM Fe.

The measured limits of detection followed a peculiar trend: they had a minimum at 2 and 10 μM DHN for ultrapure water and seawater, respectively, and raised steadily for higher DHN concentrations. This trend is due to the signal continuously increasing when DHN concentrations higher than 10 μM are used. This variability is partially offset by a giant sensitivity (up to 555 nA/nM min^{-1} in ultrapure water, 229 nA/nM min^{-1} in seawater) at very high DHN concentrations, but the S/N ratio is nevertheless decreasing. These experimental conditions, although ensuring the highest sensitivity ever registered in CSV, are not suitable for analytical purposed as the signal is constantly raising leading to a very low reproducibility. External contamination is a possible reason for such behavior. All the experiments were carried out under a laminar flow hood, but the measuring cell has four large holes (Figure 4.13), needed to

ensure the oxygen equilibrium between the solution and the atmosphere, greatly facilitating the contamination of the samples with Fe. An additional possible source of contamination is through the porous ceramic frit that separates the reference electrode salt bridge and the sample: a potential solution to this problem would be the use of a pseudo reference electrode, such as the one introduced in [119]. Experiments carried out in the 10 mL cell with the classical glass salt bridge and the polytetrafluoroethylene salt bridge with the commercial porous ceramic frit showed that the first would cancel a slow signal increment detected with the polytetrafluoroethylene salt bridge. For the same reason it has been suggested to fill the reference salt bridge with clean seawater [99]. It is interesting noting that such a behavior, i.e. increasing peak current, was observed with high DHN concentrations only, as this solution may be more easily contaminated due to the high affinity of DHN for iron.

Given these experimental results, a ligand concentration equal to 2 μM for the analysis of low ionic strength sample is proposed: these experimental conditions allow a limit of detection of 10 pM (deposition time 30 s) and a sensitivity of 49 nA nM^{-1} min^{-1}. A higher DHN concentration, 10 μM, ensured the best limit of detection for seawater: 5 pM for 30 s deposition time with a sensitivity of 49 nA nM^{-1} min^{-1}. This very high sensitivity is a peculiar feature of the cell configuration used: the same effect (i.e. signal enhancement in the presence of O_2 or H_2O_2) has been achieved with a standard 10 mL cell in the same conditions (see sections 4.1.1) and also with a different ligand (salicylaldoxime [81]), but the sensitivity values reported here were never achieved.

The higher DHN concentration required for seawater to achieve the same sensitivity as in ultrapure water, may be easily explained with the need to outcompete major ions (especially calcium) which may compete with iron for complexation with DHN.

Regarding the different sensitivity registered in ultrapure water and seawater, oxygen solubility should be firstly considered: oxygen is about 25 % more soluble in freshwater than in sea water (35 psu) at 20 °C [120], leading to a parallel increase in sensitivity (see Figure 4.6, S vs O_2 %). A second important factor is the presence of natural organic matter in the seawater sample as the procedure does not require UV digestion prior to analysis. Natural organic matter has already been demonstrated to cause a reduction in sensitivity in stripping voltammetry [121]. Differences in the electrode-solution double layer composition, in iron speciation and electron transfer

kinetics may also play a role, although such a deep knowledge of the system is presently not at hand.

Effect of pH The effect of pH on detection capabilities was systematically investigated in the range 7-9 by determining LODs and sensitivities in ultrapure water buffered at eight different pH values (Figure 4.17). The fivefold increase in sensitivity in the pH range 7-9 was analogous to the trend previously reported in the presence of bromate as the oxidizing agent (Chapter 2, [122]). Nevertheless, this increase in sensitivity was compensated by a steady decreasing of the signal at pH higher than 8.15 which led to an increase in the LOD values (see Figure 4.16 and Figure 4.17).

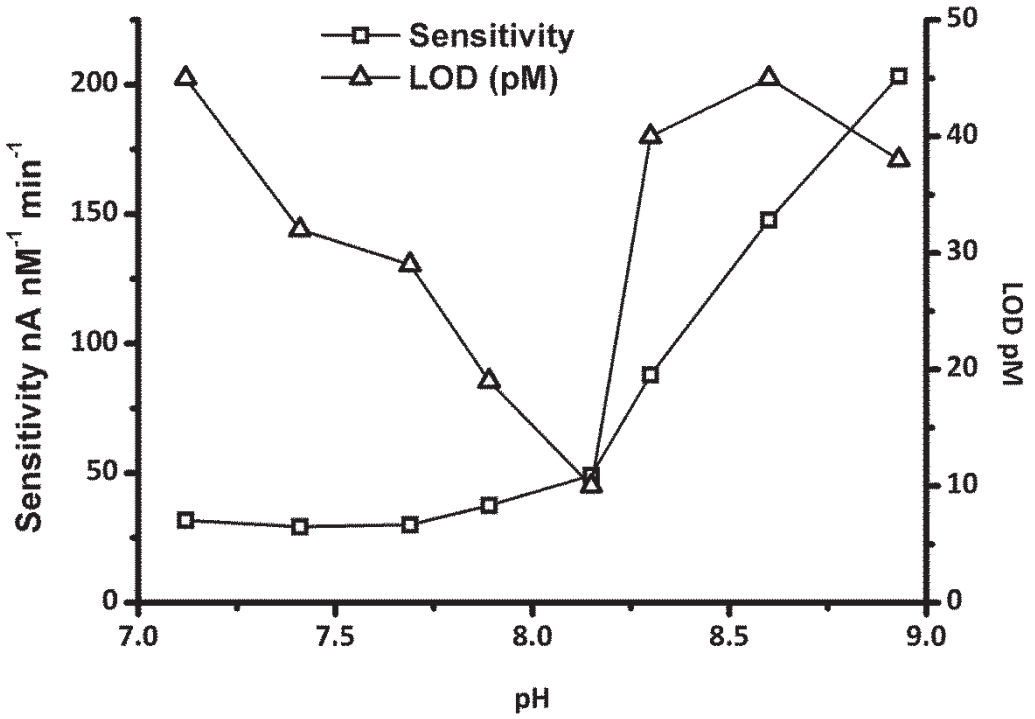

Figure 4.17 – Effect of pH on sensitivity and LOD in ultrapure water. The voltammetric cell contained 500 µL of ultrapure water, 0.5 nM of iron, 10 mM of HEPPS buffer and 2 µM of DHN, the scan was preceded by 30 sec of deposition time at - 0.1 V.

The signal was instead stable for around 20 min at pH 8.15 and 7.9 (Figure 4.18): this stability window is adequate for a two standard addition procedure with five replicates, if 30 s deposition time is used.

Accordingly, the optimal pH for the new method in low salinity waters is between 7.90 and 8.15. A much better stability was found in seawater (pH 8.15) compared to ultrapure water: a relative standard deviation of 3% was registered for 30 repeated measurements (30 min) without any clear trend. The optimum conditions

matching the range of natural seawater pH is extremely convenient as this method with minimum modifications could be used for determining the organic speciation of iron in seawater by competitive ligand equilibration – cathodic stripping voltammetry, CLE – CSV.

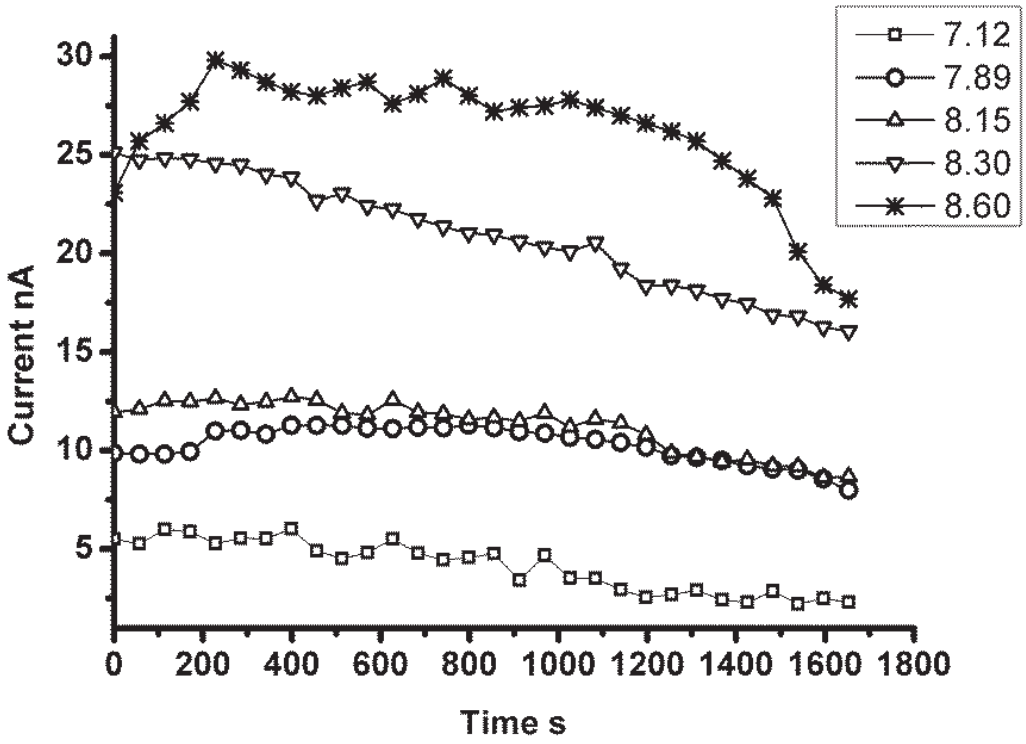

Figure 4.18 – Stability of the signal in ultrapure water as a function of pH (iron 0.5 nM, DHN 2 µM, deposition time 30 s).

4.4 Figures of Merit & Validation

4.4.1 Limit of Detection & Limit of Linearity

Under optimized conditions, the limit of detection (LOD) in ultrapure water and seawater were 10 pM (2 µM DHN) and 5 pM (10 µM DHN), respectively, with a deposition time of 30s: sensitivity close to 50 nA nM^{-1} min^{-1} was registered in the two matrices. Preliminary experiments showed that sensitivity may be further increased by increasing the deposition time: sensitivity increased up to a deposition time of 120 seconds in seawater and leveled thereafter (Figure 4.19).

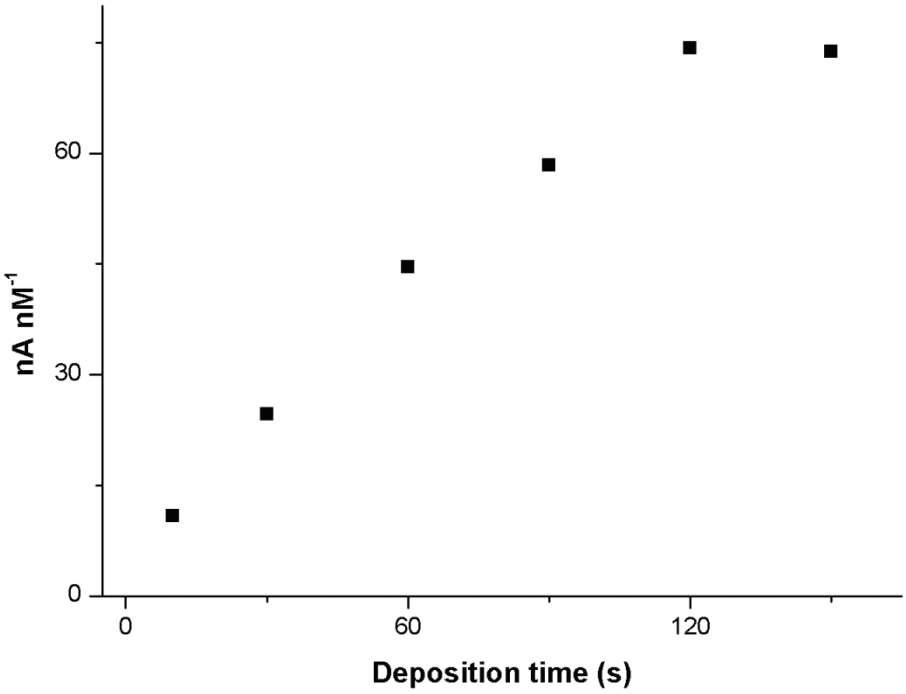

Figure 4.19 – Signal as a function of deposition time in seawater (iron 1 nM, DHN 10 µM, deposition time 30 s).

The limit of linearity (LOL) at a deposition time of 30 s was estimated as 0.6 nM in ultrapure water and 1 nM in seawater: this range may be easily expanded by reducing the deposition time if needed .

4.4.2 Validation

Two Pacific Ocean samples [85] with consensus values after interlaboratory determination of the iron concentrations were analyzed to validate this new method: the higher concentration one was diluted to keep its concentration at the ultra-trace level (Table 4.1). The iron concentration in the blank was quantified in $0.085_7 \pm 0.0016$ nM (5 replicates). It was not easy to obtain such a low level of iron in the blank, the best results were possible mixing ultrapure water and buffer in an extra container, put this mixture in the voltammetric cell, add the artificial ligand and then start the determination. The reason of this extra step is probably the ultrapure water pH, in fact the ultrapure water has an acidic pH and when it goes in contact with the cell surface can generate a contamination from the cell itself. This procedure was also adopted during the sample analysis.

The experimental data did not show statistically significant difference from the consensus values (two tailed *t* test, $p = 0.05$). The repeatability of the method proved optimal, as the relative percentage standard deviations were in the range 2-5%. Moreover, these values were obtained without the UV oxidation pretreatment. The pretreatment step absence combined with the very good performance gained and the procedure easiness make this new method a very powerful tool for the determination of dissolved iron in seawater.

Table 4.1 – Results of cathodic stripping voltammetry of Pacific Ocean samples with consensus value for ultra-trace level of iron.

Interlaboratory standard	Dilution factor	Fe consensus value nM	Fe found nM	n
SAFe S	No dilution	0.097 ± 0.043	0.096 ± 0.005	6
SAFe D2	1:10	0.91 ± 0.17	1.00 ± 0.03	5
	1:2		1.02 ± 0.02	3

All concentration data reported are in nM, n is the number of replicated analyses.

4.4.3 Application to real samples

Other real samples were analyzed with this method. The sample were collected during an oceanographic cruise in the Gulf of Mexico in June 2015 on the Weatherbird II ship (chief scientist: Prof. Kristen Buck, 18-21 June 2015). The surface water samples were collected using fish during the ship path from the St. Petersburg (FL) port to the open sea (Lat. N 25.8377, Long. E -85.7382) and back (Figure 4.20). The analyzed samples collected during the research cruise have been labeled chronologically with the suffix WB and are reported on the map (Figure 4.20)

Figure 4.20 – Sampling sites during Weatherbird II cruise in the Gulf of Mexico.

The numerical results of iron concentrations are reported in Table 4.2, every sample was analyzed in the laboratory at College of Marine Science (USF) three times in order to calculate the standard deviation.

The table above shows the relative standard deviation is consistently below the 5 %, except for one sample, indicating that the method has a very good reproducibility. The sensitivity during the measurements was variable, in general it decreased at higher iron concentrations. Iron concentrations were greater close to the shore, in these areas also the concentration of organic matter is bigger and this could be the reason for sensitivity loss.

Table 4.2 – Results from water samples collected during the research cruise on the Weatherbird II vessel. Each sample has been analyzed three times, the concentrations are in nM.

Sample	Date	Time	AV.		STD	RSD %
WB_01	18/06/2015	17:30	2.7	±	0.1	3.7
WB_02 (STN 1)	19/06/2015	13:03	0.98	±	0.027	2.8
WB_03	19/06/2015	21:50	1.14	±	0.026	2.3
WB_04	20/06/2015	0:55	0.878	±	0.0095	1.1
WB_05	20/06/2015	8:20	1.08	±	0.014	1.3
WB_06	20/06/2015	10:45	0.75	±	0.041	5.5
WB_07	20/06/2015	12:45	0.73	±	0.03	4.1
WB_08	20/06/2015	15:00	1.29	±	0.046	3.6
WB_09	20/06/2015	17:00	0.88	±	0.016	1.8
WB_10	20/06/2015	19:00	1.61	±	0.056	3.5
WB_11	20/06/2015	20:35	3.42	±	0.096	2.8
WB_12	20/06/2015	23:14	4.45	±	0.054	1.2

Moreover, the iron concentrations values are compatible with the sample origin. In fact, as is showed in Figure 4.21 (next page), the concentrations are around 1 nM for the samples from WB_02 to WB_09. Since WB_10 sample the iron concentration starts to increase moving closer to the shore. The closest to the shore sample showed a considerably higher amount of iron, over 4 nM. The monitoring of salinity, temperature, conductivity and chlorophyll a does not evidenced any particular trend or anomalous values in between the analyzed samples.

A horizontal laminar flux hood was not available during the course of the Gulf of Mexico (GoM) samples analysis in the laboratory; a vertical laminar flux hood only was available. This was a big issue at the beginning; in fact the vertical flux was not able to warrant the right oxygen exchange with the sample. For this reason an air tank was employed instead of the nitrogen tank to feed the working electrode and purging the headspace, analogously to the procedure devised by [81]. In fact, thanks to a continuous gas flux introduced in the cell headspace that is characteristic by Metrohm polarographs, air flowing from the head of the polarographic instrumentation substituted the hood air flux.

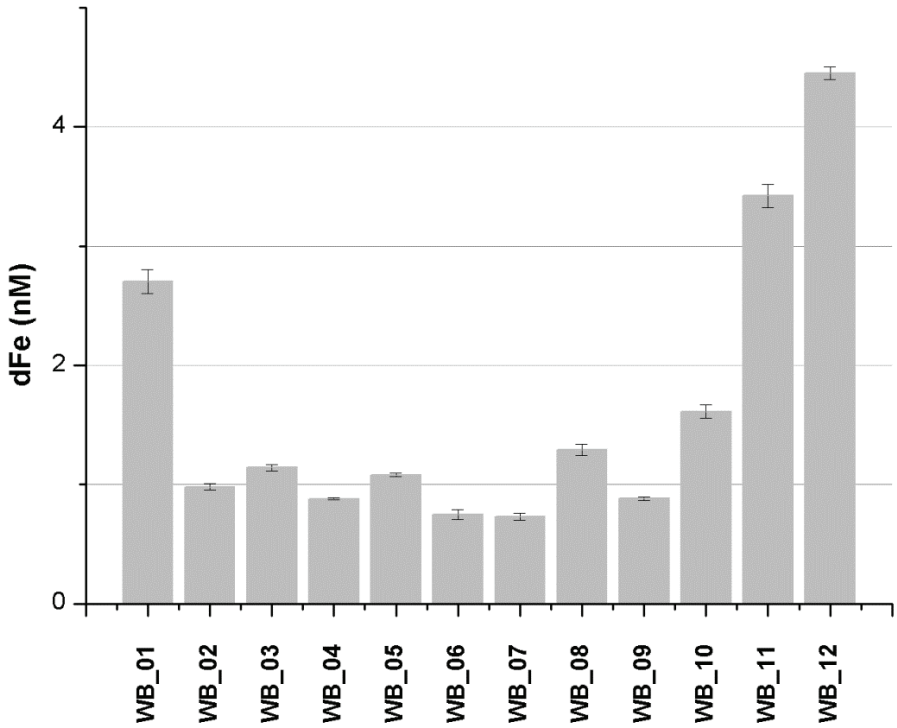

Figure 4.21 – Histogram of dissolved iron concentrations with error bars (standard deviation).

The standard stirrer was also utilized during these analyses because of an instrumentation incompatibility with the modified one. The analysis of the GoM samples showed the expected trend as a function of the distance from the coast and the replicated analyses were consistent despite these mandatory changes. Moreover, the signals showed a better stability in comparison with the previous analysis on the SAFe samples. The analysis of GEOTRACES GS sample with consensus values gave the expected result (experimental 0.569 ± 0.0031 nM, three replicates; expected 0.56_0 ± 0.047 nM).

5 Experimental

5.1 Apparatus

The measurements were performed on a 757 VA stand (Metrohm) equipped with a three electrode configuration: a mercury hanging drop electrode (0.12 mm^2 drop area), a glassy carbon rod as a counter electrode and a Ag/AgCl/3M KCl reference electrode. A 0.5 mL quartz sample cell [123] was used in the present work, details on its construction are reported in Chapter 4.

With respect to the rain samples and the speciation data (Chapter 2 & 3), the measurements were performed on a 663 VA stand (Metrohm) controlled by a micro-Autolab potentiostat (Metrohm). Also in this case, the polarograph was equipped with a standard three electrode configuration: a mercury hanging drop electrode, a glassy carbon rod as a counter electrode and a reference Ag/AgCl/3M KCl reference electrode.

A home-made UV digester was used for UV irradiation of water samples in Como ([124], Chapter 3). UV-digested seawater (UVSW) was prepared using a different home-built system with a 150W, high-pressure, mercury vapour lamp in the Palma de Mallorca laboratory. Surface seawater from the Southern Ocean was placed in 30-mL quartz tubes placed around the lamp at a distance of 10 cm for an irradiation time of 2 hours (Chapter 2).

The FIA-CL system used for intercalibration (software and hardware) was cloned from a model repeatedly used for the determination of dissolved iron in open ocean waters [72, 125] based on the analytical procedure design before [71].

An iCAP Q Inductively Coupled Plasma – Mass Spectrometer (ICP–MS) from ThermoScientific was used for the determinations of Cd, Co, Cu and Pb in rainwater samples as a reference method.

A Milestone DuoPur sub-boiling apparatus was used to produce pure hydrochcloric acid.

5.2 Materials & Solutions

All plastic materials were cleaned by successive soaking in detergent (one week) and twice in 2% HNO_3 (one week each), with ultrapure water rinsing in between steps and prior to usage.

Ultrapure water produced by a Millipore MilliQ A10 system (18.2 MΩ cm conductivity, 3 ppb TOC) was used for solution preparation and dilution.

Pure nitric acid (VWR, Ultrapure NORMATOM for trace metal analysis), hydrochloric acids (Fluka, TraceSELECT® ultra) and ammonia (Fluka, TraceSELECT® ultra) were employed.

A 1 M solution of NaOH was prepared by dissolving solid sodium hydroxide (Sigma-Aldrich, 99.99 % trace metal basis) and purified by three equilibrations with a colloidal solution of MnO_2.

A combined solution of piperazine-N,N'-bis-(2-hydroxypropanesulfonic) acid (POPSO, Sigma-Aldrich)/potassium bromate (AnalaR, BDH)/ ultrapure ammonia were prepared. One BrO_3^-/POPSO solution was prepared replacing ammonia with NaOH (Merck) at the same pH to check the effect of ammonia. Contaminating iron in all of those reagents was reduced by adsorption on a MnO_2 suspension removed by gravity filtration through 0.22 μm pore size filters.

Buffer solutions were prepared by dissolving the adequate amount of solid HEPPS (3-[4-(2-hydroxyethyl)-1-piperazinyl] propanesulfonic acid) (Sigma, ≥ 99.5 %) and adding solid sodium hydroxide (Sigma-Aldrich, 99.99 % trace metal basis) to a final pH of 8.15: the buffer was purified by two equilibrations with a colloidal solution of MnO_2 [80].

A one molar buffer solution for copper analysis was prepared by dissolving an adequate amount of solid HEPES (2-[4-(2-hydroxyethyl)piperazin-1-yl]ethanesulfonic acid) and adding pure ammonia (Suprapur, Fluka) to a final pH of 8.0. The one molar ammonia buffer was prepared by diluting adequate volumes of pure ammonia and hydrochloric acid produced by a quartz sub-boiling apparatus (Milestone DuoPur).

The 2,3-dihydroxynaphthalene (DHN) solutions (2 and 10 mM) were prepared dissolving DHN (Aldrich, ≥ 98.0 %) in ultrapure water.

A 10 millimolar salicylaldoxime (SA) solution was prepared by dissolving purified SA in 0.1 M pure hydrochloric acid. Moreover, a 0.1 M dimethylglioxime sodium salt (DMG) was prepared by dissolving purified DMG in ultrapure water.

Multistandard solutions for the calibration of Inductively Coupled Plasma – Mass Spectrometry were prepared by diluting the standard solution (10 mg L^{-1} from Merck, cat. no. 1.09498.001).

Standard iron solutions were prepared by dilution of a 1000 mg/L standard from Fluka and acidified to pH 2 or 3 (3 only for the analysis with small cell) by concentrated HCl.

All the pH measurements (buffer solutions and samples) were performed on the NBS scale.

5.3 Samplings & Methods

5.3.1 Potassium Bromate

Sampling The samples used for validation were the deep and surface reference waters collected during the SAFe (Sampling and Analysis of Fe) program [85]. Consensus values are as follows: SAFe S 0.097±0.043 nM and SAFe D2 0.91±0.17 nM[85].

The reliability of copper analysis was checked by analysis of acidified consensus samples collected during the SAFe cruise [91] (updated concentrations for different metals can be found in: http://es.ucsc.edu/~kbruland/GeotracesSaFe/kwbGeotracesSaFe.html).

Samples used for the inter-calibration were collected from the upper 300 meters of the water column by means of 8 metal free GOFLO bottles attached to a Kevlar line during the EDDY PUMP cruise in the Southern Ocean (Jan-Mar 2012) on board the research vessel Polarstern. Samples were immediately filtered online by 0.2 µm by means of filtration sterile capsules (Sartobran 300) and collected in LDPE bottles.

Analytical method Two 60 mL LDPE bottles were filled and immediately acidified to pH 2.0 by addition of 12µl HCl (30%) per 10 mL seawater for a pH of 2.0 (NBS). The bottle destined for CSV-DHN analysis was spiked also with DHN to a final concentration of 30 µM. After resting for a minimum of 24 hours at room temperature, both samples were analyzed by CSV-DHN and FIA-CL.

CSV analysis the following sequence of solutions was added to an empty glass cell in a quick succession: 500 µl of the BrO_3^-/POPSO solution, the volume of a NH_4OH (15%) solution required to raise the pH to 8.7 and 10 mL of the mix sample-HCl-DHN. The analytical sensitivity was determined for every sample by two standard additions. CSV settings were as follow: 20-90 s deposition at 0 V, quiescence period of 7 seconds, potential scan in the range -0.1 to -1.15 V at 50 mVs^{-1} (step increment of 5 mV and 10 steps s^{-1}).

Reagent blank was determined by repeated analysis of Ultrapure water tripling the concentrations of the BrO_3^-/POPSO solution (typical contamination 50 pM Fe per

500 µL addition), DHN (iron contribution lower than LOD for a concentration of 30 µM) and the HCl and NH_4OH solutions (typical contamination of ~20 pM for acidification to pH 2.0 and neutralization to pH 8.7).

5.3.2 Small Cell

Sampling Clean procedures were adopted during sample collection and treatment. Rainwater was collected in Como (Northern Italy) during a rainfall event on 15/11/2013, from 9:10 a.m. to 11:40 a.m. at half an hour intervals. The five samples were divided in two aliquots: a first 10 mL aliquot was acidified to pH 2 with quartz sub-distilled hydrochloric acid produced by a Milestone Duopur apparatus. The remaining sample aliquot (around 20 mL) was acidified with quartz sub-distilled nitric acid (final concentration 2%). Samples for the determination of total concentration by voltammetric techniques were UV irradiated for two hours in a homemade 400W apparatus[124].

Samples for analysis of organic copper speciation were collected at different depths (surface to –25 m) in Mahon Bay (Menorca Island, Balearic Islands). The samples were collected according to clean procedures and filtered online by 0.22 µm cartridges before storage in LDPE 250 mL bottles. Once on shore, the bottles were kept frozen until analysis.

Analytical methods All of the voltammetric determinations were performed in a laminar flow hood: instrumental parameters used for determination are listed in Table 5.1. A brief description of the procedures follows (see also [116]). Quantification in voltammetric determinations was performed by standard addition.

Anodic stripping voltammetry: cadmium, lead and copper. The 500 µL, UV digested, sample aliquot was transferred in the cell and concentrations quantified.

Cathodic stripping voltammetry: copper. 500 µL of the UV digested sample were transferred to the cell, 5 µL of pure concentrated ammonia, 5 µL of HEPES buffer and 5 µL of SA solution (final concentration 25 µM) were added. The potential was held at -1.1V during deposition and then switched to -0.1V before the scan as this procedure ensures higher sensitivity [114].

Cathodic stripping voltammetry: nickel and cobalt. The 500 µL of UV digested aliquot was transferred in the cell, 50 µL of ammonia buffer and 5 µL of DMG solution (final concentration 1 mM) were added (final pH around 9.5).

Metal titration (CLE–CSV), copper. The method is based on competitive ligand equilibration with salicylaldoxime and CSV detection of the labile fraction[114]. 120 mL of sample were transferred to a preconditioned bottle: 1.2 mL of HEPES buffer and 60 µL of SA solution (final concentration 2 µM) were subsequently added. Ten mL aliquots were transferred to polycarbonate 30 mL tubes and copper standard solution was added to final concentrations of 0, 1, 2 ,4 , 8, 12, 16, 20, 25, 30, 35 nM. The samples were equilibrated overnight, typically 14 hours. Signals were registered on 500 µL aliquots first: 500 µL from each tube were transferred to the small cell by a micropipette in order of increasing copper concentration and the signal read in triplicate. This procedure lasted 100 minutes on average. Subsequently, signal recording was performed using the standard 10 mL cell according to the same procedure, i.e. in order of increasing concentration, using the remaining 9.5 mL aliquots. The procedure employing the standard volume lasted 145 minutes on average. All the instrumental parameters are reported below in the Table 5.1.

Table 5.1 – Instrumental parameters employed for the differential pulse sweep.

	Cu (CSV)	Ni and Co (CSV)	Cd, Pb and Cu (ASV)
Purgin time (s)	120	150	150
Deposition potential (V)	-0.1 or -1.1	-0.7	-1.15
Deposition time (s)	60	60	60
Equilibration time (s)	10	10	10
Start potential (V)	-0.1	-0.8	-1.15
End potential (V)	-0.6	-1.1	0.05
Pulse amplitude (V)	0.050	0.050	0.050
Pulse time (s)	0.04	0.04	0.04
Voltage step (V)	0.005	0.004	0.006
Voltage step time (s)	0.3	0.3	0.15
Sweep rate (V s^{-1})	0.017	0.013	0.06

* -0.1 V was used for the speciation procedure whereas -1.1 V for the determination of total copper concentration.

Inductively Coupled Plasma – Mass Spectrometry (ICP–MS), nickel, cobalt, cadmium, lead and copper. Trace element concentrations in rainwater samples were determined by Inductively Coupled Plasma – Mass Spectrometry (ICP–MS) as a reference method, employing external calibration for quantification.

5.3.3 Atmospheric Oxygen

Sampling Two Pacific Ocean samples [85] with consensus values after inter-laboratory determination of the iron concentrations were analyzed to validate this new method (SAFe S and SAFe D2). Later, other samples from the Gulf of Mexico (GoM), sampled during a cruise in June 2015, were analyzed. The GoM samples represent surface water samples taken across a transect from the Tampa Bay area to the middle of the Gulf (Figure 4.20)

Analytical method The analyses were carried out in an open system under a laminar flow hood (Asalair 1200 FLO), to guarantee the fastest possible achievement of equilibrium between atmospheric and dissolved oxygen. This system differs from the closed one [123] in that four holes are opened in the plastic support of the small cell (see Figure 4.13). The small cell was filled with a blank (500 µL of ultrapure water, 10 mM HEPPS and 10 µM DHN) in between analyses to avoid carry over due to adsorption on the cell wall. The required amount of acidified sample (500 µL per replicate: 4 mL for SAFe and GEOTRACES GS samples; 5 mL for GoM samples) was transferred to a 60 mL bottle. 10 µL of the 1 M NaOH solution were added per 500 µL of sample aliquot to neutralize it. 500 µL of the neutralized sample were pipetted into the voltammetric cell. Ultraviolet digestion was not necessary prior to analysis, as already demonstrated in a previous paper [122]. A 25 µL aliquot of HEPPS pH buffer (final concentration 0.01 M, pH 8.15) and 50 µL of the DHN solution (final concentration 10 µM) were subsequently added. The solution was stirred for 90 sec, and three replicate measurements were registered. The measurement was repeated after a standard addition of iron (III) of appropriate concentration to calibrate the sensitivity. The instrumental parameters used for the determination are listed in Table 5.2: the optimization of the sweep mode and square wave frequency is discussed in the following sections, whereas the optimization of the deposition potential lead to the same value (-0.1V) as reported in the literature [80, 122].

Table 5.2 – Instrumental parameters used for the determination of iron in seawater with the new developed hardware.

Instrumental parameter	
Purging time (s)	0
Stirring time (s)	90
Deposition potential (V)	-0.1
Equilibration time (s)	10
Deposition time (s)	30
Start potential (V)	- 0.35
End Potential (V)	- 0.75
Voltage step (V)	0.005
Amplitude (V)	0.05
Frequency (Hz)	10

The initial 90 s stirring time was the minimum time needed to achieve a stable signal. Such an equilibration time may be needed to allow the DHN to outcompete the natural ligands (samples were not UV digested) or to reach the equilibrium oxygen concentration in the sample. Blank levels were measured for each analysis batch and subtracted from sample concentration. Contribution to the blank came mainly from the pH buffer (80 %) and from the sodium hydroxide solution (20 %).

6 Conclusions

The aim of this project was to optimize a new voltammetric method for the determination of dissolved iron in seawater. The new procedure required outstanding performance and applicability for on board analysis during research cruises.

Two CSV methods were optimized during this thesis. The first result obtained was based on a previous work on the CSV determination of iron using DHN as a ligand in the presence of bromate as a catalytic agent [80]. After significant modification of the protocol (i.e.: the need for prior acidification and the optimization of pH), it was obtained a 4 fold improvement of the sensitivity. The limit of detection obtained (5pM) was significantly better than those obtained with other pre-concentration-free techniques and close to the lowest LOD previously described for the procedures based on pre-concentration methods.

The Fe/BrO_3^- optimized method yielded good result, in fact it is suitable for any kind of seawater sample for the determination of dissolved iron thanks to its performance. Nevertheless, it comes with a few disadvantages: the procedure need potassium bromate and the required sample volume is 10 mL, like any other voltammetric method. Potassium bromate is a disadvantage because it is classified as toxic and suspected carcinogenic, causing several issues regarding its use, stock and disposal. Moreover, it is a big source of iron contamination during the analysis. At this point of the development considering all these evidences, and inspired by the principles of GAC, the mission was to build a completely new procedure avoiding the employment of carcinogenic product and limiting the sample size request for single determination. In order to achieve this goal, a small voltammetric cell was firstly developed (see section 3.1) and a new CSV method subsequently set up.

The new voltammetric cell led to a twenty fold reduction in sample size for trace and ultra-trace elemental determination and speciation by conventional voltammetric instrumentation. Reliable, validated results were obtained for the determination of trace/ultra-trace elements in rainwater (Cd, Co, Cu, Ni, Pb) and seawater (Cu). Copper speciation in seawater samples was consistently determined by competitive ligand equilibration – cathodic stripping voltammetry (CLE – CSV). The proposed apparatus (Figure 4.13) showed several advantages: 1) twenty-fold reduction in sample volume (the sample size is lowered from 120 to 6 mL for the CLE-CSV procedure); 2) the decrease in analysis time due to the reduction in purging time up to 2.5 fold; 3) twenty

fold drop in reagent consumption. Moreover, the analytical performances were not affected: similar detection capabilities, precision and accuracy were obtained. Application to sample of limited availability (e.g. pore-waters, snow, rainwater, open ocean water) and to the description of high resolution temporal trends may be easily foreseen.

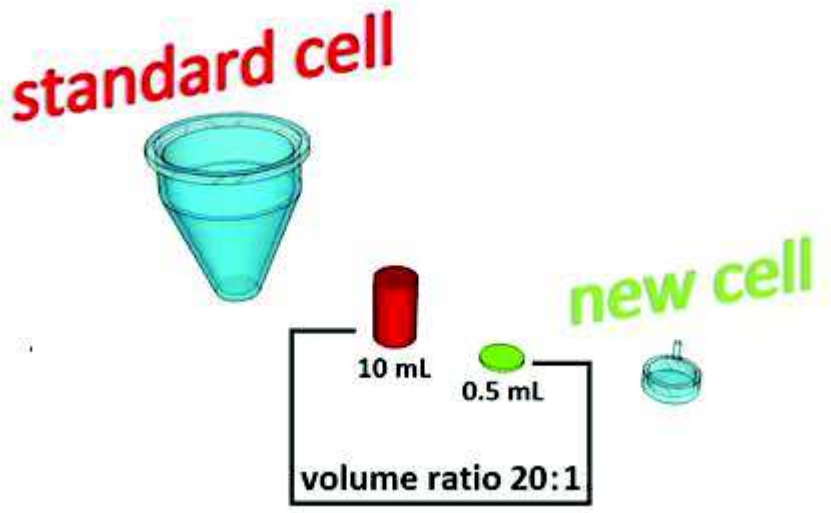

Figure 6.1 – Graphical comparison between the standard voltammetric cell (on the left) and the new voltammetric cell (on the right). The size ratio is respected.

The new cell, described in the Chapter 3, is adaptable to polarographic instrumentation without any other custom modifications: a modified stirrer was initially used, but recently, for the analysis of samples from the GoM, a standard stirrer was used without issues.

The development of this new cell was the most important step in order to achieve a greener method for the determination of dissolved iron in seawater.

The new method for iron determination in seawater at the ultra-trace level was still based on CSV of the complex formed by dihydroxynaphthalene and iron with catalytic enhancement. As opposite to the original method [126], atmospheric oxygen dissolved in solution replaced bromate ions in the oxidation of the iron complex. The analysis were carried out on 500 µL buffered sample aliquots (pH 8.15, HEPPS 0.01 M), 10 µM DHN and iron quantified by the standard addition method. The sensitivity is 49 nA nM^{-1} min^{-1} with 30 s deposition time and the LOD is equal to 5 pM. As a result, the whole procedure for the quantification of iron in one sample requires around eight

minutes, a strong reduction with respect to available procedures. In addition, the sample UV oxidation is not required.

The evolution of the detection procedure for ultra-trace iron analysis is graphically depicted in the following figure.

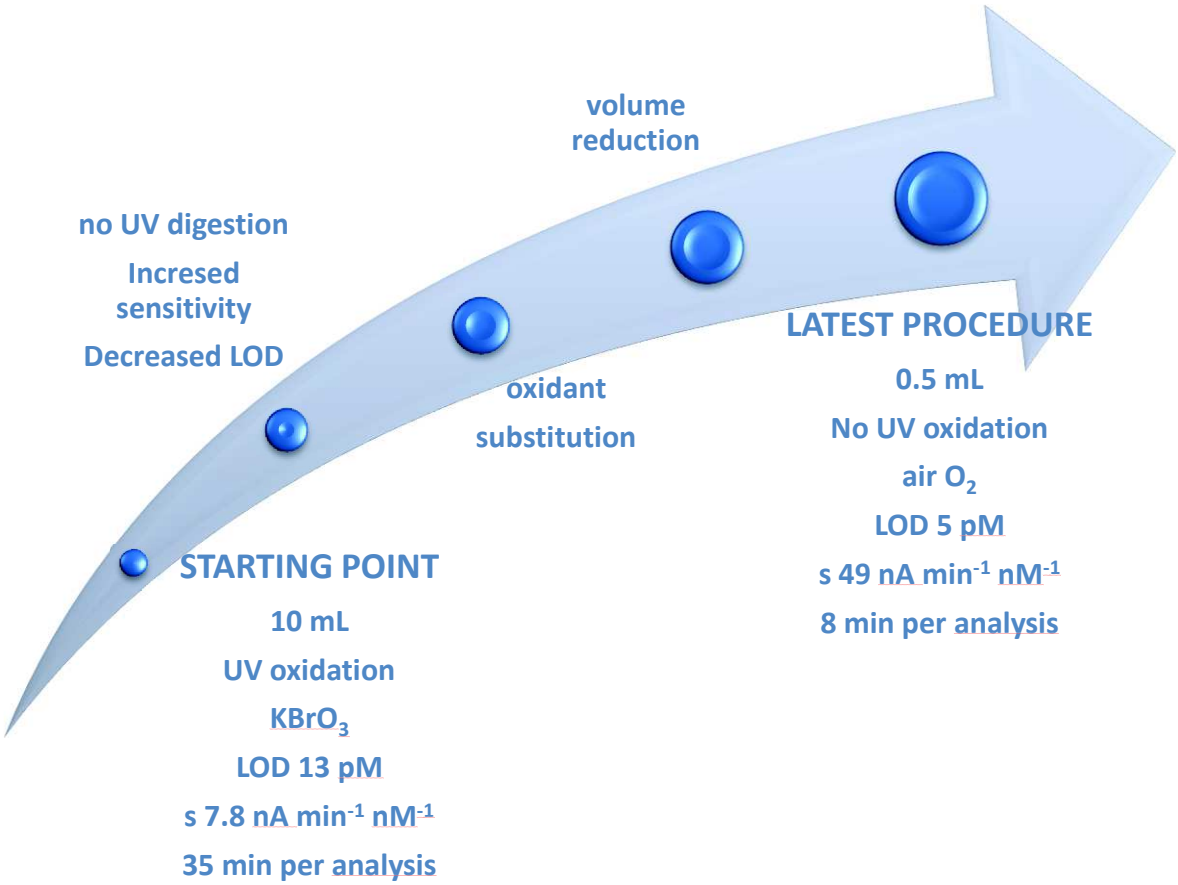

Figure 6.2 – Evolution steps during the method optimization for the determination of dissolved iron in seawater.

It is interesting noting that the evolution of the method points in the direction outlined by the green chemistry principles. These principles have been discussed by the scientific community since the early 1990s. Several definition of Green Chemistry were proposed during this period, one of the most accurate definitions states: "Green Chemistry is the use of chemistry techniques and methodologies that reduce or eliminate the use or generation of feedstocks, products, byproducts, solvents, reagents, etc. that are hazardous to human health or the environment" (see [127], page 30). The list was formed by 12 points, every one of these points was thought to encompass all the chemistry branches. Obviously some of those principles were more related to analytical chemistry than others and several years after the enunciation of the 12

principles of Green Chemistry, the 12 principles of Green Analytical Chemistry (GAC)were introduced [128], based on the Anastas P. T. and Warner J. C. works. The authors removed inadequate points, such as the atom economy and introduced others more related to analytical chemistry. After this thorough study, the 12 principals of GAC (reported below) were finalized [128].

1. Direct analytical techniques should be applied to avoid sample treatment.
2. Minimal sample size and minimal number of samples are goals.
3. In situ measurements should be performed.
4. Integration of analytical processes and operations saves energy and reduces the use of reagents.
5. Automated and miniaturized methods should be selected.
6. Derivatization should be avoided.
7. Generation of a large volume of analytical waste should be avoided and proper management of analytical waste should be provided.
8. Multi-analyte or multi-parameter methods are preferred versus methods using one analyte at a time.
9. The use of energy should be minimized.
10. Reagents obtained from renewable source should be preferred.
11. Toxic reagents should be eliminated or replaced.
12. The safety of the operator should be increased.

Most significantly, these principles note the importance of reducing volume, waste, toxic reagents and use of energy. The developed method follows many of the listed principles, especially the one related to avoiding sample treatment (no UV digestion, no purging), reduction of sample size requirements (development of a small sample cell), minimizing wastes (twenty fold reduction of reagent consumption) and elimination of one toxic reagent (substitution of potassium bromate by atmospheric oxygen). The substitution of the mercury electrode is clearly the biggest issue to be tackled to claim the development of a truly green method, although at present no viable solution has been devised yet (see also section 6.2).

The latter proposed procedure [129] for the dissolved iron determination in seawater seems the best candidate for the application of CSV methods during scientific cruises, but also for the routine laboratory analysis. It has the best performance up to

now and, more significantly, it works on 500 µL of sample eluding the use of carcinogenic products and the UV oxidation pre-treatment step. As a direct consequence, analysis time is strongly reduced because of the two-fold reduction in purge time. Moreover, a twenty fold reduction in reagent consumption was achieved. All of these features (i.e. minimal sample size, reduction in reagent use, decreased waste production and lower energy use compared to atomic spectrometric techniques) evidences advancement toward putting into practice the principles of green analytical chemistry [113].

In conclusion, a new CSV procedure for the determination of dissolved iron in seawater was reached by the combination of the substitution of potassium bromate with the atmospheric oxygen and the use of a new voltammetric cell. Moreover, the novel method follows the GAC principles ensuring the best performance in the voltammetric field and the best performance among the pre-concentration free methods (see also the following sections).

6.1 Comparison with existing methods

The optimized and developed methods will be critically compared with existing methods, firstly voltammetric ones (pre-concentration free) and subsequently with all the existing methods for trace iron detection.

Table 1.1 reports the values of LOD, sensitivity, ligand concentration and deposition time for all of the CSV methods for the determination of dissolved iron. During this time several artificial ligand were used for the determination of trace dissolved iron. The first attempts were made with SA, TAC and NN: finally, the introduction of the DHN gave a quick performance improvement. Obata et al.[80] in the work introducing DHN as artificial ligand reported a LOD equal to 13 pM for the system Fe/DHN/BrO_3^- (deposition time 300s). The optimization of this method, reported in this thesis [122], lowered this value down to 5 pM with only 30 sec of deposition time. The last procedure here presented [129] maintains the value of LOD at 5 pM, but using only 30 sec of deposition time (three-fold shorter). Moreover, the sensitivity was improved 1.5 fold, up to around 50 nA nM^{-1} min^{-1}. The value of 5 pM is, up to date, the best LOD value for CSV methods (see below for a comparison with other methods)..

Table 6.1 – Comparison with other CSV methods. LOD, sensitivity, deposition time and ligand concentration are reported.

CSV method	Ligand conc. (µM)	Deposition time (s)	LOD (pM)	Sensitivity (nA nM^{-1} min^{-1})	Cit.
Fe/TAC	10	300	100	4.3	[82]
Fe/SA*	27.5	600	10	16	[88]
Fe/NN	20	60	90	3.1	[83]
Fe/NN/BrO_3^-	20	30	80	6.2	[130]
Fe/DHN/BrO_3^- (pH 8.0)	20	300	13	7.8	[80]
Fe/DHN/BrO_3^- (pH 8.7)	30	90	5	34	[122]
Fe/SA/O_2	5	300	24 – 30	4.4	[81]
Fe/DHN/O_2	10	30	5	49	[129]

*only for speciation analysis

The very high sensitivity registered in this study may be due to several factors. The primary explanation for the high sensitivity is believed to be the possibility for oxygen to rapidly diffuse to the electrode due to the limited (around 1 mm) solution thickness needed to reach the electrode from the gas phase above the sample. This allows a much higher oxygen flux during the deposition step, resulting in a higher hydrogen peroxide concentration in the diffusion layer and finally in a higher catalytic enhancement of the signal (see Figure 4.5 and Figure 4.6). Moreover, the more oxygen is reduced, the higher the resulting pH in the diffusion layer, as this reaction consumes hydrogen ions [131]. A higher pH was shown to increase sensitivity in the bulk (see Figure 4.17) and could also cause an increase in sensitivity when the complex experience a more alkaline pH in the diffusion layer. Support for this hypothesis came from preliminary experiments in the 10 mL cell conducted in the same conditions presented here. Atmospheric oxygen gave a catalytic enhancement of the signal, but the resulting sensitivity was three times smaller.

Comparison of the latest developed method with methods other than voltammetric ones, is reported in Table 6.2. The developed voltammetric method shows an LOD similar to the best performing methods, employing the smallest amount of sample and the easiest procedure, due to the absence of any pretreatment before analysis.

Table 6.2 – Comparison of the analytical performances of the most used analytical techniques for the determination of total dissolved iron in seawater. The last section of the table is dedicated to recent developments by voltammetry.

Method	Sample acidification	Sample size mL	Preanalytical steps			Analysis	Blank pM	LOD pM (deposition time for CSV)	Ref
Catalytic spectrophotometry	0.024 M HCl	60	+50µL H_2O_2 12 mM			1.5 M HCl (eluent) 3.5 M CH_3COONH_4 DPD solution 5% H_2O_2	60	24	[132]
Chemiluminescence	0.024 M HCl	60		+ 60 µL 1‰ H_2O_2 + 0.12 M CH_3COONH_4		0.4 M HCl (eluent) 0.96 NH_3 0.35 H_2O_2 Luminol solution*	32	5.7	[133]
Preconcentration on chelatin resin + ICPMS (flow injection)	0.024 M HCl	9	Isotopic spike	+ 3 mL CH_3COONH_4 0.5 M		225 µL HNO_3 1.6M (eluent)	65	14	[134]
Preconcentration on chelatin resin + ICPMS (8 elements)	0.024 M HCl	12	Isotopic spike	+ 2 mL CH_3COONH_4 2M Preconc. on column		1 mL HNO_3 1M (eluent)	230	21	[135]
Preconcentration on chelatin resin + ICPMS (flow injection)	0.01 M HCl	~120	Isotopic spike	+1.8 g CH_3COONH_4 0.05M		15 mL of 1 M HNO3 (eluent)	26	36	[136]
$Mg(OH)_2$ single precipitation		1.4	^{57}Fe isotopic spike ~20-40 µL NH_3 Centrifugation X 2			+ 100 µL 5% HCl	89	30	[74]
$Mg(OH)_2$ double precipitation		50	^{57}Fe isotopic spike ~280 µL NH_3 Centrifugation	+2 mL 0.5 M HCl Evaporation	+ 1.6 mL of acidified seawater +~280 µL NH_3 Centrifugation	+ 100 µL 4% HNO_3	15	2	[137]

Method	Sample acidification	Sample size mL	Preanalytical steps	Analysis	Blank pM	LOD pM (deposition time for CSV)	Ref
Fe DHN BrO_3^- pH 8.7	~0.03 M HCl	10		30 µM DHN ~0.03 M NH_3 5 mM POPSO buffer 20 mM bromate	70	5 (90 s)	[122]
Fe SA O_2	~0.03 M HCl	10		5 µM SA ~0.03 M NH_3 10 mM boric buffer	na	24-30 (180 s)	[81]
Fe DHN O_2	~0.03 M HCl	0.5		10 µM DHN ~0.03 M NaOH 10 mM HEPPS buffer	86	5 (30 s)	[138]

Abbreviations (alphabetic order): DHN dihydroxynaphthalene; DPD *N*,*N*-dimethyl-*p*-phenylenediamine dihydrochloride; HEPPS (3-[4-(2-hydroxyethyl)-1-piperazinyl]propanesulfonic acid; POPSO piperazine-N,N′-bis-(2-hydroxypropanesulfonic) acid; SA salicylaldoxime
*Luminol solution: alkaline (KOH) solution of luminol with the addition of triethylenetetramine

6.2 Future Perspectives

Progresses may take place along different directions: further improvement of the existing procedure, application to new procedures/samples and hardware development.

Although the detection capabilities were demonstrated to be suitable for the determination of the lowest iron concentrations in seawater, directions for their further enhancement may be devised. In particular, other than increasing the deposition time, raising the oxygen partial pressure seems a strategy at hand, although at cost of an increase in system complexity. Alternatively, raising the ligand concentration from 10 μM to 500 μM lead to an impressive increases in sensitivity, although the deterioration in signal stability limited the gain in signal to noise ratio. A cleaner environment (a clean room) and the use of a pseudo-reference electrode free from liquid junctions could stabilize the signal as contamination was proposed to be the cause of the raising signal observed at high ligand concentrations. A further simplification in the procedure was very recently introduced for 10 mL samples: the pH buffer was not added to the solution resulting in the first method with negligible blank for iron detection at the trace level [139]. This procedure may be tested and applied to the 0.5 mL sample hardware.

The possibility of applying the developed method (oxygen plus small cell) to the speciation analysis of iron by the competitive ligand equilibration procedure (CLE-CSV) would be appealing. Nevertheless, the time stability of the signal has been verified for short periods of time only, whereas the CLE-CSV procedure requires around twelve hours of equilibration time.

Validation of the proposed procedure was achieved for open ocean samples as the focus of the research concerned trace determination of iron. Application to coastal samples with higher iron and organic matter concentrations should be tested and possibly validated.

Further hardware development may be also foreseen. Automatization of the procedure for both total concentration and speciation analysis would be highly beneficial. The small volumes involved call for the use of recent analytical platforms, lab on a chip (LoC) or lab on a valve (LoV) strategies, although at present no such hardware has ever been tested for trace conditions. On the other hand, further

reduction of sample volume in a standard three electrode configuration may be difficult to achieve due to geometric limitations: miniaturization of the electrodes and possibly different working electrodes (i.e. solid state electrodes or nano-electrodes) should be pursued, although retaining the performances of standard mercury electrode is presently out of reach. Film or alloy, mercury free macro-electrodes did not lead to satisfactory detection capabilities. Using a bismuth film, triethanolamine (TEA) as a ligand and bromate as a catalytic enhancer [140] lead to a sensitivity of and an LOD of 7.7 nM (sensitivity 0.88 nA/nM, no deposition, differential pulse sweep). More recently, a bismuth-tin alloy [141] electrode was introduced in combination with 1-(2-piridylazo)-2-naphthol (PAN) as a ligand, claiming a 0.2 nM detection limit (60 s deposition time), although the sensitivity is only 0.12 nA nM^{-1} min^{-1}.

Moving to micro-structured electrodes seems a viable option. A gold nanowire coated with mercury was proposed employing the reagent combination DHN, bromate and a pH buffer [142], with a satisfactory LOD of 0.1 nM (60 s deposition time): although not being completely mercury free, it strongly reduces the amount of metal employed. A different strategy, completely mercury free, was more recently proposed: the deposition of bismuth microcrystals over a gold macroelectrode to permit the adsorption of metal complexes [143]. The method was applied to nickel and cobalt detection by CSV in the presence of dimethylglioxime with very low detection limits (1 and 1.7 nM for Ni and Co, respectively, deposition time 120 s). The integration of these electrodes in the developed protocols could further contribute in making iron detection greener.

7 Acknowledgements

First and foremost, I would like to thank my

Family

and

friends

for their incredible level of support throughout my academic career. Also, a special thanks goes to my tutor, Dr.

Damiano Monticelli.

With his guidance as well as the experiences I have gained along my academic path, I can definitively state that Italian universities are steadfast as competitive and challenging environments in which to improve upon one's knowledge and skills. I will forever be grateful for the two study abroad opportunities I have had during my time as a PhD student. In both cases, I worked in special environments that helped me grow, not solely in the field of chemistry, but also personally. For these memorable and meaningful experiences, I would like to thank Prof.

Kristen Buck

with the College of Marine Science at the University of South Florida and Prof.

Luis Laglera

for my staying in Spain at the Universitat de les Illes Balears.

Finally, I want to say thanks to

Paige Riffe

for her precious help during the thesis writing. She spent most of her free time to read and correct my uncertain English.

8 List of publications

- ✓ Quantification of iron in seawater at the low picomolar range based on optimization of bromate ammonia dihydroxynaphtalene system by catalytic adsorptive cathodic stripping voltammetry, L. M. Laglera, J. Santos-Encheandia, S. Caprara, D. Monticelli, *Anal. Chem.*, 85 (2013), 2486-2492.

- ✓ Miniaturization in voltammetry: Ultratrace element analysis and speciation with twenty-fold sample size reduction, D. Monticelli, L. M. Laglera, S. Caprara, *Talanta*, 128 (2014), 273-277.

- ✓ Voltammetric tools for trace element speciation in fresh waters: methodologies, outcomes and future perspectives, D. Monticelli and S. Caprara, *Environ. Chem,* 12 (2015), 683-705.

- ✓ Ultrasensitive and fast voltammetric determination of iron in seawater by atmospheric oxygen catalysis in 500 µL samples, S. Caprara, L. M. Laglera, and D. Monticelli, *Anal. Chem.*, 87 (2015), 6357-6363.

- ✓ Towards a zero-blank, preconcentration-free voltammetric method for iron analysis at picomolar concentrations in unbuffered seawater, L. M. Laglera, S. Caprara, D. Monticelli, *Talanta*, 150 (2016), 449-454.

9 Communications to Conferences

- ✓ Automation of ultratrace analysis of iron by adsorptive stripping voltammetry, D. Monticelli, S. Caprara, L. M. Laglera, XXIII Congresso Nazionale della Divisione di Chimica Analitica della Società Chimica Italiana, Biodola, Isola d'Elba (Italy), 16th – 20th September 2012

- ✓ New insights and performance enhancement of the determination of total iron in seawater by catalytic cathodic voltammetry of its complexes with dihydroxynapthalene, L. M. Laglera, J. Santos-Echeandía, S. Caprara, D. Monticelli, Voltammetry and GEOTRACES ESF COST 801 Meeting, Šibenik (Croatia), 6th – 9th October 2012

- ✓ Ultratrace element analysis and speciation with twenty-fold sample size reduction, D. Monticelli, L. M. Laglera, S. Caprara, The BNASS / TraceSpec Tandem Conference, Aberdeen, Scotland (UK), 31st August – 4th September 2014

- ✓ Ultratrace element analysis and speciation with twenty-fold sample size reduction, D. Monticelli, L. M. Laglera, S. Caprara, Organic Ligands - A Key Control on Trace Metal Biogeochemistry in the Ocean, Šibenik (Croatia), 7th – 11th April 2015

- ✓ Investigating feedbacks between natural metal-binding organic ligands and particle dissolution in central California coast seawater, S. Caprara, J. Fitzsimmons, D. C. Ohnemus, B. S. Twining, P. Dreux Chappell, R. Sherrell, D. Monticelli, K. N. Buck, Trace metal speciation in seawater: measurements, modelling and impact on marine biogeochemistry, ASLO 2016 meeting, New Orleans (LA) 21st – 26th February 2016.

10 References

1. Rahmstorf, S., *Ocean circulation and climate during the past 120,000 years.* Nature, 2002. **419**(6903): p. 207-214.
2. Arrigo, K.R., *Marine microorganisms and global nutrient cycles.* Nature, 2005. **437**(7057): p. 349-355.
3. Harley, C.D.G., et al., *The impacts of climate change in coastal marine systems.* Ecology Letters, 2006. **9**(2): p. 228-241.
4. Lambeck, K., T.M. Esat, and E.K. Potter, *Links between climate and sea levels for the past three million years.* Nature, 2002. **419**(6903): p. 199-206.
5. Roemmich, D., W. John Gould, and J. Gilson, *135 years of global ocean warming between the Challenger expedition and the Argo Programme.* Nature Climate Change, 2012. **2**(6): p. 425-428.
6. Vitousek, P.M., et al., *Human alteration of the global nitrogen cycle: Sources and consequences.* Ecological Applications, 1997. **7**(3): p. 737-750.
7. Orr, J.C., et al., *Anthropogenic ocean acidification over the twenty-first century and its impact on calcifying organisms.* Nature, 2005. **437**(7059): p. 681-686.
8. Doney, S.C., et al., *Ocean acidification: The other CO2 problem.* Annual Review of Marine Science, 2009. **1**: p. 169-192.
9. Eppley, R.W. and B.J. Peterson, *Particulate organic matter flux and planktonic new production in the deep ocean.* Nature, 1979. **282**(5740): p. 677-680.
10. Diaz, R.J. and R. Rosenberg, *Spreading dead zones and consequences for marine ecosystems.* Science, 2008. **321**(5891): p. 926-929.
11. Field, C.B., et al., *Primary production of the biosphere: Integrating terrestrial and oceanic components.* Science, 1998. **281**(5374): p. 237-240.
12. Suess, E., *Particulate organic carbon flux in the oceans - Surface productivity and oxygen utilization.* Nature, 1980. **288**(5788): p. 260-263.
13. Tyrrell, T., *The relative influences of nitrogen and phosphorus on oceanic primary production.* Nature, 1999. **400**(6744): p. 525-531.
14. De Baar, H.J.W., et al., *Importance of iron for plankton blooms and carbon dioxide drawdown in the Southern Ocean.* Nature, 1995. **373**(6513): p. 412-415.
15. Martin, J.H., *Glacial-interglacial CO2 change: the iron hypothesis.* Paleoceanography, 1990. **5**(1): p. 1-13.
16. Longhurst, A.R. and W.G. Harrison, *The biological pump: profiles of plankton production and consumption in the upper ocean.* Progress in Oceanography, 1989. **22**(1): p. 47-123.
17. Martin, J.H. and S.E. Fitzwater, *Iron deficiency limits phytoplankton growth in the north-east pacific subarctic.* Nature, 1988. **331**(6154): p. 341-343.
18. de Baar, H.J.W., et al., *Importance of iron for plankton blooms and carbon dioxide drawdown in the Southern Ocean.* Nature, 1995. **373**: p. 412-415.
19. Liu, X.W. and F.J. Millero, *The solubility of iron in seawater.* Marine Chemistry, 2002. **77**(1): p. 43-54.
20. Johnson, K.S., R. Michael Gordon, and K.H. Coale, *What controls dissolved iron concentrations in the world ocean?* Marine Chemistry, 1997. **57**(3-4): p. 137-161.
21. Wells, M.L., *The level of iron enrichment required to initiate diatom blooms in HNLC waters.* Marine Chemistry, 2003. **82**(1-2): p. 101-114.
22. Strzepek, R.F., et al., *Adaptive strategies by Southern Ocean phytoplankton to lessen iron limitation: Uptake of organically complexed iron and reduced cellular iron requirements.* Limnology and Oceanography, 2011. **56**(6): p. 1983-2002.
23. Bowie, A.R., et al., *The fate of added iron during a mesoscale fertilisation experiment in the Southern Ocean.* Deep-Sea Research Part II: Topical Studies in Oceanography, 2001. **48**(11-12): p. 2703-2743.

24. Sholkovitz, E.R., E.A. Boyle, and N.B. Price, *Removal of Dissolved Humic Acids and Iron During Estuarine Mixing.* Earth and Planetary Science Letters, 1978. **40**(1): p. 130-136.
25. Laglera, L.M. and C.M.G. Van Den Berg, *Evidence for geochemical control of iron by humic substances in seawater.* Limnology and Oceanography, 2009. **54**(2): p. 610-619.
26. Bruland, K.W. and E.L. Rue, *The Biogeochemistry of Iron in Seawater.* Chichester, West Sussex: John Wiley & Sons, 2001: p. 255– 289.
27. van den Berg, C.M.G., *Evidence for organic complexation of iron in seawater.* Marine Chemistry, 1995. **50**(1-4): p. 139-157.
28. Kuma, K., et al., *Size-fractionated iron concentrations and Fe(III) hydroxide solubilities in various coastal waters.* Estuarine, Coastal and Shelf Science, 1998. **47**(3): p. 275-283.
29. Wu, J., et al., *Soluble and colloidal iron in the oligotrophic North Atlantic and North Pacific.* Science, 2001. **293**(5531): p. 847-849.
30. Millero, F.J., W. Yao, and J. Aicher, *The speciation of Fe(II) and Fe(III) in natural waters.* Marine Chemistry, 1995. **50**(1–4): p. 21-39.
31. Sunda, W.G. and S.A. Huntsman, *Iron uptake and growth limitation in oceanic and coastal phytoplankton.* Marine Chemistry, 1995. **50**(1-4): p. 189-206.
32. Kuma, K., J. Nishioka, and K. Matsunaga, *Controls on iron(III) hydroxide solubility in seawater: The influence of pH and natural organic chelators.* Limnology and Oceanography, 1996. **41**(3): p. 396-407.
33. Barbeau, K., et al., *Photochemical reactivity of siderophores produced by marine heterotrophic bacteria and cyanobacteria based on characteristic Fe(III) binding groups.* Limnology and Oceanography, 2003. **48**(3): p. 1069-1078.
34. Maldonado, M.T. and N.M. Price, *Nitrate regulation of Fe reduction and transport by Fe-limited Thalassiosira oceanica.* Limnology and Oceanography, 2000. **45**(4): p. 814-826.
35. Millero, F.J. and S. Sotolongo, *The oxidation of Fe(II) with H2O2 in seawater.* Geochimica et Cosmochimica Acta, 1989. **53**(8): p. 1867-1873.
36. Johnson, K.S., et al., *Iron photochemistry in seawater from the equatorial Pacific.* Marine Chemistry, 1994. **46**(4): p. 319-334.
37. Gordon, R.M., K.S. Johnson, and K.H. Coale, *The behaviour of iron and other trace elements during the IronEx-I and PlumEx experiments in the Equatorial Pacific.* Deep-Sea Research Part II: Topical Studies in Oceanography, 1998. **45**(6): p. 995-1041.
38. Duce, R.A., *The atmospheric input of trace species to the World ocean.* Global Biogeochemical Cycles, 1991. **5**(3): p. 193-259.
39. Hiscock, M.R., et al., *Primary productivity and its regulation in the Pacific Sector of the Southern Ocean.* Deep-Sea Research Part II: Topical Studies in Oceanography, 2003. **50**(3-4): p. 533-558.
40. Gledhill, M. and C.M.G. van den Berg, *Determination of complexation of iron(III) with natural organic complexing ligands in seawater using cathodic stripping voltammetry.* Marine Chemistry, 1994. **47**(1): p. 41-54.
41. Martin, J.H., et al., *Vertex: phytoplankton/iron studies in the Gulf of Alaska.* Deep Sea Research Part A, Oceanographic Research Papers, 1989. **36**(5): p. 649-680.
42. Boyd, P.W., et al., *A mesoscale phytoplankton bloom in the polar Southern Ocean stimulated by iron fertilization.* Nature, 2000. **407**(6805): p. 695-702.
43. Martin, J.H., et al., *Testing the iron hypothesis in ecosystems of the equatorial Pacific Ocean.* Nature, 1994. **371**(6493): p. 123-129.
44. Chavez, F.P., et al., *Phytoplankton variability in the central and eastern tropical pacific.* Deep-Sea Research Part II: Topical Studies in Oceanography, 1996. **43**(4-6): p. 835-870.
45. Thomas, W.H., *Phytoplankton Nutrient Enrichment Experiments off Baja California and in the Eastern Equatorial Pacific Ocean.* Journal of the Fisheries Research Board of Canada, 1969. **26**(5): p. 1133-1145.
46. Hart, T.J., *Red 'water-bloom' in South African seas [5].* Nature, 1934. **134**(3386): p. 459-460.
47. Coale, K.H., et al., *A massive phytoplankton bloom induced by an ecosystem-scale iron fertilization experiment in the equatorial Pacific Ocean.* Nature, 1996. **383**(6600): p. 495.

48. Martin, J.H., R.M. Gordon, and S.E. Fitzwater, *The case for iron.* Limnology & Oceanography, 1991. **36**(8): p. 1793-1802.
49. Price, N.M., L.F. Andersen, and F.M.M. Morel, *Iron and nitrogen nutrition of equatorial Pacific plankton.* Deep Sea Research Part A, Oceanographic Research Papers, 1991. **38**(11): p. 1361-1378.
50. Hutchins, D.A., G.R. Ditullio, and K.W. Bruland, *Iron and regenerated production: evidence for biological iron recycling in two marine environments.* Limnology & Oceanography, 1993. **38**(6): p. 1242-1255.
51. Timmermans, K.R., et al., *Iron stress in the Pacific region of the Southern Ocean: Evidence from enrichment bioassays.* Marine Ecology Progress Series, 1998. **166**: p. 27-41.
52. Coale, K.H., et al., *Phytoplankton growth and biological response to iron and zinc addition in the Ross Sea and Antarctic Circumpolar Current along 170°W.* Deep-Sea Research Part II: Topical Studies in Oceanography, 2003. **50**(3-4): p. 635-653.
53. Sedwick, P.N., et al., *Resource limitation of phytoplankton growth in the Crozet Basin, Subantarctic Southern Ocean.* Deep-Sea Research Part II: Topical Studies in Oceanography, 2002. **49**(16): p. 3327-3349.
54. Takeda, S. and H. Obata, *Response of equatorial Pacific phytoplankton to subnanomolar Fe enrichment.* Marine Chemistry, 1995. **50**(1-4): p. 219-227.
55. Dixon, J.L., *Macro and micro nutrient limitation of microbial productivity in oligotrophic subtropical Atlantic waters.* Environmental Chemistry, 2008. **5**(2): p. 135-142.
56. Gervais, F., U. Riebesell, and M.Y. Gorbunov, *Changes in primary productivity and chlorophyll a in response to iron fertilization in the Southern Polar Frontal Zone.* Limnology and Oceanography, 2002. **47**(5): p. 1324-1335.
57. Hoffmann, L.J., et al., *Different reactions of Southern Ocean phytoplankton size classes to iron fertilization.* Limnology and Oceanography, 2006. **51**(3): p. 1217-1229.
58. Smetacek, V., et al., *Deep carbon export from a Southern Ocean iron-fertilized diatom bloom.* Nature, 2012. **487**(7407): p. 313-319.
59. Peloquin, J., et al., *Control of the phytoplankton response during the SAGE experiment: A synthesis.* Deep-Sea Research Part II: Topical Studies in Oceanography, 2011. **58**(6): p. 824-838.
60. Tsuda, A., et al., *Evidence for the grazing hypothesis: Grazing reduces phytoplankton responses of the HNLC ecosystem to iron enrichment in the western subarctic pacific (SEEDS II).* Journal of Oceanography, 2007. **63**(6): p. 983-994.
61. Boyd, P.W., et al., *The evolution and termination of an iron-induced mesoscale bloom in the northeast subarctic Pacific.* Limnology and Oceanography, 2005. **50**(6): p. 1872-1886.
62. Coale, K.H., et al., *Southern Ocean Iron Enrichment Experiment: Carbon Cycling in High- and Low-Si Waters.* Science, 2004. **304**(5669): p. 408-414.
63. Buesseler, K.O., et al., *The Effects of Iron Fertilization on Carbon Sequestration in the Southern Ocean.* Science, 2004. **304**(5669): p. 414-417.
64. *The Law of the Sea.* Nature Geosci, 2009. **2**(3): p. 153-153.
65. Strong, A.L., J.J. Cullen, and S.W. Chisholm, *Ocean fertilization: Science, policy, and commerce.* Oceanography, 2009. **22**(SPL.ISS. 3): p. 236-261.
66. Boyd, P.W., et al., *Mesoscale iron enrichment experiments 1993-2005: Synthesis and future directions.* Science, 2007. **315**(5812): p. 612-617.
67. Banse, K., *Rates of phytoplankton cell division in the field and in iron enrichment experiments.* Limnology & Oceanography, 1991. **36**(8): p. 1886-1898.
68. de Baar, H.J.W., et al., *Synthesis of iron fertilization experiments: From the iron age in the age of enlightenment.* Journal of Geophysical Research C: Oceans, 2005. **110**(9): p. 1-24.
69. Mitchell, B.G., et al., *Light limitation of phytoplankton biomass and macronutrient utilization in the Southern Ocean.* Limnology & Oceanography, 1991. **36**(8): p. 1662-1677.
70. Jickells, T.D., et al., *Global iron connections between desert dust, ocean biogeochemistry, and climate.* Science, 2005. **308**(5718): p. 67-71.

71. Obata, H., H. Karatani, and E. Nakayama, *Automated-determination of iron in seawater by chelating resin concentration and chemiluminescence detection.* Analytical Chemistry, 1993. **65**(11): p. 1524-1528.
72. Sarthou, G., et al., *Atmospheric iron deposition and sea-surface dissolved iron concentrations in the eastern Atlantic Ocean.* Deep-Sea Research Part I: Oceanographic Research Papers, 2003. **50**(10-11): p. 1339-1352.
73. Lohan, M.C., A.M. Aguilar-Islas, and K.W. Bruland, *Direct determination of iron in acidified (pH 1.7) seawater samples by flow injection analysis with catalytic spectrophotometric detection: Application and intercomparison.* Limnology and Oceanography: Methods, 2006. **4**(JUN.): p. 164-171.
74. Wu, J. and E.A. Boyle, *Determination of iron in seawater by high-resolution isotope dilution inductively coupled plasma mass spectrometry after Mg(OH)2 coprecipitation.* Analytica Chimica Acta, 1998. **367**(1-3): p. 183-191.
75. Wu, J.F., *Determination of picomolar iron in seawater by double Mg(OH)(2) precipitation isotope dilution high-resolution ICPMS.* Marine Chemistry, 2007. **103**(3-4): p. 370-381.
76. Biller, D.V. and K.W. Bruland, *Analysis of Mn, Fe, Co, Ni, Cu, Zn, Cd, and Pb in seawater using the Nobias-chelate PA1 resin and magnetic sector inductively coupled plasma mass spectrometry (ICP-MS).* Marine Chemistry, 2012. **130–131**(0): p. 12-20.
77. Bowie, A.R., P.N. Sedwick, and P.J. Worsfold, *Analytical intercomparison between flow injection-chemiluminescence and flow injection-spectrophotometry for the determination of picomolar concentrations of Iron in seawater.* Limnology and Oceanography: Methods, 2004. **2**(FEB.): p. 42-54.
78. Achterberg, E.P., et al., *Determination of iron in seawater.* Analytica Chimica Acta, 2001. **442**(1): p. 1-14.
79. Worsfold, P.J., et al., *Determination of dissolved iron in seawater: A historical review.* Marine Chemistry, 2014. **166**: p. 25-35.
80. Obata, H. and C.M.G. van den Berg, *Determination of picomolar levels of iron in seawater using catalytic cathodic stripping voltammetry.* Analytical Chemistry, 2001. **73**(11): p. 2522-2528.
81. Abualhaija, M.M. and C.M.G. van den Berg, *Chemical speciation of iron in seawater using catalytic cathodic stripping voltammetry with ligand competition against salicylaldoxime.* Marine Chemistry, 2014. **164**: p. 60-74.
82. Croot, P.L. and M. Johansson, *Determination of iron speciation by cathodic stripping voltammetry in seawater using the competing ligand 2-(2-thiazolylazo)-p-cresol (TAC).* Electroanalysis, 2000. **12**(8): p. 565-576.
83. Gledhill, M. and C.M.G. van den Berg, *Measurement of the redox speciation of iron in seawater by catalytic cathodic stripping voltammetry.* Marine Chemistry, 1995. **50**(1-4): p. 51-61.
84. Bowie, A.R., et al., *A community-wide intercomparison exercise for the determination of dissolved iron in seawater.* Marine Chemistry, 2006. **98**(1): p. 81-99.
85. Johnson, K.S., et al., *Developing standards for dissolved iron in seawater.* Eos, Transactions American Geophysical Union, 2007. **88**(11): p. 131-132.
86. Tagliabue, A., et al., *A global compilation of dissolved iron measurements: Focus on distributions and processes in the Southern Ocean.* Biogeosciences, 2012. **9**(6): p. 2333-2349.
87. Boye, M., et al., *Organic complexation of iron in the Southern Ocean.* Deep-Sea Research Part I-Oceanographic Research Papers, 2001. **48**(6): p. 1477-1497.
88. Rue, E.L. and K.W. Bruland, *Complexation of iron(III) by natural organic ligands in the Central North Pacific as determined by a new competitive ligand equilibration/adsorptive cathodic stripping voltammetric method.* Marine Chemistry, 1995. **50**(1-4): p. 117-138.
89. Gledhill, M. and C.M.G. van den Berg, *Determination of complexation of iron(III) with natural organic complexing ligands in sea water using cathodic stripping voltammetry.* Marine Chemistry, 1994. **47**: p. 41-54.

90. Croot, P.L. and K.A. Hunter, *Determination of Fe(II) and total iron in natural waters with 3-(2-pyridyl)-5,6-diphenyl-1,2,4-triazin (PDT).* Analytica Chimica Acta, 2000. **406**(2): p. 289-302.
91. Johnson, K.S., et al., *Developing standards for dissolved iron in seawater.* Eos, 2007. **88**(11): p. 131-132.
92. Gledhill, M. and C.M.G. van den Berg, *Measurement of the redox speciation of iron in seawater by catalytic cathodic stripping voltammetry.* Marine Chemistry, 1995. **50**: p. 51-61.
93. Gordon, R.M., K.H. Coale, and K.S. Johnson, *Iron distributions in the equatorial Pacific: Implications for new production.* Limnology and Oceanography, 1997. **42**(3): p. 419-431.
94. Aguilar-Islas, A.M., et al., *Micro- and macronutrients in the southeastern Bering Sea: Insight into iron-replete and iron-depleted regimes.* Progress in Oceanography, 2007. **73**(2): p. 99-126.
95. Measures, C.I., J. Yuan, and J.A. Resing, *Determination of iron in seawater by flow injection analysis using in-line preconcentration and spectrophotometric detection.* Marine Chemistry, 1995. **50**: p. 3-12.
96. Wu, Q.G. and G.E. Batley, *Determination of Sub-Nanomolar Concentrations of Lead in Sea-Water by Adsorptive Stripping Voltammetry with Xylenol Orange.* Analytica Chimica Acta, 1995. **309**(1-3): p. 95-101.
97. Saito, M.A. and J.W. Moffett, *Complexation of cobalt by natural organic ligands in the Sargasso sea as determined by a new high-sensitivity electrochemical cobalt speciation method suitable for open ocean work.* Marine Chemistry, 2001. **75**(1-2): p. 49-68.
98. Laglera, L.M., G. Battaglia, and C.M.G. van den Berg, *Effect of humic substances on the iron speciation in natural waters by CLE/CSV.* Marine Chemistry, 2011. **127**(1-4): p. 134-143.
99. van den Berg, C.M.G., *Chemical speciation of iron in seawater by cathodic stripping voltammetry with dihydroxynaphthalene.* Analytical Chemistry, 2006. **78**(1): p. 156-163.
100. Baars, O. and P.L. Croot, *Comparison of alternate reactants for pM level cobalt analysis in seawater by the use of catalytic voltammetry.* Electroanalysis, 2011. **23**(7): p. 1663-1670.
101. Johnson, J.D. and R. Overby, *Bromine and bromamine disinfection chemistry.* Journal of the Sanitary Engineering Division-Asce, 1971. **97**(NSA5): p. 617-&.
102. Heaton, V.R., *A Study of the Oxidation of 2,3-dihydroxynaphthalene*. 1950: Western Illinois University.
103. Vega, M. and C.M.G. van den Berg, *Determination vanadium in sea water by catalytic adsorptive cathodic stripping voltammetry.* Analytica Chimica Acta, 1994. **293**: p. 19-28.
104. Job, P., *Formation and stability of inorganic complexes in solution.* Annali di Chimica Applicata, 1928. **9**: p. 113-203.
105. Bard, A.J. and L.R. Faulkner, *Electrochemical methods. Fundamentals and applications*. 1980, New York: John Wiley & Sons. 718.
106. Mirceski, V. and R. Gulaboski, *The surface catalytic mechanism: a comparative study with square-wave and staircase cyclic voltammetry.* Journal of Solid State Electrochemistry, 2003. **7**(3): p. 157-165.
107. Quentel, F. and V. Mirceski, *Catalytic adsorptive stripping voltammetry of molybdenum: Redox kinetic measurements.* Electroanalysis, 2004. **16**(20): p. 1690-1696.
108. Zotou, A., *An overview of recent advances in HPLC instrumentation.* Central European Journal of Chemistry, 2012. **10**(3): p. 554-569.
109. Tur'yan, Y.I., *Microcells for voltammetry and stripping voltammetry.* Talanta, 1997. **44**: p. 1-13.
110. Wang, J., *Electrochemical detection for microscale analytical systems: a review.* Talanta, 2002. **56**: p. 223-231.
111. Nyholm, L., *Electrochemical techniques for lab-on-a-chip applications.* Analyst, 2005. **130**: p. 599-605.
112. Vandaveer IV, W.R., et al., *Recent developments in electrochemical detection for microchip capillary electrophoresis.* Electrophoresis, 2004. **25**: p. 3528-3549.

113. Gałuszka, A., Z. Migaszewski, and J. Namieśnik, *The 12 principles of green analytical chemistry and the SIGNIFICANCE mnemonic of green analytical practices.* TRAC Trends in Analytical Chemistry, 2013. **50**(0): p. 78-84.
114. Campos, M.L.A.M. and C.M.G. van den Berg, *Determination of copper complexation in sea water by cathodic stripping voltammetry and ligand competition with salicylaldoxime.* Analytica Chimica Acta, 1994. **284**: p. 481-496.
115. Monticelli, D., C. Dossi, and A. Castelletti, *Assessment of accuracy and precision in speciation analysis by competitive ligand equilibration-cathodic stripping voltammetry (CLE-CSV) and application to Antarctic samples.* Analytica Chimica Acta, 2010. **675**(2): p. 116-124.
116. Monticelli, D., E. Ciceri, and C. Dossi, *Optimization and validation of an automated voltammetric stripping technique for ultratrace metal analysis.* Analytica Chimica Acta, 2007. **594**(2): p. 192-198.
117. Kolthoff, I.M. and E.P. Parry, *Catalytic polarographic waves of hydrogen peroxide. I. The kinetic wave for the ferric iron-hydrogen peroxide system.* Journal of the American Chemical Society, 1951. **73**(8): p. 3718-3723.
118. Bobrowski, A. and J. Zarębski, *Catalytic systems in adsorptive stripping voltammetry.* Electroanalysis, 2000. **12**(15): p. 1177-1186.
119. Beati, A.A.G.F., et al., *Development and Evaluation of a Pseudoreference Pt//Ag/AgCl Electrode for Electrochemical Systems.* Industrial & Engineering Chemistry Research, 2012. **51**(14): p. 5367-5371.
120. Weiss, R., *The solubility of nitrogen, oxygen and argon in water and seawater.* Deep Sea Research and Oceanographic Abstracts, 1970. **17**: p. 721-735.
121. Louis, Y., et al., *Speciation of trace metals in natural waters: The influence of an adsorbed layer of natural organic matter (NOM) on voltammetric behaviour of copper.* Analytica Chimica Acta, 2008. **606**(1): p. 37-44.
122. Laglera, L.M., et al., *Quantification of Iron in Seawater at the Low Picomolar Range Based on Optimization of Bromate/Ammonia/Dihydroxynaphtalene System by Catalytic Adsorptive Cathodic Stripping Voltammetry.* Analytical Chemistry, 2013. **85**(4): p. 2486-2492.
123. Monticelli, D., L.M. Laglera, and S. Caprara, *Miniaturization in voltammetry: Ultratrace element analysis and speciation with twenty-fold sample size reduction.* Talanta, 2014. **128**: p. 273-277.
124. Monticelli, D., et al., *Design and development of a low cost, high performance UV digester prototype: Application to the determination of trace elements by stripping voltammetry.* Microchemical Journal, 2010. **95**(2): p. 158-163.
125. Chever, F., et al., *An iron budget during the natural iron fertilisation experiment KEOPS (Kerguelen Islands, Southern Ocean).* Biogeosciences, 2010. **7**(2): p. 455-468.
126. Laglera, L.M., et al., *Quantification of iron in seawater at the low picomolar range based on optimization of bromate/ammonia/dihydroxynaphtalene system by catalytic adsorptive cathodic stripping voltammetry.* Analytical Chemistry, 2013. **85**(4): p. 2486-2492.
127. Anastas, P.T., *Green Chemistry and the role of analytical methodology development.* Critical Reviews in Analytical Chemistry, 1999. **29**(3): p. 167-175.
128. Gałuszka, A., Z. Migaszewski, and J. Namieśnik, *The 12 principles of green analytical chemistry and the SIGNIFICANCE mnemonic of green analytical practices.* TrAC - Trends in Analytical Chemistry, 2013. **50**: p. 78-84.
129. Caprara, S., L.M. Laglera, and D. Monticelli, *Ultrasensitive and Fast Voltammetric Determination of Iron in Seawater by Atmospheric Oxygen Catalysis in 500 µl Samples.* Analytical Chemistry, 2015. **87**(12): p. 6357-6363.
130. Aldrich, A.P. and C.M.G. van den Berg, *Determination of Iron and Its Redox Speciation in Seawater Using Catalytic Cathodic Stripping Voltammetry.* Electroanalysis, 1998. **10**(6): p. 369-373.

131. Aguilar, D., et al., *Non-purged voltammetry explored with AGNES.* Physical Chemistry Chemical Physics, 2013. **15**(40): p. 17510-17521.
132. Lohan, M.C., A.M. Aguilar-Islas, and K.W. Bruland, *Direct determination of iron in acidified (pH 1.7) seawater samples by flow injection analysis with catalytic spectrophotometric detection: Application and intercomparison.* Limnology and Oceanography: Methods, 2006. **4**(6): p. 164-171.
133. Klunder, M.B., et al., *Dissolved iron in the Southern Ocean (Atlantic sector).* Deep Sea Research Part II: Topical Studies in Oceanography, 2011. **58**(25–26): p. 2678-2694.
134. Lagerström, M.E., et al., *Automated on-line flow-injection ICP-MS determination of trace metals (Mn, Fe, Co, Ni, Cu and Zn) in open ocean seawater: Application to the GEOTRACES program.* Marine Chemistry, 2013. **155**(0): p. 71-80.
135. Milne, A., et al., *Determination of Mn, Fe, Co, Ni, Cu, Zn, Cd and Pb in seawater using high resolution magnetic sector inductively coupled mass spectrometry (HR-ICP-MS).* Analytica Chimica Acta, 2010. **665**(2): p. 200-207.
136. Sohrin, Y., et al., *Multielemental determination of GEOTRACES key trace metals in seawater by ICPMS after preconcentration using an ethylenediaminetriacetic acid chelating resin.* Analytical Chemistry, 2008. **80**(16): p. 6267-6273.
137. Wu, J., *Determination of picomolar iron in seawater by double Mg(OH)2 precipitation isotope dilution high-resolution ICPMS.* Marine Chemistry, 2007. **103**(3–4): p. 370-381.
138. Caprara, S., L.M. Laglera, and D. Monticelli, *Ultrasensitive and fast voltammetric determination of iron in seawater by atmospheric oxygen catalysis in 500 µl samples.* Analytical Chemistry, 2015. **87**: p. 6357-6363.
139. Laglera, L.M., S. Caprara, and D. Monticelli, *Towards a zero-blank, preconcentration-free voltammetric method for iron analysis at picomolar concentrations in unbuffered seawater.* Talanta, 2016. **150**: p. 449-454.
140. Bobrowski, A., K. Nowak, and J. Zarębski, *Application of a bismuth film electrode to the voltammetric determination of trace iron using a Fe(III)-TEA-BrO3 - Catalytic system.* Analytical and Bioanalytical Chemistry, 2005. **382**(7): p. 1691-1697.
141. Lin, M., et al., *A tin-bismuth alloy electrode for the cathodic stripping voltammetric determination of iron in coastal waters.* Analytical Methods, 2015. **7**(12): p. 5169-5174.
142. Salaün, P., B. Planer-Friedrich, and C.M.G. van den Berg, *Inorganic arsenic speciation in water and seawater by anodic stripping voltammetry with a gold microelectrode.* Analytica Chimica Acta, 2007. **585**(2): p. 312-322.
143. Mardegan, A., et al., *Simultaneous Adsorptive Cathodic Stripping Voltammetric Determination of Nickel(II) and Cobalt(II) at an In Situ Bismuth-Modified Gold Electrode.* Electroanalysis, 2013. **25**(11): p. 2471-2479.

Author's contacts

e-mail: salvatore.caprara@gmail.com

Skype: salvatore.caprara